UNIVERSITAT POLITÈCNICA DE CATALUNYA
BARCELONATECH
Escola d'Enginyeria de Barcelona Est

FINAL DEGREE PROJECT

Biomedical engineering degree

QUANTIFYING THE EFFECTIVE RANGE OF ELECTRIC FIELD VALUES FOR TRANSCRANIAL ELECTRIC STIMULATION

Memory and Annexes

Author: Fernández Asunción, Víctor

Director: Salvador, Ricardo

Tutor: Nescolarde Selva, Lexa

Announcement: February, 2020

Resumen

La estimulación eléctrica transcraneal (tES) es una técnica qué consiste en la colocación de diversos electrodos en la cabeza y mediante la aplicación de corrientes de bajo amperaje se modula la excitabilidad neuronal. En este trabajo revisaremos primero los documentos más importantes relacionados con tES, para establecer el estado del arte de esta técnica. En esta revisión cubriremos todos los aspectos; desde la instrumentación, los mecanismos de acción y las aplicaciones. Principalmente nos enfocaremos en métodos numéricos para determinar la distribución del campo eléctrico.

A continuación, presentaremos una revisión de los montajes utilizados en las aplicaciones de tES que constan de más apoyo para un efecto clínico: fibromialgia, depresión y adicción, según (Lefaucheur et al. 2017). De este estudio, obtendremos la información requerida para replicar las posiciones, corriente, forma y tipo de electrodos típicamente empleados.

Finalmente, haremos uso de estos montajes para modular la distribución del campo eléctrico inducido en un conjunto de modelos de cabeza computacional. Los modelos de cabeza computacional se crearán utilizando diferentes softwares y recursos de modelado de Neuroelectrics. Para realizar dichos modelos, utilizaremos imágenes de resonancia magnética de sujetos, obtenidas de una base de datos pública, la base de datos IXI (IXI Dataset, 2020). Para cada montaje, se calcularán los valores promedio del campo eléctrico en diferentes regiones de interés en el cerebro, el rango de estos valores y su variación entre los sujetos. Para cada sujeto y cada área cortical objetivo (que depende de la aplicación que se está estudiando), también presentaremos montajes optimizados multicanal alternativos. Cuantificaremos la importancia de la personalización de los montajes y discutiremos las posibles ventajas de usarlos.

En la sección de resultados, se ha cuantificado el rango de valores de campo eléctrico necesarios para inducir una respuesta. Estos valores divergen dependiendo del área estudiada; sin embargo, la variabilidad calculada permanece entre el 15-35% de la magnitud del campo eléctrico inducido para la mayoría los casos. La ubicación de las zonas con más influencia de campo eléctrico también difiere según el área estudiada y las diferencias anatómicas individuales.

Hemos demostrado la efectividad de los montajes multicanal para dar un mejor resultado en términos de focalización. Además, estos montajes tienen la capacidad de obtener un mayor valor para el campo eléctrico con las mismas corrientes de entrada que una distribución bipolar común.

Resum

L'estimulació elèctrica transcranial (tES) és una tècnica què consisteix en la col·locació de diversos elèctrodes al cap i mitjançant l'aplicació de corrents de baix amperatge es modula l'excitabilitat neuronal. En aquest treball revisarem primer els documents més importants relacionats amb tES, per establir l'estat de l'art d'aquesta tècnica. En aquesta revisió cobrirem tots els aspectes; des de la instrumentació, els mecanismes d'acció i les aplicacions. Principalment ens enfocarem en mètodes numèrics per determinar la distribució de camp elèctric.

A continuació, presentarem una revisió dels muntatges utilitzats en les aplicacions de tES que consten de més suport per a un efecte clínic: fibromiàlgia, depressió i addicció, segons (Lefaucheur et al. 2017). D'aquest estudi, obtindrem la informació requerida per replicar les posicions, corrent, forma i tipus d'elèctrodes típicament empleats.

Finalment, farem ús d'aquests muntatges per modular la distribució de camp elèctric induït en un conjunt de models de cap computacional. Els models de cap computacional es crearan utilitzant diferents programaris i recursos de modelatge de Neuroelectrics. Per realitzar aquests models, utilitzarem imatges de ressonància magnètica de subjectes, obtingudes d'una base de dades pública, la base de dades IXI (IXI Dataset, 2020). Per a cada muntatge, es calcularan els valors mitjans de camp elèctric en diferents regions d'interès en el cervell, el rang d'aquests valors i la seva variació entre els subjectes. Per a cada subjecte i cada àrea cortical objectiu (que depèn de l'aplicació que s'està estudiant), també presentarem muntatges optimitzats multicanal alternatius. Quantificarem la importància de la personalització dels muntatges i discutirem els possibles avantatges d'usar-los.

A la secció de resultats, s'ha quantificat el rang de valors de camp elèctric necessaris per induir una resposta. Aquests valors divergeixen depenent de l'àrea estudiada; però, la variabilitat calculada roman entre el 15-35% de la magnitud de el camp elèctric induït per a la majoria dels casos. La ubicació de les zones amb més influència de camp elèctric també difereix segons l'àrea estudiada i les diferències anatòmiques individuals.

Hem demostrat l'efectivitat dels muntatges multicanal per donar un millor resultat en termes de focalització. A més, aquests muntatges tenen la capacitat d'obtenir un major valor per al camp elèctric amb les mateixes corrents d'entrada que una distribució bipolar comú.

Abstract

Transcranial electrical stimulation (tES) is a technique that consists of using electrodes placed on the scalp to deliver weak currents and modulate neuronal excitability. In this work we will first review the most important papers related to tES, in order to establish the state of the art of this technique. In this review we will cover all aspects ranging from instrumentation, mechanisms of action and applications. We will focus especially in numerical methods to determine the E-field distribution.

After this initial review, we will present a review of the montages used in the applications of tES that show more evidence of a clinical effect (fibromyalgia, depression and addiction/craving, according to (Lefaucheur et al. 2017)). From this review we will obtain the information required to replicate the positions, current, shape and type of electrodes typically employed.

We will then model the (E-field) distribution induced in a set of computational head models by these montages. The computational head models will be created using Neuroelectrics' segmentation and modelling pipeline. As an input to this step we will use MRIs of subjects from a public database, the IXI database (IXI Dataset, 2020). For each montage, the average E-field values in different regions of interest in the brain, the range of these values and their variation across subjects will be calculated. For each subject and each target cortical area (which depends on the application being studied), we will also present alternative multichannel optimized montages. We will quantify the importance of personalization of montages and discuss possible advantages of using them.

In the results section, the range of electric field values needed to induce a response has been quantified. Those values diverge depending on the studied area; however, the computed variability remains at 15-35% of the induced electric field magnitude for the majority of the cases. The location of the E-field hotspots diverges also depending on the studied area and the individual anatomical differences.

We have demonstrated the effectiveness of multichannel montages to give a better result in terms of focality. Furthermore, these montages have the ability to obtain bigger values for electric field with the same input currents as a common bipolar distribution.

Acknowledgments

I would like to express my sincere gratitude to my tutor in Neuroelectrics (Ricardo Salvador), his constant effort, with weekly meetings and his dedication is admirable. Without his knowledge and optimism, I would not have finished this article, his implication made this project possible.

I would also like to express my thanks to the whole Neuroelectrics team. It was a pleasure for me to be working with them for months in the curricular practices. Specially I want to mention (Maria Chiara and Carla Sendra) who helped me at different stages of this project. Both are members of the neuro-modelling team in Neuroelectrics, the team I joined.

Glossary

tES (also known as tCS)	Transcranial electrical stimulations (also known as Transcranial current stimulation)
tDCS	Transcranial direct current stimulation
MRI	Magnetic Resonance Image
NE	Neuroelectrics
E-field	Electric field
TMS	Transcranial magnetic stimulation
tPCS	Transcranial pulse current stimulation
tODCS	Transcranial oscillating direct current stimulation.
GVS	Galvanic Vestibular Stimulation.
CSF	Corticospinal Fluid
gui	Graphical user interface
FE	Finite element
WM	White-matter
GM	Gray-matter
FEM	Finite Element Method
lDLPFC	Left dorsolateral prefrontal cortex
lPMC	Left primary motor cortex
TC	Total current injected
MCPE	Maximum current per electrode
TE	Target Electric field
ERNI	Error relative to no intervention
WCC	weighted cross correlation coefficient

Table 1: *Abbreviations used*

Index

RESUMEN 4

RESUM 5

ABSTRACT 6

ACKNOWLEDGMENTS 8

GLOSSARY 9

LIST OF TABLES 13

LIST OF FIGURES 14

1. PREFACE 17

1.1 Origin of the work 17
1.2 Motivation 17
1.3 Skills developed 17

2. INTRODUCTION 18

2.1 Project objectives 18
2.2 Project scope 18

3. STATE OF THE ART 19

3.1 Instrumentation 20
3.2 Safety of tES 23
3.3 Generation of electric field 23
3.4 Spatial distribution 24
3.5 Mechanisms underlying tDCS 26
3.6 Effects of tES in neurons 27
3.7 Variability of the E-field 28
3.8 Electrode montages 29
3.9 Optimization of a multifocal tES 30

4. DISEASES TREATED WITH TDCS 33

4.1 Fibromyalgia 33
4.2 Depression 34
4.3 Addiction/craving 35
4.4 Other diseases 36

5. METHODS ____ 37
5.1 Generation of a mesh ... 37
5.1.1. 'Headreco' steps ... 38
5.1.2. Corrections ... 39
5.1.3. Freesurfer processing ... 39
5.2 Calculations of the lead matrix files ... 40
5.3 Bipolar and customized montages ... 42
5.4 Multichannel montages optimization ... 43
5.5 Target definition ... 44

6. IMPORTANCE OF MANUAL CORRECTIONS ON E-FIELD CALCULATION ____ 45
6.1 Manual Corrections made ... 45
6.2 Optimization results ... 49

7. E-FIELD VARIABILITY ACROSS SUBJECTS ____ 52
7.1 Characteristics and corrections for each subject ... 52
7.2 Montages characteristics ... 54
7.3 Results and discussion ... 56

8. ANALYSIS OF ENVIRONMENTAL IMPACT ____ 69

9. CONCLUSIONS ____ 70

10. ECONOMIC ANALYSIS ____ 71

11. BIBLIOGRAPHY ____ 73

ANNEX A NUMERICAL RESULTS FOR THE MANUAL CORRECTIONS. ____ 77

ANNEX B RESULTS FOR THE TARGET AREA 'LDLPFC' ____ 79
B1. Numerical results ... 79
B2. Graphical results for the average E-field ... 85
B3. Bipolar configuration results (V/m) ... 88

ANNEX C RESULTS FOR THE TARGET AREA 'LPMC' ____ 89
C1. Numerical results ... 89
C2. Graphical results for the average E-field ... 95
C3. Bipolar configuration results (V/m) ... 98

ANNEX D CODE CREATED FOR MESHING INTO COLIN'S SPACE ____ 99

List of tables

Table 1: Abbreviations used *9*

Table 2: Commercial tES systems for clinical and neuroscience research *21*

Table 3: Conductivity values for different tissues *41*

Table 4: Maximum relative error of the average electric field value obtained when comparing Colin with Colin corrected, and Colina with Colina corrected. Several optimizations have been computed for each study case, here we just show the maximum error obtained. (TC: Total current injected; MCPE: Maximum current per electrode; TE: Target Electric field) *51*

Table 5: Characteristics of the subjects studied on the project *52*

Table 6: Descriptions of the corrections made for each subject *53*

Table 7: Different optimization constraints for the multichannel optimization montages. *55*

Table 8:Electric field mean obtained for the 8 electrode montages over the lDLPFC and the lPMC with 0.25V/m demanded E-field. *63*

Table 9 Electric field mean obtained for the 8 electrode montages over the lDLPFC and the lPMC with 0.5V/m demanded E-field. *64*

Table 10: Electric field mean and standard deviation obtained for the bipolar montage over the lDLPFC and the lPMC *65*

Table 11: Economic analysis *71*

List of figures

Figure 1: Subject on a tES session with the instrumentation of NE (A), more details on section 2.1. (B) represents an example of the electric field distribution on the brain when applying tES. 19

Figure 2: Instrumentation needed for a tES session, electrode cables cap and device (shown on the back part, (A) Enobio model, (B) StarStim model) 20

Figure 3: Different types of electrodes used in tES. (A) spongy electrodes, (B) Ag/AgCl pellets, (C) earlobe electrode. 22

Figure 4: Positions of the 10/10 international EEG system 22

Figure 5: Different steps followed, from the MRI acquisition up to the calculation of the E-field (in the last image, the distribution over a concert montage done in this project can be seen, units in (V/m)). 25

Figure 6: Electric field distribution for 2 different subjects with the same electrodes positions and currents used, units in (V/m). 29

Figure 7: multichannel montage optimized with 8 electrodes over the left dorsolateral prefrontal cortex. Restrictions made: 4 mA maximum total injected current, 2 mA maximum current per electrode, 0.25 V/m desired for the case (A), 0.5 V/m desired for (B). Units of the figure in (V/m). 30

Figure 8: World population affected by fibromyalgia and depression 34

Figure 9: Default subject folder structure for the SimNibs pipeline (Source: Maria Chiara, SimNIBS3.x_user manual_vBeta, Neuroelectrics 2020) 40

Figure 10: Different views for the selected areas of the study. In red the lDLPFC and in blue the lPMC. 44

Figure 11: Corrections made on Colin's CSF (A) and Colin's skin mask (B) 46

Figure 12: Final masks segmentations for Colin's subject. Bone mask (A), grey matter (B), ventricles (C), white matter (D), corticospinal fluid (E) and eyes (F)..... 47

Figure 13: Colina's masks segmentation corrected, bone mask with a concavity in the forehead (A), CSF mask with the presence of different bulging areas (B). In (C) it is shown the different views as for the CSF marking the defaults found on these layers. 48

Figure 14: Final masks segmentations for Colina's subject. Bone mask (A), grey matter (B), white matter (C), corticospinal fluid (D), eyes (E), skin (F) and ventricles (G), ... 49

Figure 15: Plots of the surface average electric field values (normal component of the E-field) obtained for Colina, Colina, Colin corrected and Colina corrected, for the different parameters of the optimization. The average values were calculated in the surface. 50

Figure 16: CSF mask correction for IXI 033..... 53

Figure 17: Bone mask correction for IXI 013 53

Figure 18: Skin mask for IXI 050..... 54

Figure 19: (B) 10/10 Electrodes position with the chosen electrodes for the bipolar montages printed. In red the configuration for the lDLPFC (A) and in blue for the lPMC (C). 54

Figure 20: Boxplots representing the electric field distribution on multichannel montages targeting the lPMC (left primary motor cortex). The title of the plots shows the optimization constraints: target E-field, TC and MCPE, respectively..... 57

Figure 21: Electric field distribution over the lPMC on IXI002 with a target -field value of 0.5V/m. (A) and (B) were restricted to 2 mA maximum injected current and 1 mA of maximum current per electrode, with 4 and 8 electrodes used, respectively. (C) and (D) had restrictions of 2 mA/2 mA, with 4 and 8 electrodes used, respectively..... 58

Figure 22: Electric field induced over the lDLPFC on IXI016. (A) was targeted at 0.5 V/m, giving a total injected current (uA): 1354 $\boldsymbol{\mu A}$ *and maximum current any electrode (uA): 1354*

μA. (B) was targeted at 0.25 V/m, giving a total injected current (uA): 677 μA and maximum current any electrode (uA): 677 μA . (units of the scale: V/m)……59

Figure 23: Maximum current injected on the IXI subjects, Colin and Colina over the lDLPFC..60

Figure 24: Boxplots representing the electric field distribution on multichannel montages made over the lDLPFC (left dorsolateral prefrontal cortex). ……61

Figure 25: Boxplots of the ERNI and WCC value for the lDLPFC……62

Figure 26: Boxplots of the ERNI and WCC value for the lPMC……62

Figure 27: Multichannel electrode montage made for IXI045 over the lDLPFC with 0.5V/m demanded electric field, 4mA maximum injected current and 1mA maximum current per electrode. (A) 2 electrode montage, (B) 4 electrode montage, (C) 6 electrode montage and (D) 8 electrode montage. (units of the scale V/m)……63

Figure 28: Barr plots of maximum current per electrode obtained over the lPMC. In both graphs the restrictions for currents were 2mA of maximum injected current and 2mA of maximum current per electrode. On (A) the targeted E-field is 0.25V/m while on (B) is 0.5V/m. ……65

Figure 29: Electric field induced with bipolar montages over the LDLPF and the lPMC……65

Figure 30: Transformation into Colin space for (A) IXI 016 and (B) IXI 002……66

Figure 31 Median values and standard deviation obtained for the different subjects into Colins space over the Left dorsolateral prefrontal cortex. (A) frontal view, (B) top view. (units of the scale: V/m)……67

Figure 32: Median values and standard deviation obtained for the different subjects into Colins space over the Left primary motor context. (A) frontal view (B) back view. (units of the scale: V/m)……68

1. Preface

1.1 Origin of the work

We can find the origin of this work in Barcelona Neuroelectrics S.L.U (NE), this is a high-tech company that offers non-invasive medical devices with the best technology for electrical brain stimulation and monitoring. Transcranial electrical stimulation (tES) has proved to help patients with different neuropsychiatric diseases for who there are no alternative forms of treatment, leading to a minimization of disability and an improvement in the quality of life.

After taking there the extracurricular practices I knew I would like to do my final project in the same company, as I was attracted by the different studies that were taking place at NE and the working environment is very comfortable. So, I got in touch with some of the company's members and they accepted my request.

1.2 Motivation

The electric field (E-field) is the physical agent for the effects of tES on a neuronal level. Many mechanisms are described that explain the interaction of the E-field with neurons, and how potentially this can lead to the reported effects of tES on cortical excitability or other functional measurements of cortical activity. However, to this day, precise quantification of the range of E-field values that are required to achieve an effect is still unreported. This lack of knowledge makes a determination of dose parameters in tES imprecise. The most important dose parameters that can be modified are the position of the electrodes used in the stimulation as well as the input current of each one of those electrodes.

1.3 Skills developed

During this project, some skills using required software will be developed. The main programmes that will be used are: Matlab, Python, as well as some other software tools available in the field of neuroscience and MRI data analysis: Freesurfer (MRI data analysis and visualization), SimNIBS (head model creation and E-field calculation using the finite element method) and MRI visualization software (3D-Slicer, ITK-Snap).

2. Introduction

In this work, a total of 11 subjects have been studied, starting from a magnetic resonance image of their brain. These images have been segmented with the use of existing software's, thus obtaining reconstructions of the different brain parts. The precise computational models generated have been used to quantify the induced electric field over different brain regions with different study protocols.

The main objective of this project is ranging the E-field values required for an effect and quantifying the existent variability between subjects. This information can be used in subsequent studies for *in vivo* tES applications.

2.1 Project objectives

We aim at estimating the E-field in a number of common montages (typical applications of tES). First creating a database of head models covering a wide range of age-groups and second, evaluating the E-field. We also include some personalized multichannel montages using typical current constraints that may be a step-up from these typical bipolar montages.

2.2 Project scope

This project will help us to understand the range of E-field values that are required to generate an effect in specific applications. This is critical because, nowadays, tools with information about E-field values in a range of protocols/head models are still missing. Numerical head models allow for precise prediction of the E-field distribution. This is the only way to do it, as *in vivo* methods are not available to measure the E-field non-invasively. However, these models are time consuming and not everyone may have the needed expertise/data to create them.

3. State of the art

During the last decade, it has been observed that the number of publications related to transcranial stimulation have increased. Transcranial current brain stimulation (tCS, also known as transcranial electrical stimulation, tES) includes three principal subfamilies that apply this non-invasive technique in order to obtain positive results in patients: transcranial direct current stimulation (tDCS) transcranial alternating current stimulation (tACS), and transcranial random noise current stimulation (tRNS).

The basic concept under this methodology remains the same while applying these different techniques, generically, we define tES as a stimulation of the brain by generating electric fields (E-fields) in different areas with the delivery of currents transcranially from the scalp. The currents delivered on the scalp are weak (in this study a maximum total injected current[1] of 4 mA total and 2 mA maximum for each electrode have been applied) and their waveform varies at low frequencies (typically lower than 1 kHz). The result of applying this is a weak electric field in the brain (with a magnitude range of about 0.02-2 V/m), as shown in *Figure 1*. The electrodes in the scalp are connected to an electrical stimulator. This is a current controlled device that can output the different waveforms typically used in tES (See table 2 for a comparison of several commercial electrical stimulators, based on (Pedro C. Miranda et al. 2018)).

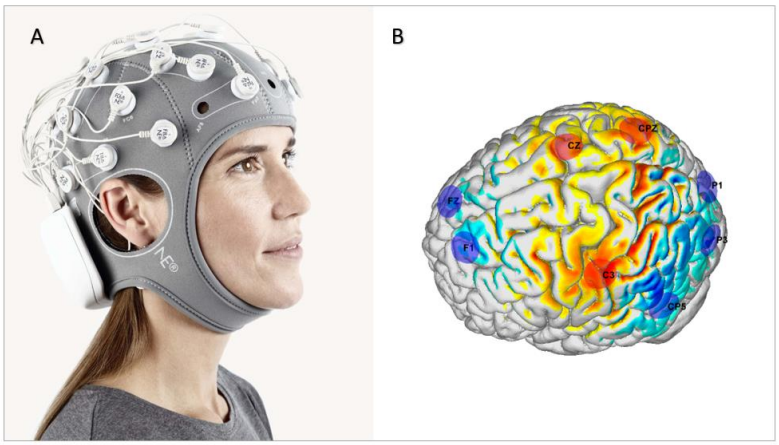

Figure 1: *Subject on a tES session with the instrumentation of NE (A), more details on section 2.1. (B) represents an example of the electric field distribution on the brain when applying tES. (Source A: Neuroelectrics 2020. Neuroelectrics: Reinventing Brain Health. Accessed June 13. https://www.neuroelectrics.com/.)*

[1] Here defined as the sum of all the positive currents in the electrodes (anodes). This value is the same as the absolute value of the sum of all negative currents in the electrodes (cathodes).

Specifically, this study has been focused on the application of tDCS. This technique uses DC currents in order to modulate brain excitability (Nitsche and Paulus 2000). Depending on the desired target area to stimulate, the magnitude and polarity of the currents and positions of the electrodes can change. Several possible beneficial effects of tDCS are still in study, however it has already shown some effectiveness in depression, chronic pain and/or stroke recovery (Lefaucheur et al. 2017). Applying this technique on a patient can cause long term modifications on cortical excitability due to brain plasticity, i.e., dynamic changes in the central nervous system connectivity due to normal external and internal stimuli or brain damage (Ruffini et al. 2018).

3.1 Instrumentation

When carrying out a tDCS session, the instrumentation is mandatory. Neuroelectrics offers a great variety of products to cover the customer specific needs. In this section the different products as well as their function on a tDCS session will be explained.

- Device

  This instrument is the most important part of the kit and different models are designed. Among all the different varieties that we can find, these are mainly divided into two different families. On the one hand, Enobio is a precise device with 8, 20 or 32 channels that allows the user to record and visualize a high-resolution EEG. On the other hand, Startstim is a class of device prepared for wireless multi-channel brain stimulation and recording functions (EEG). Table 2 shows some of the available devices on the market, as well as their basic characteristics (Pedro C. Miranda et al. 2018).

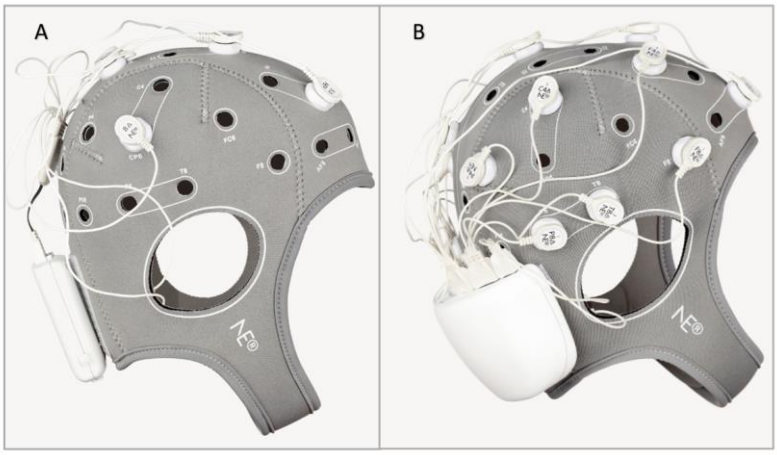

Figure 2: *Instrumentation needed for a tES session, electrode cables cap and device (shown on the back part, (A) Enobio model, (B) StarStim model) (Source A and B: Neuroelectrics 2020. Neuroelectrics: Reinventing Brain Health. Accessed June 13. https://www.neuroelectrics.com/.)*

Model	StarStim R32	MxN HD Transcranial Stimulation	DC-STIMULATOR MC	GTEN 100 Research
Stimulation types	tDCS tACS tRNS tODCS	tDCS tACS tPCS tRNS tODCS	tDCS tACS tRNS GVS	tDCS tACS tPCS tRNS
Stimulation channels	(up to) 32	5–82	16	32, 64, 128, 256
EEG	Yes	Allows integration with third party products	Can be combined with NeuroPrax TMS/tES	Yes
EEG Channels	(up to) 32	None	32,46,128	32, 64, 128, 256
Targeting software	Yes	Yes	No	Yes
Maximum injected current	2 mA per electrode, 4 mA total	2 mA	4 mA	0.2 mA per electrode, 1 mA total
Electrode Impedance Check	Yes	Yes	Yes	Information N/A
MRI-compatible	Yes	Information N/A	Yes (optional)	Information N/A
Manufacturer	Neuroelectrics	Soterix Medical	NeuroConn	EGI

Table 2: *Commercial tES systems for clinical and neuroscience research*

- Electrodes

  As in the previous case, there is more than one type of electrode that can be used for tES. Large spongy electrodes are the most common between the huge variety offered. Basically, this electrode consists of a sponge soaked in saline solution that surrounds a conductive rubber with a metallic pin. These electrodes are usually large, with surface areas between 9 and 35 cm^2.

Another type of electrode are Ag/AgCl pellets of circular area (1 cm radius electrodes in the case of the NGPiStim electrodes commercialized by Neuroelectrics). This electrode can be used for EEG monitoring and/or for transcranial electrical stimulation. As in the previous case, this electrode cannot directly touch the scalp of a patient. A conductive gel is needed in order to operate with this product. The specific characteristics of this type of electrode, for instance the durability, varies depending if we want them for EEG functions, stimulation, or both at the same time.

Finally, the last electrode that will be explained is the ear clip. This electrode design consists of a dual reference connection that is placed in the earlobe, allowing like this to suit EEG, tES and hybrid applications.

Figure 3: *Different types of electrodes used in tES. (A) spongy electrodes, (B) Ag/AgCl pellets, (C) earlobe electrode. (Source A, B and C: Neuroelectrics 2020. Neuroelectrics: Reinventing Brain Health. Accessed June 13. https://www.neuroelectrics.com/.)*

- Caps

  As discussed in section 2.5, different factors can influence the variability between subjects of the electric field. One of those factors is the electrodes position, a 1 cm displacement can alter up to +-20% the results (Opitz et al. 2015). In order to maintain the positions of the electrodes fixed, neoprene headcaps are used. These caps cover a big range of ages and dimensions, basically, the idea consists of a head cover with holes on preestablished electrode positions. For most tES applications these positions consist of those defined by the 10/10 international EEG system, Figure 4 (Jurcak, Tsuzuki, and Dan 2007).

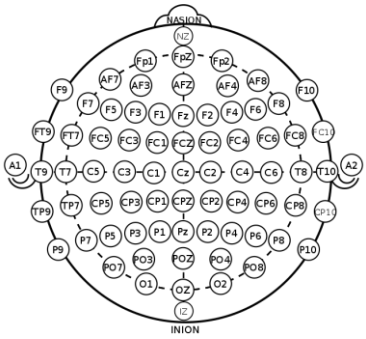

Figure 4: *Positions of the 10/10 international EEG system (Source: International 10-20 System for EEG Wikimedia Commons. 2020. Commons.Wikimedia.Org. Accessed April 25. https://commons.wikimedia.org/wiki/File:International_10-20_system_for_EEG-MCN.svg.)*

- Electrode Cables
  The main function of the cables is the connection between the device and the different electrodes. For this purpose, this type of cables has at one end an elongated connection port to be inserted on the electrical stimulator. The other extreme consists of different cables to be connected with the electrodes. Depending on the application desired, the number of cables will vary. As in the case of the devices, this product can be found with 8,20 or 32 cables.

- Gels and solutions
  For obtaining a good recording of the brain activity or having an accurate stimulation, the conductivity values are a key factor. The use of saline solutions or conductivity gels are mandatory in almost all cases for improving the contact between the electrode and the skin.

3.2 Safety of tES

There is no evidence, that a session of tES can cause adverse serious effects, see (Lefaucheur et al. 2017). No serious adverse events have been reported over 18,000 sessions administered to healthy subjects, neurological and psychiatric patients (Antal et al. 2017). Some adverse events have been reported, including skin burn for bad electrode-skin contact, however the presence of this effects occurs very rarely. A total of 11 subjects on this article reported the presence mania or hypomania time after the tES session, but the low incidence rate makes it difficult to prove the relation.

3.3 Generation of electric field

The electric field distribution in tES can be calculated considering a set of quasi-static approximations, see (Ruffini et al. 2013):

1. Neglecting propagation effects, since the electromagnetic frequency is in the range DC-1 KHz, the wavelength generated is many times larger than the dimensions of the human head. That leads to a no significant variation of phases in the electric field while it goes through the brain.
2. It is assumed that the effect of the magnetic field produced by the currents is negligible
3. Capacitive effects are neglected, considering the tissue as a purely resistive medium. This effect must be taken into account when using currents above 10KHz.As said before, it is considered the brain as a dielectric, so the relationship between the current density $\vec{J}$ $(\text{Ampères per meter squared}, \text{A}/m^2)$ and the applied electric field $\vec{E}$ (in Volts per meter, V/m) is given by the equation 1.

$$\vec{J} = \sigma\vec{E} \quad (1)$$

$$\sigma^* = \sigma + j\omega\varepsilon_0\varepsilon_R \quad (2)$$

In the frequency domain, the complex conductivity equation of the tissue remains as the equation 2. Where σ is the conductivity of the tissue (in Siemens per meter, S/m), ω is the angular frequency (defined as $\omega = 2\pi f$, where f is the frequency of the current waveform in Hz; in units of Radians per second, Rad/s), and ε_0 ($8{,}854 \times 10^{-12}\ F/m$) and ε_R are the vacuum electrical permittivity and relative permittivity of the tissue, respectively (Ruffini et al. 2020).Even though the relative permittivity tends to increase while decreasing the frequency, it is not enough to make us consider the second term in expression (2), since its value still so much lower compared with the electrical conductivity. In tDCS, of course the conductivity is a real number, so no capacitive effects are present.

Regarding the values of the conductivity of tissues, several authors and papers have investigated its variability. As this topic is not fully covered it must be taken with care. The last reports tend to show a constant value of conductivity from 10Hz-10KHz, but considerable variability of values for lower frequencies. One of the causes of this variability at lower frequencies stems from instrumentation difficulties in measuring conductivities in this frequency range (Reato et al. 2019).

Some examples can be found for instance in (Baumann et al. 1997), those reported a constant value of 1.79 S/m for the conductivity of cerebrospinal fluid (CSF) at 37 °C in the range 10 Hz to 10 kHz. An average value of 0.404 S/m was reported for the conductivity of grey matter, that is practically frequency independent in the range 1 Hz to 10 kHz. One of the main problems regarding the different conductivities can be found in the skull, as its value of conductivity is considerably lower in comparison with the surrounding tissues. It is important to notice that conductivities are not always isotropic and homogeneous, for instance white matter presents different values of conductivities depending on the area (heterogeneity), and it is not an anisotropic tissue, i.e., the conductivity along different directions is different. As mentioned by most authors, the skull is also considered anisotropic and non-uniform.

3.4 Spatial distribution

The next question that has to be solved is how the electric field distributes inside the patient's brain.
In steady state, as it is the case, the electric potential (φ) in a conductor obeys Laplace's equation (3) (Plonsey and Heppner 1967). This equation has a unique solution if the boundary conditions applied are the appropriate ones: continuity of normal component of current density and continuity of electrostatic potential. The currents in each electrode can be enforced by imposing that the surface integral of the normal component of the current density in the outer surface of each electrode is equal to the current in the montage protocol.

$$\vec{\nabla} \cdot \vec{J} = -\vec{\nabla}\left(\sigma \vec{\nabla} \varphi\right) = 0 \qquad 3$$

If the electric potential is known, the electric field as well as the current density can be computed. However, for complex head and electrode geometries numerical methods are required to solve (3).

Rush and Driscoll (Rush and Driscoll 1969) obtained a first analytical solution for a head model composed from scalp, skull and brain; however, this result had some limitations, such as the electrode model (point electrodes). This method was improved in (Pedro Cavaleiro Miranda et al. 2013) where an implementation of the spherical head model using the finite element method (FEM) was made. One of the most notorious conclusions that came out of this investigation was that only about 40-60% of the injected current penetrate the brain, and it depends on the inter-electrode distance. The rest of the current fails to penetrate the brain due to a process called current shunting: current goes from anode to cathode following the low impedance route provided by the scalp. More realistic head FE model for tDCS were later developed (Datta et al. 2009). The models are based on MR images which are then segmented into five tissue types: scalp, skull, CSF, grey and white matter. The technique of using structural MRI images to generate realistic volume conductor models continues being the most efficient nowadays.

As it has been indicated in the previous paragraph, FEM is a very important tool to numerical solve Laplace's equation for complex geometries. Methods employing the FEM modelling approach typically employ the following steps (Pedro C. Miranda et al. 2018).

1. Segment head MRIs of the patient and generate 3D surfaces of the head tissues (with electrodes)
2. Discretize the head geometry into small shapes (finite elements, usually tetrahedra, comprising a finite element mesh)
3. Simplify the behaviour of the electrostatic potential inside each FE (linear combination of linear functions)
4. Equation 3 then becomes a linear system of equations that we can invert to obtain the potential ((φ) in each node of the mesh (each vertex of the finite element mesh).

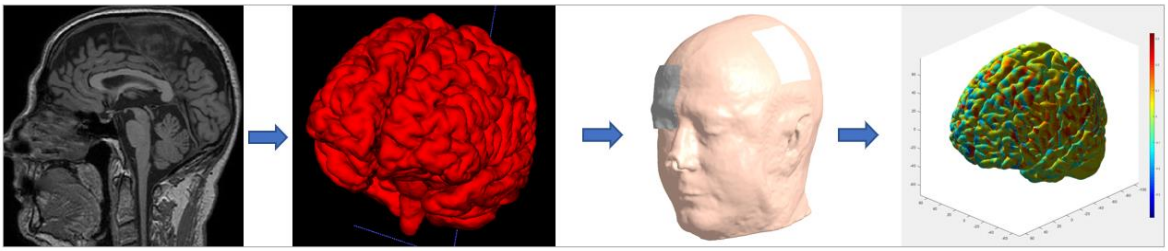

Figure 5: *Different steps followed, from the MRI acquisition up to the calculation of the E-field (in the last image, the distribution over a concert montage done in this project can be seen, units in (V/m)).*

3.5 Mechanisms underlying tDCS

Nowadays it is still unclear what mechanisms underlie the observed effects of tCS. Even though we do not know it exactly it surely depends on the spatial distribution of the electric field (Pedro Cavaleiro Miranda et al. 2013), especially in the WM and GM. There are also other factors that must be taken into account, as the orientation of the E-field, the cell type or the brain state.

The different effects that tCS sessions are thought to produce are:

- Membrane potential variation based on neuron morphology (Radman et al. 2009). This article determines the neural response to subthreshold and suprathreshold uniform electric fields. This *in vitro* study tested the response for an applied uniform E-field on coronal slices of primary motor, extracted from clinical rats. After testing 51 neurons the magnitude of cortical subthreshold somatic polarization increased linearly with increasing electric field steps (5 mV/mm electric field steps). This change was shown to be small: 0.27 mV per V/m of induced E-field. This proved that tES is a subthreshold technique. The relatively low E-field induced in tES affect brain functionality due to an amplification at cell and network levels due to changes in spike timing. Also, tES sessions produces plastic effects, for instance with the prolonged depolarization.
- Changes in synaptic strength mediated by NMDA receptors in a polarity-dependent manner (Lefaucheur and Wendling 2019).
- Cortical excitability changes, as a consequence of the last two statements (Nitsche and Paulus 2000).
- Changes in glial cells (Ruohonen and Karhu 2012)

There is a big importance in computing the direction of the electric field, as it is known that a strong directional component effect exists. Neurons only get affected by the component of the electric field tangential to its direction. Regarding the cortical surface, investigating the perpendicular and tangential components of the E-field is of special interest. Since the pyramidal cells tend to align perpendicular to the surface, while cortical interneurons tend to align themselves parallel to it. The small changes produced in membrane potential are thought to be stronger in pyramidal cells due to its orientation. The fact that pyramidal cells are aligned perpendicular makes them be more stimulated by the normal component of the E-field. This simple model also explain why anodal stimulation leads to predominantly increases in cortical excitability, whereas cathodal stimulation has the opposite effect. These changes are not enough to elicit action potentials in cells. However even small changes can lead to changes in action potential timing that may lead to plastic changes (synaptic plasticity is an example), which may lead to long term changes in brain connectivity.

3.6 Effects of tES in neurons

As mentioned before, the principal neurons that interact with the effects of tES are thought to be pyramidal cells. There are other neurons that are thought to play an important role, such as basket cells or glia cells, however, nowadays there is not enough information to understand the roles that these neurons have in the process.

Physically, what a session of tES makes to neurons is a displacement of intracellular ions, altering in this way the internal charge distribution and modifying the transmembrane potential.

Mathematically this physical effect can be described by using the cable equation (Ruffini et al. 2013). The latter describes the changes in transmembrane potential of a neuron when submitted to an external electric field. In the case of a long straight finite fiber (like pyramidal cells), the equation predicts a polarization of the membrane that is proportional to the following activation function (f in units of Volts, V):

$$f = \lambda \vec{E} * \vec{n} \qquad 4$$

Where n is a vector aligned with the main direction of the neuron and λ is the spatial constant of the neuron's membrane (in mm) which determines how much a localized change in transmembrane potential attenuates with distance from this source. In this study, we will assume that $\vec{n}$ points into the cortical surface; thus an anodal electrode produces predominantly a normal E-field (E_n) that is positive, ie, it leads to an increase in cortical excitability of the soma (on the other hand, under the cathode(s), E_n is predominantly negative, pointing out of the cortical surface, thus leading to a decrease of excitability of cortical neurons). Other E-field components might have other effects in other components of neurons (or neuron populations), but that is not completely understood today.

For model the effect of the E-field some papers generate realistic models of neurons. One of the most recent papers regarding the effects of TMS is (Aberra et al. 2020), in this article a method for computing electric fields on realistic neuronal models is developed. The main conclusion obtained is that TMS activated with lowest intensity intracortical axonal terminations in the superficial gyral crown and lip regions. As for the pyramidal cells, the effects diverge depending on the affected layer. The layer 5 of pyramidal cells reported the lowest thresholds, but layer 2/3 pyramidal cells were activated at almost all intensities. Neural activation reported variations depending on the magnitude, the larger magnitude of electric field applied, the more activation obtained. The field component normal to the cortical surface does not seems to have a direct effect on neural activation.

3.7 Variability of the E-field

As said before the electric field induced in the brain is the main physical agent of tES. However, with the same electrode position and the same currents injected some variability is found in the induced electric field (Laakso et al. 2015), see Figure 6. One of the potential sources of variation in the induced electric field are the individual's anatomical difference, these variations induce some variability in the inputs and outputs of tES protocols.

The article (Laakso et al. 2016) covers the topic of inter subject variability regarding different montages. Especially interesting the generation of 62 fixed bipolar montages constructed from T1 and T2 weighted MRI images and uses the finite-element method in order estimate the E-field. From this article two important conclusions can be drawn. On the one hand the variability of the electric field depends on the target region of the stimulation. As shown in the mentioned paper, there are regions that tend to have less variable values of electric field across the different subjects tested. Meanwhile there are other regions that show a big variability on the E-fields obtained: one example being the frontal cortex. Depending on the individual the strength and direction of the E-field is found to be different. This suggests that in specific zones, in order to obtain the desired E-field distribution for a specific patient, there is the need of quantifying previously the different parameters with computational models and plan the montage based on the results obtained.

Another source of variability are small changes in electrode positions. In (Opitz et al. 2015) the differences obtained by displacing the electrodes over different positions are tested. In this case the conclusion was that a displacement of 1 cm could alter the results +-20% of its original value. That shows that, in order to make a study over different subjects, the conditions used must be the same in order not to alter the results.

During a session of tES a complex electric field distribution is induced on the brain of the participant and, as it has been discussed, this electric field is very variable from subject to subject. This variation is explained up to a 50% due to some physiological aspects (Opitz et al. 2015) that must be taken into account. The thickness of the CSF and the cortical bone, the gyral depth and the distance between electrodes are the most important factors. The inhomogeneity of the electric field distribution between subjects makes the results obtained from a tES session highly variable. One of the key factors on this variation regards on the thickness and composition of the skull and the CSF. Since the skull has the lower value of conductivity it determines the amount of current that passes into the brain. It is shown that the thinner skull regions lead to a higher electric field value. To this effect is also added the larger proportion of conducting spongy bone in the thicker regions, which enhances the radial conductivity. The models that do not have into account the presence of spongy bone in skull shows have changes up to 20%.

Another factor that has a big effect on E-field distribution is the cortical curvature: it has been shown (Pedro Cavaleiro Miranda et al. 2013) that at the bottom of cortical sulci, there are hot-spots of E-field's normal component, due to the funnelling effect of the CSF. Once the current spread, it results in lower current densities and hence electric field strengths in regions further down in the sulci. Peaks of the normal electric field component have been reported to occur in deeper sulcal regions.

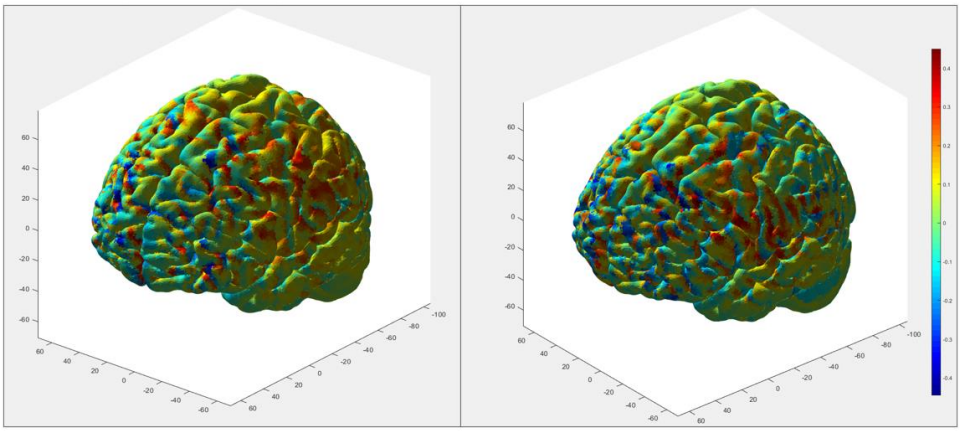

Figure 6: *Electric field distribution for 2 different subjects with the same electrodes positions and currents used, units in (V/m).*

This study also showed that smaller electrodes result in a better focality for the tangential component of the electric field. However, the normal component does not seem to be influenced by the electrode dimensions (Pedro Cavaleiro Miranda et al. 2013).

3.8 Electrode montages

Typically, the electrode montage used for tDCS consisted in two large saline soaked sponges with areas of 35 cm^2. The anode, the one with the positive current is placed over the area that is targeted for stimulation (in the case of anodal stimulation), and the other electrode (cathode) is placed over a faraway region or a region targeted for inhibition.

In order to be more precise and increase the focality of the induced E-field, multichannel electrode montages with smaller electrodes can be used (Datta et al. 2009). These montages place different electrodes over the head of the patient, each one with a specified positive (anode) or negative (cathode) current. The anodes are placed over the area to be excited and the negative current electrodes (cathodes) are placed on strategic positions in order to minimize the unwanted electric field or in order to inhibit those regions. In these multichannel montages there are some options to increase the E-field under a specific target area: either by increasing the total injected current, or by spreading the electrodes with negative current away from the area of interest. These approaches will result in a loss of focality, i.e., the zone affected by this electric field will be larger, as can be observed in Figure 7.

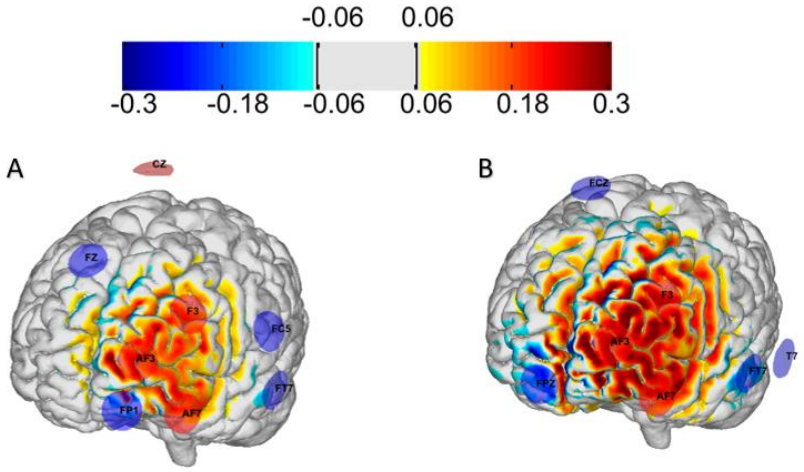

Figure 7: *multichannel montage optimized with 8 electrodes over the left dorsolateral prefrontal cortex. Restrictions made: 4 mA maximum total injected current, 2 mA maximum current per electrode, 0.25 V/m desired for the case (A), 0.5 V/m desired for (B). Units of the figure in (V/m).*

It is very important to choose the best parameters for the electrodes in the experimental montages. There are three principal factors that define an electrode: their dimensions and geometry; the materials that compose each electrode and their position in the scalp.

In order to have the less variability possible between subjects, electrodes are usually placed in the EEG standard positions of the 10-10 (or 10-20) system. Also, smaller electrodes offer more degrees of freedom in achieving a desired target E-field.

Multichannel montages are more versatile and they have the potential to achieve a more focal E-field distribution than bipolar montages with big electrodes. However, it is not always clear how to best position these electrodes and which currents to use. This can be achieved by a family of techniques called montage optimization algorithms.

3.9 Optimization of a multifocal tES

As it has been discussed in previous sections, it exists a huge variability of this E-field distribution across subjects. In order to find the best combination of electrodes and currents for each patient that better approximate a desired electric field distribution map, montage optimization algorithms have been developed. Several of these methods have been published, but we will focus on the one that was developed by Neuroelectrics.

The first thing that will be required by the optimization algorithm is a target map indicating the brain region that we want to stimulate with a target E-field value. The map is usually defined in the cortical

surface (triangulated surface of the brain, obtained from the head model). For this project, it will target the normal component of the E-field, because that is the component that explains better the effects of tDCS at the level of pyramidal cells. These target maps are usually defined in template reference space (like the MNI space) and then mapped to the anatomical space of the subject's brain (a RAS space: x Left to Right; y Posterior to Anterior; z Inferior to Superior) by means of an affine linear transformation.

Another condition that we need to constrain is the maximum total injected current (maximum of 4.0 mA in the StarStim stimulator commercialized by Neuroelectrics) and the maximum current per channel (2.0 mA in StarStim). The last condition we need to input is the relative importance for each region as well as the target electric field value. In the case of the algorithm we will be describing here (Stimweaver, (Ruffini et al. 2014)), the relative importance is specified by weights assigned to each node of the mesh (integers ranging from 2-10). In most optimizations as the maximum weight (10) is specified in the areas of the target map that we want to stimulate and for the remaining areas the minimum weight (2) is specified. Regarding the target E-field value, Stimweaver optimizes for the normal component of the E-field (E_n), since this component is the one that better predicts the coupling of the E-field with the pyramidal cells: positive E_n values (E_n directed into the cortical surface) lead to increases in cortical excitability, whereas negative E_n values have the opposite effects. Regarding the actual values, a value of $\pm$0.25 V/m is chosen for most optimizations (Ruffini et al. 2014), however this value is higher in some studies.

In order to approximate a solution with a limited number of electrodes we will follow the method presented in (Ruffini et al. 2014). It can be done using the previously computed E-field distribution files. These files are the E-field distribution in the cortical surface for the N-1 bipolar electrode montages (N is the number of available electrodes in the scalp) with one common cathode (Cz, -1 mA). These E-field distribution files are also called lead-field matrices in some references (a lead is the set of two electrodes in each montage: anode and Cz). These files are obtained for a computational head model of each subject, so they are subject specific. In the Stimweaver algorithm, the electrodes were represented as cylindrical gel disks with 1.0 cm of radius and a height of 2.5mm (NGPiStim electrodes). The E_n-field can then compute as a combination of the different lead matrix files (Ruffini et al. 2014) (principle of superposition):

$$[E_1(x) \dots E_{N-1}(x)] * I = E(x) \qquad 5$$

Where I is a column vector with the currents in each electrode of the montage and x is each node in the cortical surface triangulated mesh.

This calculation requires memory intensive calculations, as the meshes that have been created have a big number of nodes in each segmented section. The WM mesh, for instance, has about 88.000 nodes for each subject.

The objective function in the optimization process, is the ERNI (Error relative to no intervention, in units of V^2/m^2) defined as the least squares error at each mesh point, comparing it with a case of no intervention, equations 6 and 7.

$$ERNI(\mathrm{x};\mathrm{I}) = \frac{\left(\mathrm{y_w(x)} - \mathrm{E_w(x)}\right)^2 - \left(\mathrm{y_\omega(x)}\right)^2}{(1\ /\ \mathrm{N_x})\Sigma_\mathrm{x}\mathrm{w(x)}^2} \quad 6$$

$$\mathrm{y_w(x)} = E_0(x)w \quad 7$$

The new variables that appear in this equation are: $\mathrm{N_x}$, the number of mesh points; $E_w(x)$, the normal component of the electric field induced by the montage being tested in node x multiplied by the weight in that node ($w(x)$) and $y_w(x)$, the normal component of the target electric field in node x multiplied by the weight in that node.

The sum of ERNI over all mesh points provides us with a measurement of how close our solution is with respect to a case of no intervention, in other words, a case where all the currents are set to 0. That leads to an increase in the negativity of the ERNI value at each iteration (notice that the best possible ERNI is always negative, since in this case the first term in the numerator is null).

Another value that is extracted from the montages in order to ensure the viability of the results is the WCC (weighted cross correlation coefficient). The result from that equation is a number between -1 and 1:

$$WCC = \frac{\Sigma_x y_w(x) E_w(x)}{\sqrt{\Sigma_x\left(y_w(x)\right)^2 \Sigma_x\left(E_w(x)\right)^2}} \quad 8$$

Minimization of equation 8 may result in impractical montages with many channels involved. In order to limit the number of electrodes in the solution, a genetic algorithm is employed. This is an evolutionary iterative minimization algorithm where populations are defined based on DNA strands (electrodes active in each montage) with a specific number of active sites (the max number of electrodes we desire in the montage). These strands are then combined during several iterations until the value of ERNI remains stable (Ruffini et al. 2014).

4. Diseases treated with tDCS

In this section, we will review the different uses that tES has had in the recent decades. Because tDCS is more established and its mechanisms are better understood, we will focus on this modality of tES. This information is extracted from (Lefaucheur et al. 2017), a manuscript published in 2017 were a group of European experts was commissioned by the European Chapter of the International Federation of Clinical Neurophysiology to review the state of the art of the therapeutic use of tDCS. The methodology used in this article consists in first, search in PubMed with the key words relating the topic and collect the different papers that appears. For instance, a search could be tDCS combined with Tinnitus. Then this paper is classified depending on different criteria and an analysis is what proceeds. A summary of those illness that reported beneficial effects can be found here, focusing on the different montages as well as the effectiveness they had.

However, before starting, a few concepts must be clarified. First of all, the class of the studies; class I studies: those with more than 25 patients involved, the conditions should be defined with a clear criterion. All the data used has to be reported and a placebo control should be included, randomized factors have to be also taken into account. Class II studies includes a smaller number of patients, between 10 and 25 and can avoid some of the characteristics presented in the Class I studies. Class III studies have a number of patients around 10 but a clear luck in the resources used, that limit the results and the conclusions obtained. Finally, the Class IV studies are the uncontrolled studies.

The second concept to be clarified is the 'level', defined as the efficacy that has a specific montage to respond the way it is considered. Level A evidence requires at least two class I studies or one class I study and two class II that proof its efficiency. Level B requires one Class I study and less that two Class II studies, and finally level C requires one convincing Class II study and at least two class III studies.

4.1 Fibromyalgia

Fibromyalgia is characterized by generalized musculoskeletal pain and painful pressure sensation at specific points. The same montage as for chronic neuropathic pain is applied in this case, placing the anode over the primary motor cortex (M1) and the cathode in the supraorbital region. As for intensities, the values used are 1 or 2mA. Multiple sessions were applied in all cases, having a duration no longer that 30 minutes, otherwise it can harm the patient's integrity.

As for treating pain in the lower limbs, this montage seems to be efficient in reducing the pain score. In this case all the studies shown to have benefits for the patients, with a mean pain reduction of 35%. The level of recommendation given to this montage is a level B of efficiency.

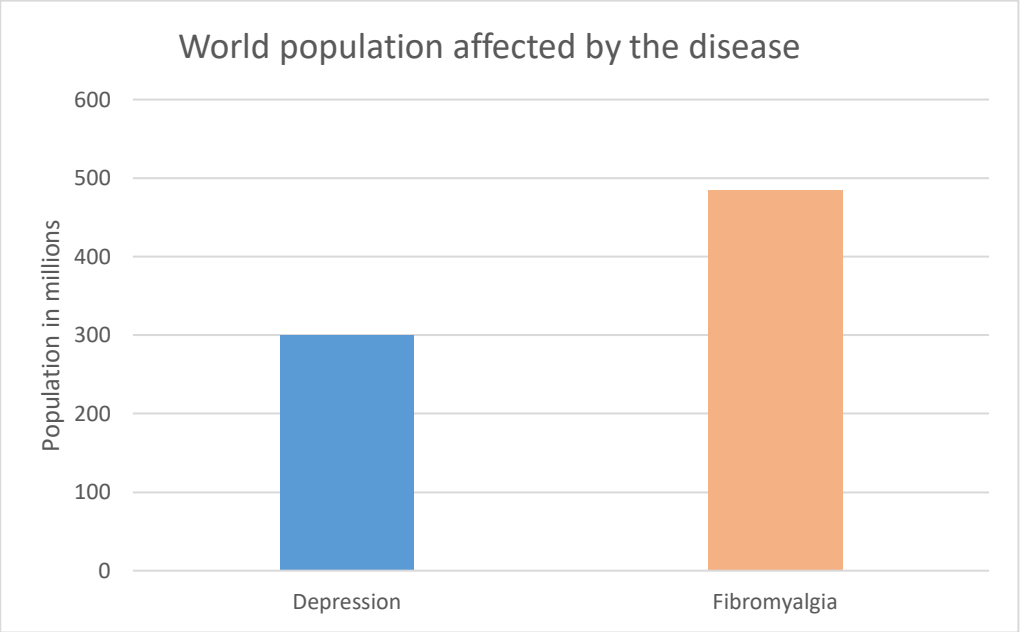

Figure 8: *World population affected by fibromyalgia and depression (Source: World Health Statistics 2020 Visual Summary". 2020. Who.Int. Accessed June 23. https://www.who.int/data/gho/whs-2020-visual-summary.)*

4.2 Depression

Depression is a psychiatric and psychological diagnosis that describes a mood disorder, characterized by feelings of despondency, unhappiness and guilt, in addition to causing a total or partial inability of everyday life.

Regarding depression there is a total of four class II articles and one class I. In all cases the montage used was as follows, the anode was placed over the left dorsolateral prefrontal cortex and the cathode was placed over the right orbitofrontal region. The sessions were standardized as: 2mA delivered in multiple sessions over several weeks with a maxim duration of 30 minutes.

The results in this case were different depending on the subject who took the treatment. On the one hand, those subjects with no drug-resistant showed an improvement in neurophysiological state, as well as with working memory tests, therefore, a level B of recommendation due to possible efficacy is obtained.

On the other hand, a level of recommendation B of possible inefficacy is also obtained in those patients with drug-resistant and major depressive episodes. Two independent studies proved the absence of results in patients with drug resistance.

Another configuration of electrodes was also tried in order to treat depression, in this case it can be found a total of three articles, one class I, one class II and one class III. In this experiment the anode was placed over the left dorsolateral prefrontal cortex while the cathode was over the right dorsolateral prefrontal cortex. The intensities and durations applied were similar to the conditions used when the cathode was placed over the right orbitofrontal region. The results obtained from that configuration where: a mood improvement after the tDCS session, having the older patients the better performance in cognitive tasks. However, some articles failed to demonstrate any clinically relevant effect of this active treatment, so no recommendation can be made for this configuration.

4.3 Addiction/craving

The addiction theme is treated by splitting it out in three different subtopics (alcohol, crack and smoking). However, as the montages used in all cases and the conclusions obtained are similar it will be here summarized as just one.

The montage consists in placing the anode over the right dorsolateral prefrontal cortex and the cathode over the left dorsolateral prefrontal cortex. In all cases the intensity delivered was 2mA with a maximum time of 30m. interesting to note that this montage is opposed to the one proposed in the treatment of depression.

In the case of alcohol, it can be seen an overall improvement. It exists a class II article that reported improvement in the perception of life after a session of tDCS. No difference was reported in frontal function nor in the mental status or anxiety. The number of subjects that at 6 months still abstinent was quantified as for alcohol, and the results prove the efficacy (8/16 vs/ 2/17). As for Crack addiction, a class II article reported an improvement in the craving scores, anxiety levels, and overall performance. Finally, for smoking a reduction in the number of cigarettes smoked after the tDCS sessions is appreciable in just one week.

Despite it is still early to affirm that these positive effects are valid for all people and can last over time, the recommendation level obtained in this case is B, as this method seems to be efficient for addiction/craving.

4.4 Other diseases

Other diseases have been treated with tES with positive results, as chronic pain, showing a reduction of the pain between 14 and 58%, with more benefits and a higher reduction in those studies that applied a greater number of sessions. Parkinson has also proved to produce beneficial effect on gait and motor performance with the application of multiple tDCS sessions over the primary motor cortex.

Other reports show to have no benefits while applying a tES sessions, that is the case of Tinnitus, that reported no results while placing the anode over the left temporo-parietal cortex.

In conclusion, different diseases have been treated with tDCS, however, only some of them have the validation enough to prove beneficial effects on patients (Fibromiàlgia, depression and addiction/craving).

5. Methods

In this section we will go through the process required to obtain a processable finite element mesh of a head from a structural MRI. It is important to guide the reader through which the different software that are needed and how they work.

In this work I have used already existing scripts (created by Neuroelectrics) in different programming languages and different software to implement each step in this study. All manual segmentations were performed by me, as well as all the data analysis. This includes all the head model creations for each of subjects in this study. I also did small changes in the programming scripts, whenever required, to specifically adapt them to the objectives as well as creating some short new scripts when needed.

5.1 Generation of a mesh

One of the most important software used during this project is SimNIBS (Simnibs, 2020). SimNIBS is a free software package that runs in MATLAB and Python. It allows the user to model non-invasive brain stimulation techniques including both TMS (transcranial magnetic stimulation) and tES (transcranial electric stimulation). SimNIBS allows us to generate hight quality head model meshes, set up and run the preferred stimulation and visualise the results obtained.

As a minimum input to SimNIBS a T1 weighted MRI is typically needed, however, before calling the reconstruction function that will generate the different segmentations, a few added packages are required.

On one hand, Iso2mesh which is a free Matlab/octave-based that will be used to visualize distributions of E-field components on surface meshes. On the other hand, NIFTI _toolbox, that is needed in order to handle the nifti files (a format to store MRIs, (Nifti, 2020)) that will be created in the process.

Once it is all installed, the next step is calling the function 'headreco' from a terminal. This function will reconstruct a tetrahedral head mesh from at least a T1 weighted structural MRI images. For achieving a more reliable skull and CSF segmentation, a T2-weighted MRI is needed. This function takes from 2-5 hours to complete the whole process.

The reconstruction steps followed after applying the function 'headreco' are as follows. It starts with a segmentation of the different masks (air, bone, grey matter, white matter, ventricles, corticospinal fluid, eyes and skin), followed by a clean-up of the tissue maps, a surface mashing and finally a volume

meshing. In order to do the segmentation, the toolboxes used are SPM12 and CAT12 (Matlab toolboxes).

The output obtained from the 'headreco' function is a folder called m2m, containing the segmentation results files. The inside structure of this folder is as follows:

- A msh file, which is the FEM head model used for the stimulations, this is in the RAS space of the original T1 used.
- A folder containing the 10-10 electrode position for the subject.
- A folder with the different mask preparations generated. In case those masks needed corrections, it can be used and added software in order to manually correct it
- A log file with output from the headreco run.
- Two different T1 files, being one an exact copy from the original T1 and the other in the same space as the mesh nodes, and as we didn't change the space from the nodes it means that both are the same.

5.1.1. **'Headreco' steps**

As said before, 'headreco' allows us to reconstruct a tetrahedral mesh from a T1 and/or T2 MRI images. This process can be divided in 5 different steps.

1. Preparevol: This step runs in SPM12 in order to co-register the T2 to the T1, generate the transforms to the MNI space and segment all tissues.
2. Preparecat: This step runs in CAT12, a computational anatomy toolbox similar to Freesurfer. It generates the different files related to the green matter as well as the white matter.
3. Cleanvols: In this step the binarized masks previously created in the Preparevol and the Preparecat are cleaned
4. Surfacemesh: In this step the .stl files are generated, those are built up in an inner-to-outer order. Inside the Surfacemesh process it can also be found a series of steps that apply to all masks except GM and WM
    a. decouple its voxel mask from the next-inner voxel mask
    b. build a surface from the updated voxel mask
    c. decouple surface from next-inner surface
    d. update its voxel mask using the decoupled surface.
5. Volumemesh: In this step it is taken the .stl files in order to mesh them with the gmsh, the output from this step is the volume mesh file.

5.1.2. **Corrections**

Some of the masks generated from the 'headreco' function need to be fixed, as some defects in the image voxels or some errors in the process may generate distortions in the reconstruction. These results from misclassifications of the voxels that occur during image segmentation. Those errors can lead to big errors in the calculus of intensities. In order to quantify the errors produced by not manually correcting the masks we performed a study with MRI datasets from two subjects.

Not all masks tend to have the errors mentioned. These errors are found more often on CSF masks. After each segmentation, all the masks were checked one by one (with special attention being given to the CSF) in order to identify and correct regions with segmentation problems. This will be done using the software ITK-Snap, a free software where the T1 overlapped with the segmentation mask can be visualized. The mask is represented by red layer over the images of the MRI. Thanks to the tools provided by ITK-Snap, regions of the different tissues' masks can be manually added or deleted. This is a time-consuming process that needs to be done layer by layer. After overwriting the masks with the corrections done, we have to rerun the 'headreco' function but specifying only for surface and volume, in other words, it is only necessary to rerun the steps 4 and 5.

After this last step a processable finite element mesh will be created. These steps work for minor corrections, not for extensive lesions of the tissues.

5.1.3. **Freesurfer processing**

Different systems of coordinates are defined for the MRI images and to understand the differences and similarities between them some concepts must be clarified. A system of coordinates is defined by: firstly, the origin of coordinates, secondly, the directions in which the axis is pointing and finally, if the MRI is scaled to the individuals head.

The first concept we will describe here is of RAS anatomical space: i.e. a space where the shape and dimensions of the subject head are only re-oriented in such a way that the x-axis points to the right ear (left to right direction), the y-axis to and front of the head (posterior-anterior direction) and the z-axis to the top of the head (inferior-superior direction). All head models are originally in this space, since it preserves the size and shape of the subject's head.

In order to define standard positions in a patient's brain and to make it easy to compare data across multiple subjects, standard template spaces have been defined. In this project, the Montreal Neurological Institute (MNI) space has been used to define such a common template space. After transformation to an MNI space, the patient's brain remains in a RAS orientation, with the origin of the

coordinate system set to the anterior commissure. In this transformation, the patient's brain is scaled in order to match it to an averaged template (Chau and McIntosh 2005). This can be done with a linear affine transformation and Freesurfer can be used to obtain such a transformation. This affine transformation is defined by a 3x3 matrix ($\boldsymbol{A}$) (rotation, scaling and shear of the brain) and a translation ($\boldsymbol{p}$, 3x1 column vector). The coordinates of each node ($\boldsymbol{r_{RAS}}$) of the original mesh of the patient's brain in anatomical space can be converted to MNI space using this transformation:

$$\boldsymbol{r_{MNI}} = A\boldsymbol{r_{RAS}} + \boldsymbol{p} \qquad 9$$

5.2 Calculations of the lead matrix files

Before continuing with the process, there is the need of generating a structured folder where all the files from the subject will be contained. From now on, we will assume this default structure shown in Figure 9.

Figure 9: *Default subject folder structure for the SimNibs pipeline (Source: Maria Chiara, SimNIBS3.x_user manual_vBeta, Neuroelectrics 2020)*

As can be seen, there is a file named tailarach.auto.xfm, located in the transforms folder. This is the only file that must be copied previously from the generation of the lead matrix files. The functionality of this file is to transform the head geometry into the MNI space. In order words, the file contains the parameters of the affine transformation required to convert from a template MNI space to anatomical space.

In order to obtain this file, it is needed to have Freesurfer installed, an open source software suite for processing and analysing brain MRI images. This software is not still adapted to Windows, so, in order to use it there are different paths that can be taken, as installing a virtual machine to run Linux within a Windows environment.

If the m2m folder as well has the tailarach.auto.xfm file ready on its correct place, you can proceed to run the lead matrix calculation script, that will run in Matlab. The output from this script are the 75 text files with the different E-field components in each node of the mesh induced by the base bipolar montages (see section 2.7).

Fundamentally, when running the lead-field matrix calculation script, we will assume the electrodes are in the 75 positions of the 10-10 system. In this head models we added PiStim electrodes. The script ran 3 main steps, comparing these electrodes with Cz, the common cathode. Each of the 75 lead-field matrix files results from the calculation of the E-field of a bipolar montage involving the two PiStim electrodes placed on the scalp of the head model generated with the current set to 1 mA in each case. Runs the gmsh solver in order to calculate the electric field of the bipolar montage (this bipolar montage consists in considering each of the electrodes presents in the list compared with Cz). This step is done by calling SimNibs, and as an output we have data for conductivity, voltage, electric field vector and current density vector. Some of the parameters as the geometry of the electrodes can be changed on the script for concrete situations. Those parameters are set by default as 1cm radius, 3mm height for the gel, 2mm height for the electrode.

All the tissues present in the head model were represented as homogeneous and isotropic with conductivity values adequate to the low-frequency range. See Table 3 for a list of conductivity values (Knotkova et al. 2019).

Tissue	Conductivity value (S/m)
White matter	0.15
Grey matter	0.4
Skull	0.008
Scalp	0.33
Corticospinal fluid	1.79
Eye balls	0.33

Table 3: *Conductivity values for different tissues*

As mentioned before, the first step that runs performs a calculation of the E-field and current density for each bipolar montage in a loop. It uses a first order FEM solver (GetDP) to calculate the electric potential in each mesh node, then uses built-in post-processing functions to calculate E-fields and current density in each mesh tetrahedra and triangle.

Since the brain geometry does not change, at the first iteration the WM and GM geometry are extracted and saved in two different files:

- Nodes_struct.mat, a structure with nodes and faces WM and GM and their division in hemispheres, in RAS space
- Nodes_struct_mni_uns.mat and Head_geom_RAS.mat, two identical structures with the nodes and faces of WM and GM but in MNI space. That is done thanks to the tailarach.auto.xfm

On each iteration of the process normal and tangential E-fields are derived out of the calculated current density vector (J) and E-field vector (E), equation 10.

$$nE = \pm \frac{Jx * nx + Jy * ny + Jz * nz}{\sigma_{\frac{GM}{WM}}} \quad 10$$

The faces that combined generate our mesh are triangular faces. The different parameters obtain from this process are referred to the nodes of this triangles, so SimNibs find the triangles common to each node, and we attribute to that node the weighted average of the variable of interested multiplied by the area of those triangles, equations 11 and 12

$$x_i = \frac{\sum_j x_j \ Area_j}{\sum_j Area_j} = \frac{\sum_j x_j \cdot \frac{1}{2} \left\| \overrightarrow{A_J B_J} \cdot \overrightarrow{A_J C_J} \right\|}{\sum_j \frac{1}{2} \left\| \overrightarrow{A_J B_J} \cdot \overrightarrow{A_J C_J} \right\|} \quad 11$$

$$x_i = \frac{\sum_j x_j \ Volume_j}{\sum_j Volume_j} = \frac{\sum_j x_j \cdot \frac{1}{6} \left\| \left(\overrightarrow{A_J B_J} \times \overrightarrow{A_J C_J}\right) \cdot \overrightarrow{A_J D_J} \right\|}{\sum_j \frac{1}{6} \left\| \left(\overrightarrow{A_J B_J} \times \overrightarrow{A_J C_J}\right) \cdot \overrightarrow{A_J D_J} \right\|} \quad 12$$

Finally, it exports the resulting data as a text file.

5.3 Bipolar and customized montages

We will also compare these multichannel optimized montages with bipolar montages that uses big sponge electrodes typically used in many of the tDCS applications we mentioned before.

The E-field distribution in each montage will also be calculated using SimNibs. To evaluate this part, three different scripts developed by Neuroelectrics will be applied. As a remainder, both bipolar and customized multichannel montages need as an input the default subject structure folder and the lead-field matrix files calculated previously.

The first script that is run is called *'setup_tCDS_sponge.m'*. Here the different parameters of the montage are specified. The first condition that you have to define is the number of electrodes that you

are adding [2,3…] and the position of this electrode [C3, Fp2…]. Then it is required to set-up the electrode definition, here there are two possibilities: it can be plane, so it is defined in 2D, or conf, that defines the electrode vertices directly in the head mesh. Following the conditions, the next point that has to be determined is the shape of our electrode, that can be either rectangular, ellipse or customized shape. Finally, the last parts that have to be taken into account are the dimensions of our electrode: the longitude and the amplitude as well as the thickness of the different layers that it can have.

As an output from the previous script a document with the definition of the parameters set before will be created. By running the script *'customized montage.m'*, the previous conditions will be applied on a selected subject. That will generate a mesh file located in the pipeline folder of the subject. All variables are calculated in the elements and faces of the mesh, except the voltage, which is calculated in the nodes.

The third step consists in running *'standalone_export_results_from_Simnibs.m'***,** in order to export the results automatically. This script needs as an input two different options: the surface where we will export the results from ('GM' or 'WM'); the the data extracted: 'nE' (normal component of the E-field) ,'tE' (magnitude of the tangential component of the E-field),'V' (electrostatic potential),'normE' (magnitude of E),'tEx','tEy','tEz' (cartesian components of the tangential E-field vector).

5.4 Multichannel montages optimization

In this study, the aim is to quantify the variations of the electric field on a group of subjects. In order to do that, a bipolar montage will first be calculated for each subject, as presented in the previous section. With the results obtained it will be possible to discuss the variations among different population with the same conditions of stimulation.

We will then perform subject specific montage optimizations to determine the optimal montage parameters to stimulate the same areas that are thought to be modulated by the bipolar montages: the left dorsolateral prefrontal cortex and the left premotor cortex.

As explained in section 2.7, the optimization algorithm (based on the Stimweaver algorithm, explained before) will calculate the best solution possible maintaining certain constraints on the currents, max number of electrodes and target E-field value. These optimizations ran in Python (version 3.7), and with the max number of electrodes that are demanded during the project it took about 4 hours to finish every case.

5.5 Target definition

An important aspect of the optimization algorithm is the target definition. In this algorithm, the target areas are defined on the surface of the GM triangulated surface. Since different subjects are used in this study, we defined standard target areas in MNI coordinates (a template head in MNI space) and then mapped them individually to each of the subject's mesh using the affine linear transformation defined before. Target definition in this project was done using the Neuroelectric's online target editor tool (Stimtargeter, 2020), that allows for a specification of the desired weight and target E-field value in the template subject's brain surface. This tool includes also target definition based on parcellations of the cortical surface (standard divisions of the cortical surface). In this project we used a parcellation based on cytoarchitecture: Brodmann areas.

Two stimulation areas have been selected to be studied, Figure 10. The left dorsolateral prefrontal cortex (lDLPFC) is printed in red, while the left primary motor cortex (lPMC) can be seen in blue.

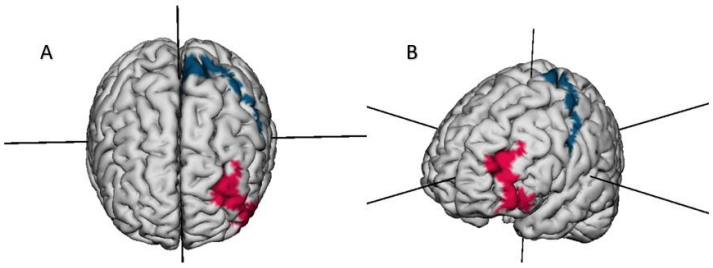

Figure 10: *Different views for the selected areas of the study. In red the lDLPFC and in blue the lPMC. (Source: Stimtargeter. 2020. Neuroelectrics: Reinventing Brain Health. Accessed June 23. https://www.neuroelectrics.com/solutions/target-editor/.)*

The lDLPFC mask was selected by choosing Brodmann area 46 and the lPMC by choosing Brodmann area 4. Note that the brain geometry shown in Figure 10 does not represent any of the models studied in this project. It represents, instead, the MNI template. The areas defined in this template were then mapped to each subject's brain surface using the inverse of the affine transformation that transforms from RAS to MNI coordinates.

The choice of these stimulation areas is determined by the degree of efficacy shown in past studies. As explained in section 2.8, different diseases have been treated by tDCS, most of the studies are not conclusive enough to show a degree of validation or disapproval against a particular montage. However, there are certain cases that show strong evidence of positive results. For instance, fibromyalgia treated with anodal tDCS on the lPMC, obtained a degree of recognition B of efficacy. Another example is depression; showing a decrease in negative symptoms on those patients who had not taken drugs, by applying multiple sessions of anodal tDCS on the lDLPFC (Lefaucheur et al. 2017).

6. Importance of manual corrections on E-field calculation

The software used for calculating the E-field induced by different multichannel montages, as said before, is a script from Python. This software is applied to the mesh file with the different masks and segmentations associated. However, how much do the segmentation errors that can happen during the *headreco* reconstruction influence the E-field calculations?

In order to answer that question, it was decided to do a comparison with two subjects. For each subject, two head models were created: one with manually corrected masks and another one with the masks as they came out from segmentation. We used two MRIs for this study, one from a male subject ("Colin") and another one from a female subject ("Colina").

Both segmentations were made with SimNibs, following the approach described before. Each T1 weighted MRI was segmented into scalp, skull, grey matter, white matter, cerebrospinal fluid, bone, skin, air, ventricles, and eyes.

The manual corrections have been made for each one of the subjects following a careful visual inspection of the masks. As both, the original and the corrected masks are saved, in this study we worked effectively with a total of 4 subjects: 2 of them with corrected masks and two without. Lead matrix files were then calculated for each of the four subjects.

6.1 Manual Corrections made

In the case of Colin, some masks needed little corrections. Those corrections took no more than 5 minutes per each one of them, except in the case of the CSF and the skin.

CSF had lots of regions out printed that had to be deleted, as this error propagates in every layer of the MRI. For instance, it can be seen in Figure 11A, how those out-printed regions generate some convexities on the CSF mask. This then affects the three-dimensional reconstruction.

Colin's skin mask showed a very bad segmentation so it needed big corrections. Those were not made in agreement with the tutor, due to the low relevance that the skin has on this process. So, this segmentation was left as it can be seen on Figure 11B, there is a presence of a concavity on the frontal part of the head, as well as an excess in width on the top part.

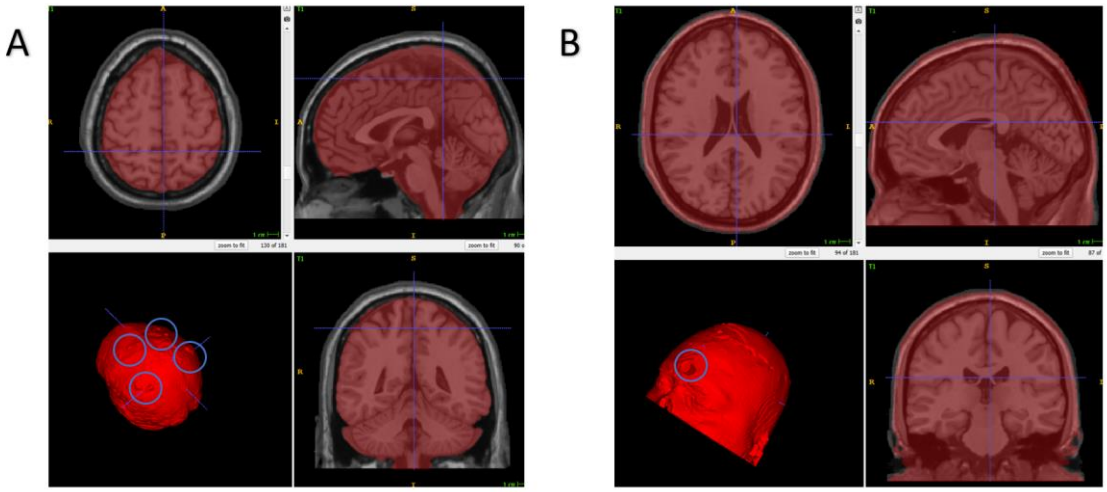

Figure 11: *Corrections made on Colin's CSF (A) and Colin's skin mask (B)*

The remaining masks received little corrections or no corrections at all, since the segmentation done by SimNibs was good enough. In Figure 12 we present the rest of the masks for Colin. It is important to notice that Colin only has partial coverage of the head (up to the node), as shown in Figure 12A. This only happened to Colin, since the other subjects presented a complete head coverage. This partial coverage is a limitation especially when it comes to calculation of the E-field in lower electrode positions.

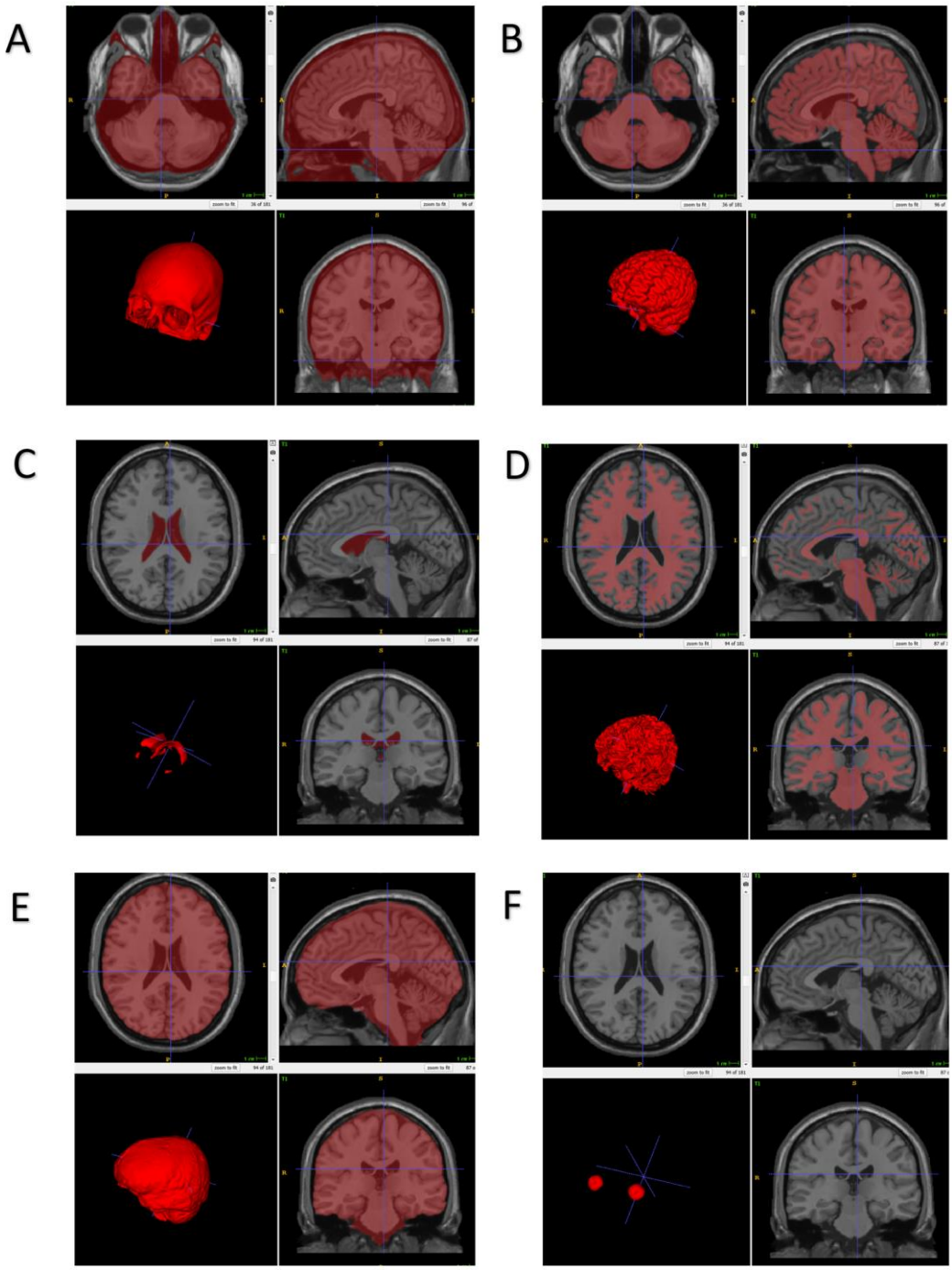

Figure 12: *Final masks segmentations for Colin's subject. Bone mask (A), grey matter (B), ventricles (C), white matter (D), corticospinal fluid (E) and eyes (F)*

Regarding Colina, it can be seen that the main issues came while looking at the CSF and the bone masks. The other masks received small corrections that did not make them very different from the original masks. The main corrections made (CSF tissue) can be seen in Figure 13B. As with Colin, several regions where the CSF mask was over segmented (eating into the skull segmentation) were observed.

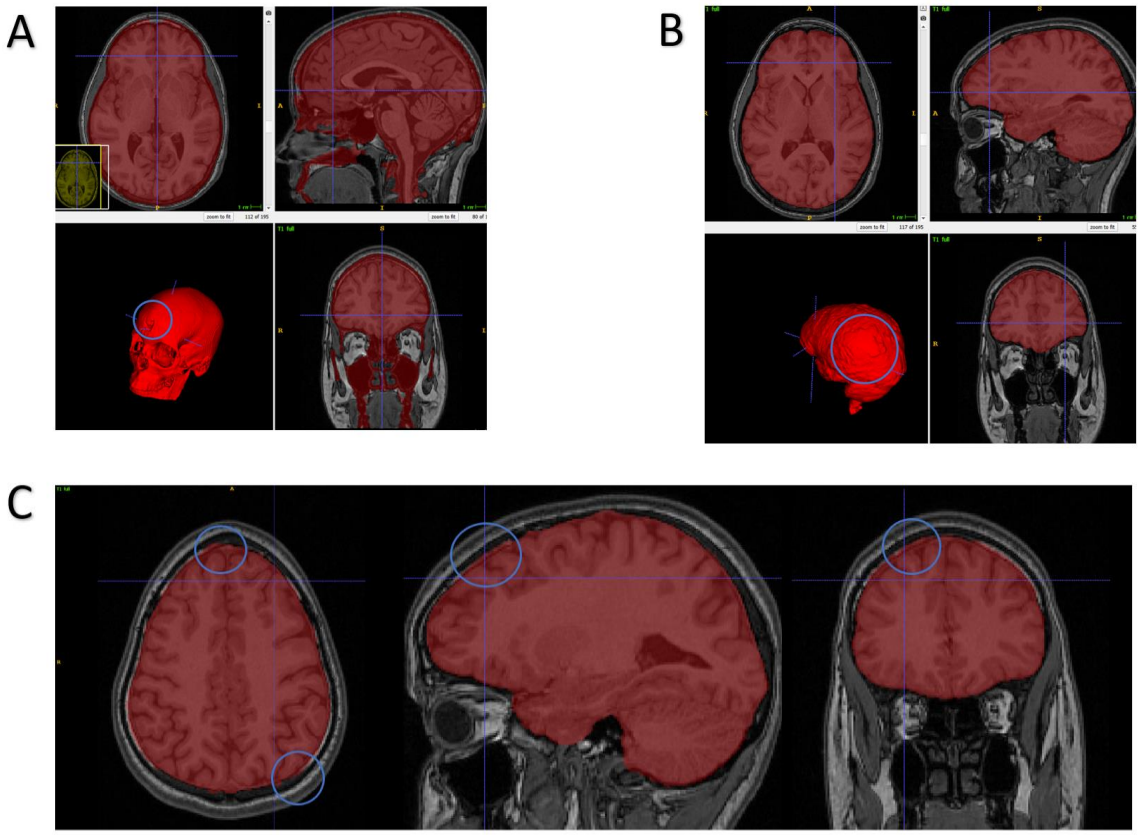

Figure 13: *Colina's masks segmentation corrected, bone mask with a concavity in the forehead (A), CSF mask with the presence of different bulging areas (B). In (C) it is shown the different views as for the CSF marking the defaults found on these layers.*

The bone mask, shown in Figure 13A, presented a big hollow space at the front, this was corrected manually by modifying the affected layers of the MRI.

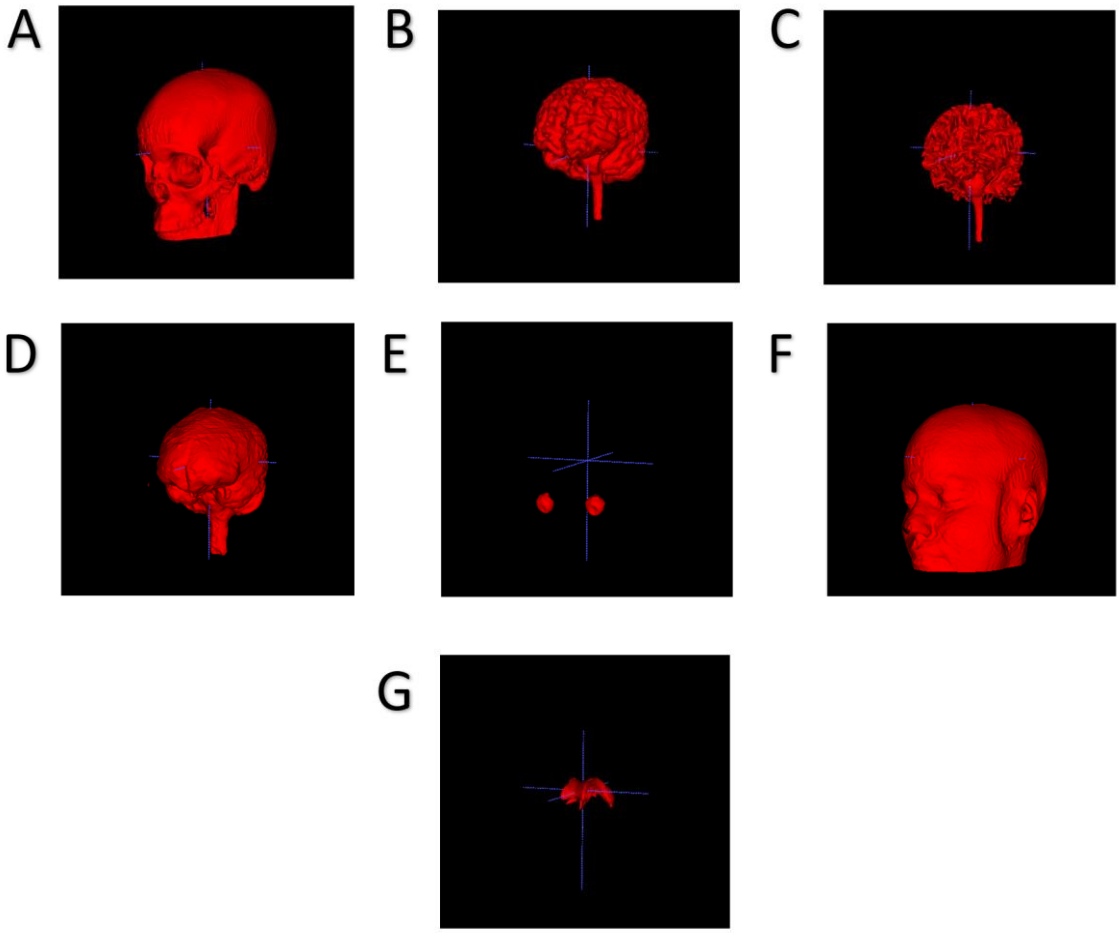

Figure 14: *Final masks segmentations for Colina's subject. Bone mask (A), grey matter (B), white matter (C), corticospinal fluid (D), eyes (E), skin (F) and ventricles (G),*

6.2 Optimization results

Once the masks were corrected, the next step was generating the lead-field matrix files in order to optimize the montages using the Stimweaver algorithm. With this ready it was necessary to plan the different optimization parameters for each of our subjects. In this case it was chosen that each subject would go through 5 different montages, resulting in a total of 20 different optimizations. In our concrete case the target electric field was set to either 0.15V/m, 0.25V/m or 0.5V/m, and the currents were constrained to 4/2mA of 2/1 mA of maximum total injected current /max current per channel. The five combinations made can be seen on Figure 15. The target defined in this optimization was the left dorsolateral prefrontal cortex (lDLPFC, BA46 as shown in Figure 10), using the methods described before. The montages were evaluated with respect to ERNI, WCC and surface average value of E_n in the target region, (complete results on Annex A).

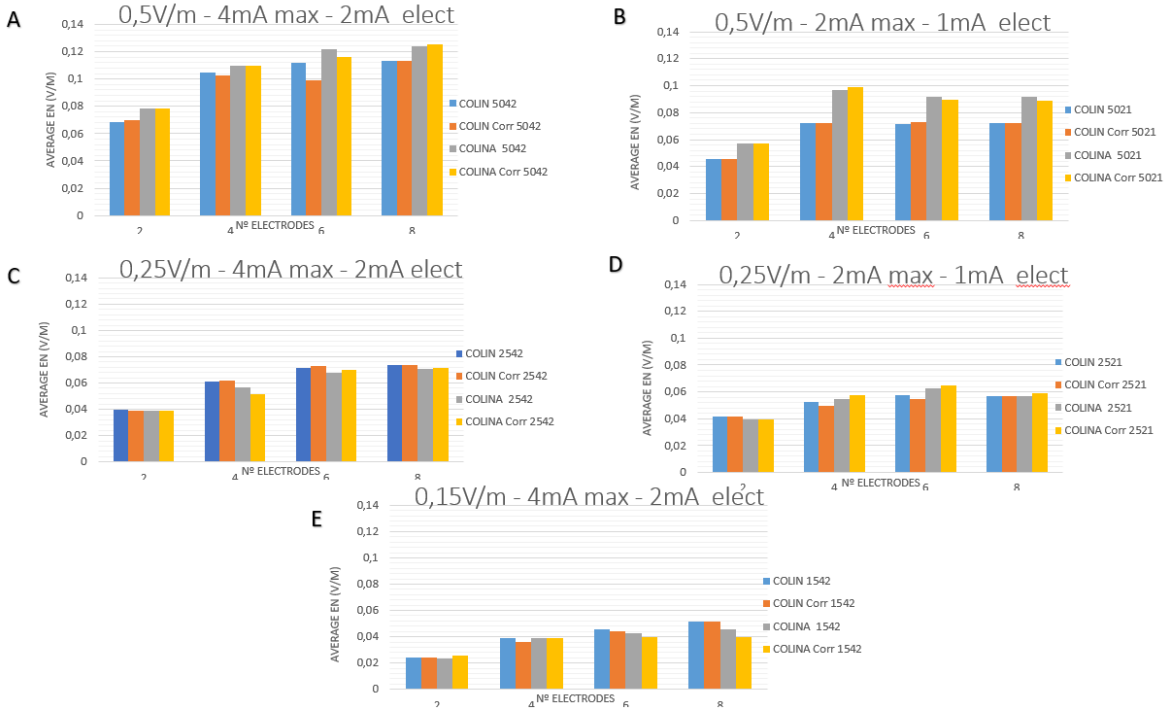

Figure 15: *Plots of the surface average electric field values (normal component of the E-field) obtained for Colina, Colina, Colin corrected and Colina corrected, for the different parameters of the optimization. The average values were calculated in the surface.*

Now it is possible to start seeing differences between the cases. The first point that is appreciable is the fact that the electric fields generated increases as we demand more to the optimization (by increasing the target value of the E-field). Also, making more currents available to the optimizer (by increasing the current constraints), allows for higher electric field values to be achieved.

Taking a closer look at the results some differences in the electric field values can be seen between corrected and non-corrected subjects.

In the graph shown in Figure 15B, it can be seen how the effects of the corrections vary for each subject. We can see how there exists a relation between Colin and Colina. Taking a look at those results, Colin tends to have similar values to its corrected version and diverge from the results obtained in Colina. Meanwhile Colina acts exactly in the same manner, presenting similarities values also with its corrected version. That makes sense, taking into account that both solutions come from the same MRI.

There seems to be no relation between the montage chosen and the variability of the results with and without corrections. The current constraints do not seem to modify in a systematic way the electric field differences between the corrected and non-corrected head models. However, this statement cannot be confirmed with this short number of subjects tested in this section.

In order to quantify the variations on all the different aspects for both of the subjects we calculated the difference between the subject with and without corrections (as a percentage of the value obtained with the correction), as shown in Table 4.

Subjects/Study case	Colin (%)	Colina (%)
4mA (TC) – 2mA (MCPE) – 0.25 V/m (TE)	2%	8%
2mA (TC) – 1mA (MCPE) – 0.25 V/m (TE)	6%	6%
4mA (TC) – 2mA (MCPE) – 0.50 V/m (TE)	13%	5%
2mA (TC) – 1mA (MCPE) – 0.50 V/m (TE)	2%	3%
4mA (TC) – 2mA (MCPE) – 0.15 V/m (TE)	7%	15%

Table 4: *Maximum relative error of the average electric field value obtained when comparing Colin with Colin corrected, and Colina with Colina corrected. Several optimizations have been computed for each study case, here we just show the maximum error obtained. (TC: Total current injected; MCPE: Maximum current per electrode; TE: Target Electric field)*

In view of the results shown, we can state that the corrections made on the masks prior to the current calculations is a necessary step. It can be seen how in the case of Colin there is a variation of up to 13% of the electric field between the corrected and the uncorrected versions. In the case of Colina, the maximum in this case is to 15%. As for Colin the mean error of the electric field voltage is 3±5%, and in the case of Colina the mean error is 3±4% (taking into account all the values, not just the maximums).

It can also be seen how the currents delivered in each one of the cases tends to present different values if the mask has been corrected. However, in some cases no variation is present. This happens when the currents saturated, i.e., they have reached the maximum value allowed by the constraints. Current saturation happens anytime the E-field target value is too high. Once this occurs, the way that the algorithm proceeds to increase the E-field is spreading the anodes and the cathodes more a part. That causes in some cases, variable electric field values, as well as the WCC and ERNI but no variation of the current. The effects of the corrections on the currents, are more visible for the less stringent optimizations: lower target -field and/or higher currents. This can be seen by calculating the total injected current variation between Colin and Colin corrected in the case with 0.5 V/m (with TC limited to 2.0 mA and MCPE limited to 1.0 mA) is 2% as compared to 10% in the case with 0.15 V/m target E-field (with TC and MCPE limited to 4.0 mA and 2.0 mA, respectively).

To summarize this part, the need of correcting the masks prior to any kind of montage has been demonstrated. As the average E-field differences obtained without correction could be up to 15% different with respect to the corrected model. These variations can subsequently lead to imprecise estimation of the results of tDCS sessions.

7. E-field variability across subjects

7.1 Characteristics and corrections for each subject

The purpose of this part of the project, as a reminder, is the study and quantification of the electric field variability induced in different subjects under the same conditions. For this purpose, the IXI database (IXI Dataset, 2020) has been selected for the MRI image acquisition. This database has collected over 600 MRI T1-weighted images from three different London hospitals. The high quality offered and the wide range of demographics for this population (age, sex…) led us to choose the IXI Database for our project. E-field calculations will be performed for typically used bipolar montages that target the lDLPFC and the lPMC. Montage optimizations will also be performed for each subject, targeting the two areas mentioned before.

In this section we will first present the different subjects involved in the project as well as the different corrections made to them. Those corrections will be shown on a list to notify the most important aspects that have been modified. In the case that some large modifications were made, those will be presented as a figure.

The realistic head models created in this section were built with the SimNibs *headreco* tool (as explained before). The software *Freesurfer* was used to obtain the affine transformation to MNI space for each subject.

Age	Sex	Ethnicity	ID
21.38	Male	White	38
24.76	Male	White	33
30.67	Male	White	22
35.8	Female	White	2
40.04	Female	White	45
46.71	Male	White	13
55.17	Male	White	16
63.19	Male	White	50
74.03	Male	White	28

Table 5: *Characteristics of the subjects studied on the project*

ID	Corrections made
38	Little correction on the CSF
33	Little corrections on the skin mask and big corrections on CSF
22	Little correction on the CSF
2	Little correction on the CSF
45	Little correction on the CSF
13	Little correction on the CSF and big corrections on the bone
16	Little correction on the CSF
50	Little correction on the CSF and nose problem
28	Little correction on the CSF

Table 6: *Descriptions of the corrections made for each subject*

- IXI 033

  As it can be observed in Figure 16, the CSF mask on this subject presents lots of out-printed regions that generates lumps once the reconstruction is made. Those regions were deleted slice by slice in order to obtain a better reconstruction.

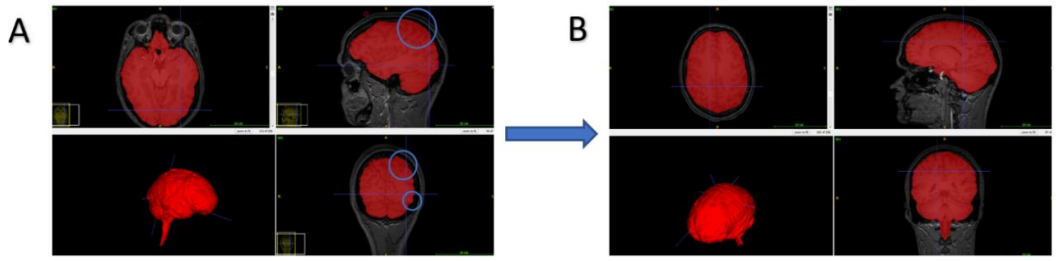

Figure 16: *CSF mask correction for IXI 033*

- IXI 013

  This subject had some issues on the top part of the bone. Here the program detected an inexistent hole and deleted some tissue generating an inconformity, see Figure 17A. This issue was solved by adding bone mask to the top of those layers affected.

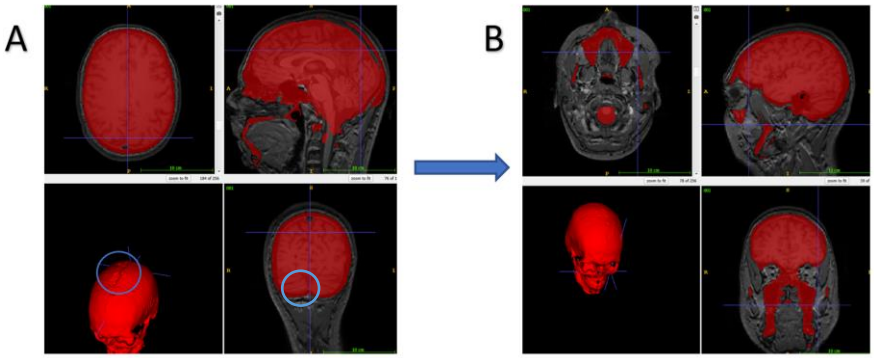

Figure 17: *Bone mask correction for IXI 013*

- IXI 050

  This subject was an interesting case since the image cropped the end of the individual's nose, see Figure 18. That makes impossible having a perfect reconstruction of the skin of the patient. However, it is not expected to have significant variations on the result with this problem unsolved.

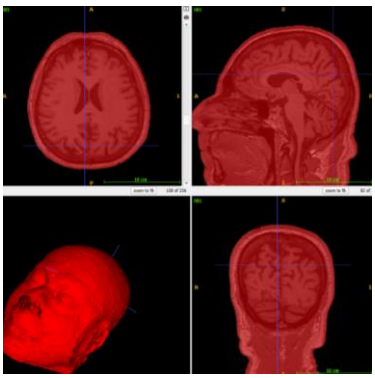

Figure 18: *Skin mask for IXI 050*

7.2 Montages characteristics

In order to see how the electric field changes across subjects, two different types of tests have been performed. Firstly, a bipolar montage was defined for each one of the target areas mentioned before, obtaining the electric field generated in each subject by the presence of two sponges, as defined in section 3.3. These large sponge electrodes delivered 2 mA and -2 mA, respectively for the anode and the cathode. For the case of the lDLPFC the anode was placed over F3 and the cathode over Fp2. Meanwhile, for stimulating the lPMC, the anode was placed over C3 and the cathode over Fp2, see Figure 19.

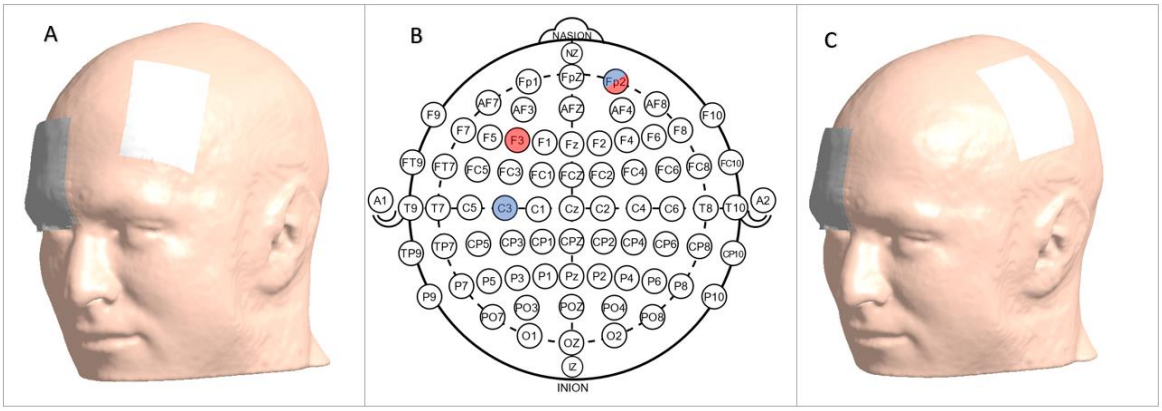

Figure 19: *(B) 10/10 Electrodes position with the chosen electrodes for the bipolar montages printed. In red the configuration for the lDLPFC (A) and in blue for the lPMC (C). (Source (B): International 10-20 System for EEG Wikimedia Commons. 2020. Commons.Wikimedia.Org. Accessed April 25. https://commons.wikimedia.org/wiki/File:International_10-20_system_for_EEG-MCN.svg.)*

The characteristics of the sponge electrodes were the same for all the subjects: rectangular electrodes, with dimensions of 50 mmx70 mm (35 cm^2 area) and two layers of thickness 3mm (the conductive material) and 2mm (metallic connector). These sponge models are typically used in several studies. The E-field results obtained for each subject were stored, with the aim to study the differences that may arise between individuals. These results will also be used to make a comparison with the optimization montages. he second type of test done in the subjects was a series of optimized montages. Eight optimized montages have been computed for each subject and each area, comprising a total of 16 optimizations for each of the subjects. As explained in section 3.4, optimizations were performed with Stimweaver, as implemented in Python by scripts developed by Neuroelectrics. The inputs for each optimization were (see also Table 7): the target electric field value in the target areas (0.25 V/m or 0.50 V/m) and maximum values of total injected current (2.0 mA or 4.0 mA) and the individual currents in each electrode (1.0 mA or 2.0 mA). Then, by minimizing the value of ERNI, the scripts provide the best combination possible of electrodes and intensity values.

Target electric field (V/m)	Maximum total current (mA)	Maximum current per electrode (mA)
0.5	4	2
	4	1
	2	2
	2	1
0.25	4	2
	4	1
	2	2
	2	1

Table 7: *Different optimization constraints for the multichannel optimization montages.*

For each set of optimization constraints we ran 4 different sub-optimizations, each having a maximum number of electrodes in the montage of either 2, 4, 6 or 8 electrodes. The time expend for each one of the solutions diverges depending on the currents and electric field limitations, as well as on the maximum number of electrodes. The 2 electrodes case does not take more than 5 minutes to finish, however, as we increase the number of electrodes used, the times seems to increase in an exponential way, with the 8-electrode solution taking several hours to finish. Seeing how the different subjects act, the time for obtaining a complete result (going from the 2 electrodes case up to 8) varies depending on the area and the type of montage. Exact calculations have not been made to validate this claim, but it was observed that the lDLPFC area optimizations take 15-20% more time than the lPMC optimizations. In addition, the more freedom we offer to our program to obtain the desired solution the faster it gets. For this reason, those montages limited to 4 mA maximum current and 2 mA of maximum current per electrode, take a third time less than a montage limited to 2 mA and 1 mA respectively. At the end, the estimated average time per calculation was of about 3.5h.

7.3 Results and discussion

Figure 20 and Figure 23 are boxplots representing the electric field variability on the left dorsolateral prefrontal cortex and the left primary motor cortex respectively (Annex B and C shows the complete results). These plots represent the average electric field over the area of interest for each of the subjects tested. In these graphs the first and third quartiles are shown as a rectangle, we can also see the mean value represented with an 'x', the median as a straight line dividing the quartiles and the maximum/minimum values, for each of the cases. Notice that the graphs include a boxplot for each one of the maximum number of electrodes cases, as well as the boxplot for the bipolar montage. The bipolar plot is the result of calculating the average electric field within the studied areas by using two rectangular electrodes (details about this montage can be found in section 7.2). This boxplot serves as a visual reference, allowing for a quick comparison between the optimized and bipolar montages.

Observing the values represented in Figure 20 and Figure 23, the first thing to notice is that the lDLPFC shows bigger values of electric field in almost every case. More specifically, the average value of the electric field is doubled in most studies carried out if we compare the values of lDLPFC with respect to those of lPMC. This difference is explained in (Laakso et al. 2016). This article explains how depending on the brain geometry, different values of electric field can appear under similar current conditions depending on the area stimulated. The different sulci distribution present in different brain areas directly affects the electric field induced, thus explaining the difference of mean values between both regions.

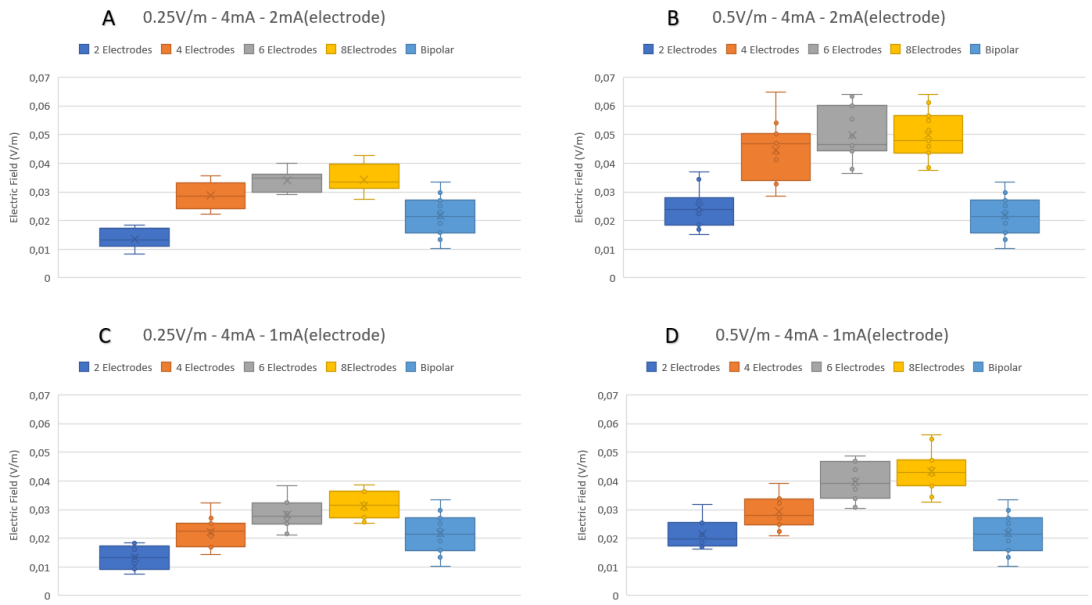

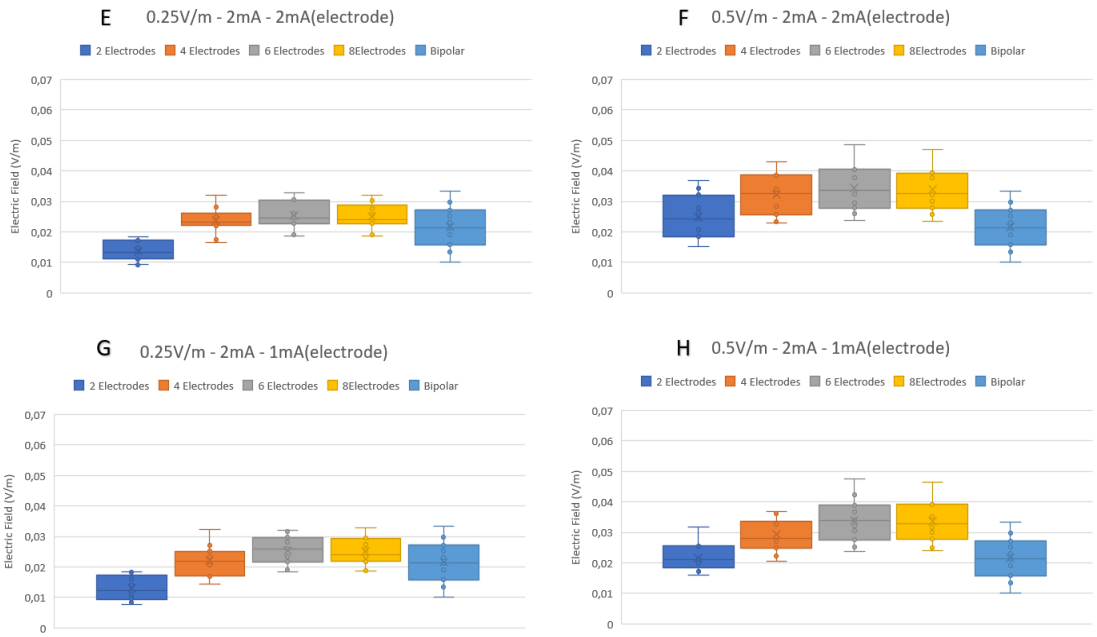

Figure 20: *Boxplots representing the electric field distribution on multichannel montages targeting the lPMC (left primary motor cortex). The title of the plots shows the optimization constraints: target E-field, TC and MCPE, respectively.*

In order to closely examine the impact of optimization constraints, we will start by analysing the results of Figure 20, the lPMC. The general trend is that increasing the number of electrodes available, increases the average value of the electric field on the target area. In Figure 20A-C (TC limited to 4.0 mA and MCPE to 2.0/1.0 mA), this trend is clearly seen. However, this does not happen in all cases. In Figure 20E-H after moving from 4 to 6 electrodes, the values seem to stabilize. Clearly this behaviour is due to current saturation: optimizations that are more limited in the current benefit less from the increase in the number of electrodes. The optimization that benefited more with increasing the number of electrodes was the one with TC set to 4.0 mA and MCPE set to 2.0 mA (Figure 20C –D). The limitation in MCPE makes the increase in the number of electrodes an effective way of injecting more current, which benefits montages with more electrodes. In solutions that are constrained in the TC to lower values, current saturates at lower electrode counts and increasing the number of electrodes will just affect the E-field due to a change in electrode configuration (more on that later).

We must remember that the parameter to be maximized is the ERNI and not the electric field value. As can be seen in Figure 25 and Figure 26, the absolute value of ERNI increases as we provide a bigger number of electrodes availed. This increase in ERNI is seen as a better focality of the E-field distribution, as shown in Figure 21. The top cases, Figure 21A and Figure 21B, are the most restrictive cases regarding the parameters imposed (TC of 2.0 mA and MCPE of 1.0 mA). Moving from the case with 4 electrodes into the 8-electrode montage, results in a better fit and focality of the E-field distribution. In addition, the negative electric field generated mainly in the frontal part of the brain, is reduced with the incorporation of several cathodes. This effect is clearly appreciable in Figure 21C and Figure 21D,

here the limiting currents are reached in both figures, whereby changes in the area affected by a positive electric field are not appreciable. However, if we look at the areas far from lPMC, we will see how the negative electric field is substantially reduced with the incorporation of new electrodes.

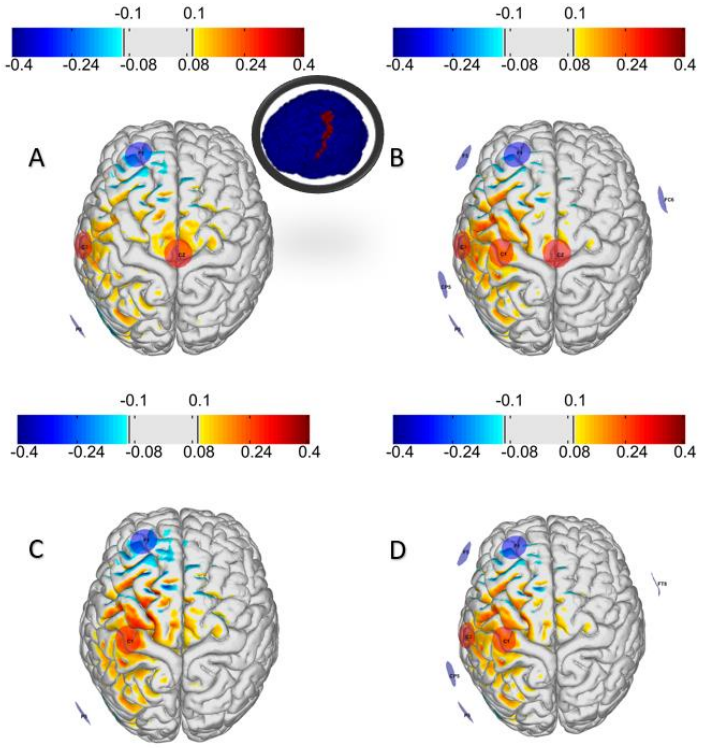

Figure 21: *Electric field distribution over the lPMC on IXI002 with a target -field value of 0.5V/m. (A) and (B) were restricted to 2 mA maximum injected current and 1 mA of maximum current per electrode, with 4 and 8 electrodes used, respectively. (C) and (D) had restrictions of 2 mA/2 mA, with 4 and 8 electrodes used, respectively.*

Regarding the influence of target E-field value on the results, it stands out that generally higher average E-field values on target are obtained in those cases with target E-field of 0.5 V/m, as compared to those with 0.25 V/m. However, this increase in average E-field values also brings a greater variability in the results. This fact makes perfect sense, since by requiring a greater electric field within the area, one of the priorities of the optimization algorithm will be to get as close as possible to this value. It is known that: the generation of the electric field acts proportionally to the injected current (if by injecting a current X[mA] we obtain an electric field Y [V/m], injecting from the same electrodes 2X[mA] it will generate an electric 2Y[V/m]). This is clearly visible in montages with two electrodes., when comparing 0.25 V/m to 0.5 V/m. In those cases where the current is not saturated, the intensity values are doubled to obtain the electric desired, see Figure 22. However, increasing the current is not always possible since, as we have explained in the previous paragraph, the current constraints must be taken into account. Therefore, the variability of the induced average E-field values in target will increase in those cases. This is partially offset by the increase of the distances between the anodes and cathodes, which increases average E on target, at cost of losing focality. Mathematically, the variability of results will be

always larger when demanding a greater electric field. Brain structure differences between subjects is another factor to be considered as a contributing factor to this variability. In (Laakso et al. 2016) it is explained how different people present slight differences in the brain sulcal and gyral areas, and the importance of these areas when inducing a certain electric field. In the 0.5 V/m montages, different areas in the patient's brain shows an increase in the point electric field. A higher electric field acts different depending on the sulcal and gyral distribution, thus causing a higher variability.

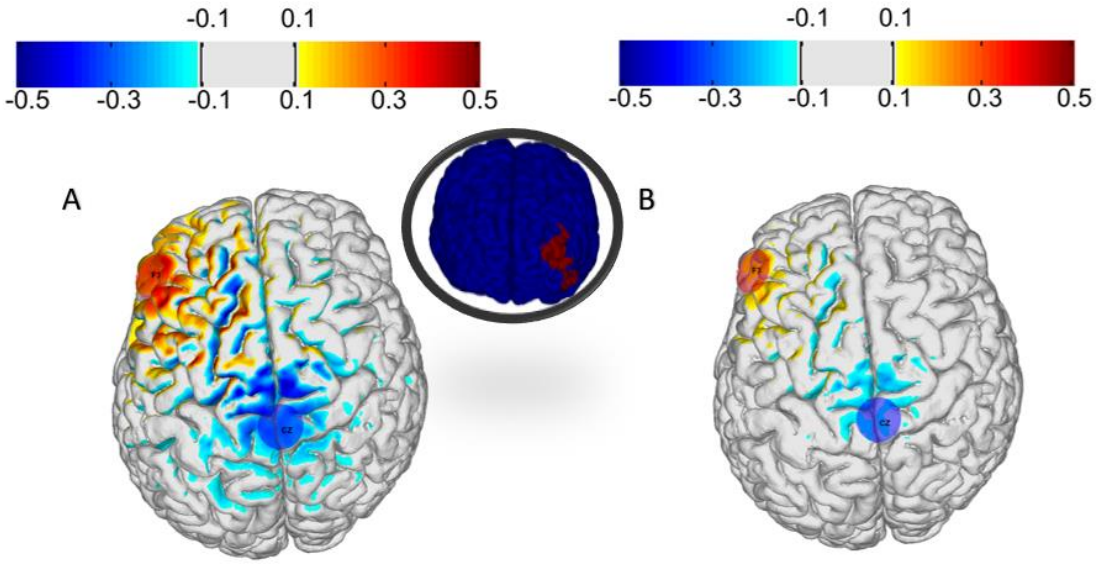

Figure 22: *Electric field induced over the IDLPFC on IXI016. (A) was targeted at 0.5 V/m, giving a total injected current (uA): 1354* μA *and maximum current any electrode (uA): 1354* μA*. (B) was targeted at 0.25 V/m, giving a total injected current (uA): 677* μA *and maximum current any electrode (uA): 677* μA *. (units of the scale: V/m)*

Comparing the boxplot generated with the bipolar montage with respect to the rest, the greatest similarities found are with the Figure 20F case, more specifically with the 2 electrodes solution. This fact is explained taking into account that the bipolar montage has been carried out by using two electrodes, a cathode and an anode with 2 mA and -2 mA respectively. The montage resulting from the optimization with two electrodes of the case Figure 20F ends up being very similar to the bipolar one, as the E-field demanded is the heights, the currents tends to saturate and reach values similar to 2 and -2mA (in the Figure 20 F case, the currents are limited to 2mA for maximum total current and 2mA for maximum current per electrode). Moreover, by looking at the width of the area between the two quartiles, it can be observed how the bipolar montage resembles most of the configurations with 0.5V/m. However, these multichannel montages have higher values in terms of electric field. Making a comparison with the 0.25V/m cases, with the exception of the 6 and 8 electrodes montages limited to 4 mA of maximum injected current, the rest of the montages have maximum values similar to those of the bipolar configuration. In all cases, the standard deviation obtained is lower than the bipolar montage, meaning that, in terms of variability, the best results are obtained for the optimized solutions with a target E-field of 0.25 V/m solutions.

As for the lDLPFC results, shown in Figure 24, similar conclusions can be drawn. At the beginning of this section, the reason for the main difference between the results obtained with lPMC and lDLPFC has been explained. However, despite this difference in the magnitudes, it can be seen how the general behaviour in both cases is similar. Under the same restrictions, both stimulation areas tend to act in the same way. Therefore, we can say that the trends shown in these graphs (the multichannel boxplots) are mainly determined by the limiting current factor. To graphically show how the limiting current works, the graphs of Figure 23 have been generated. In those montages with low electric field demand and permissive restrictions for currents (Figure 23A) the subjects do not reach the current limits. Figure 23D is a perfect example when current saturation is reached.

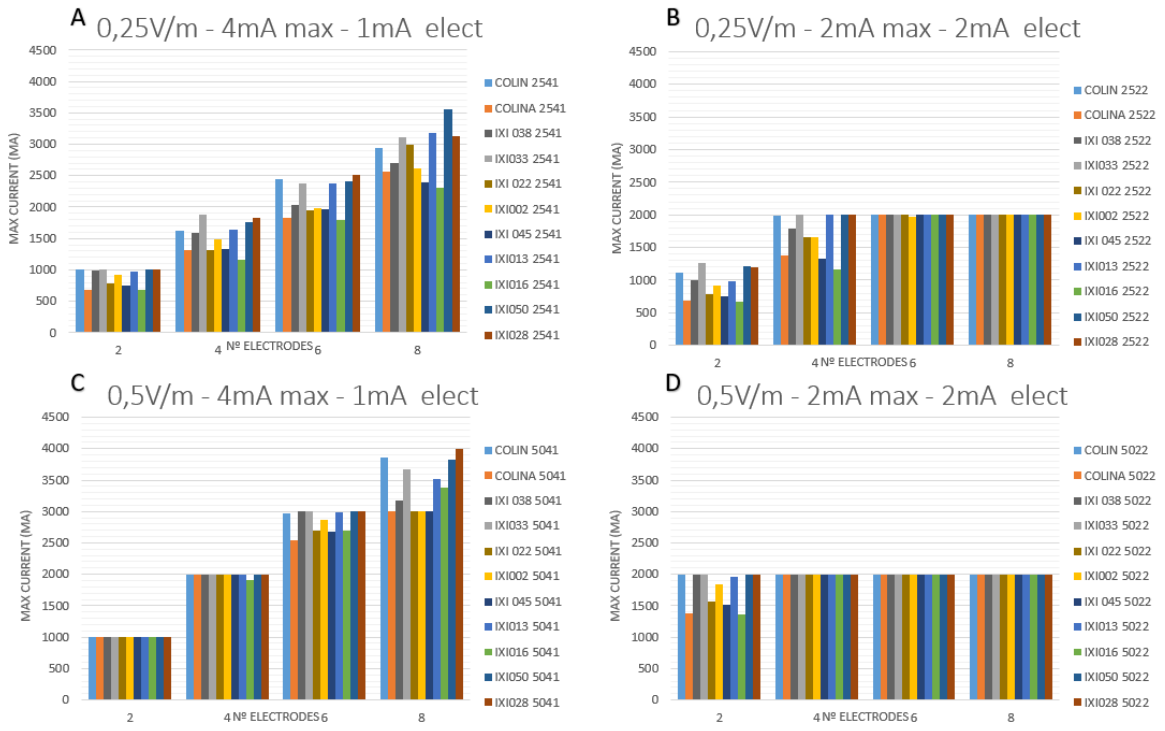

Figure 23: *Maximum current injected on the IXI subjects, Colin and Colina over the lDLPFC*

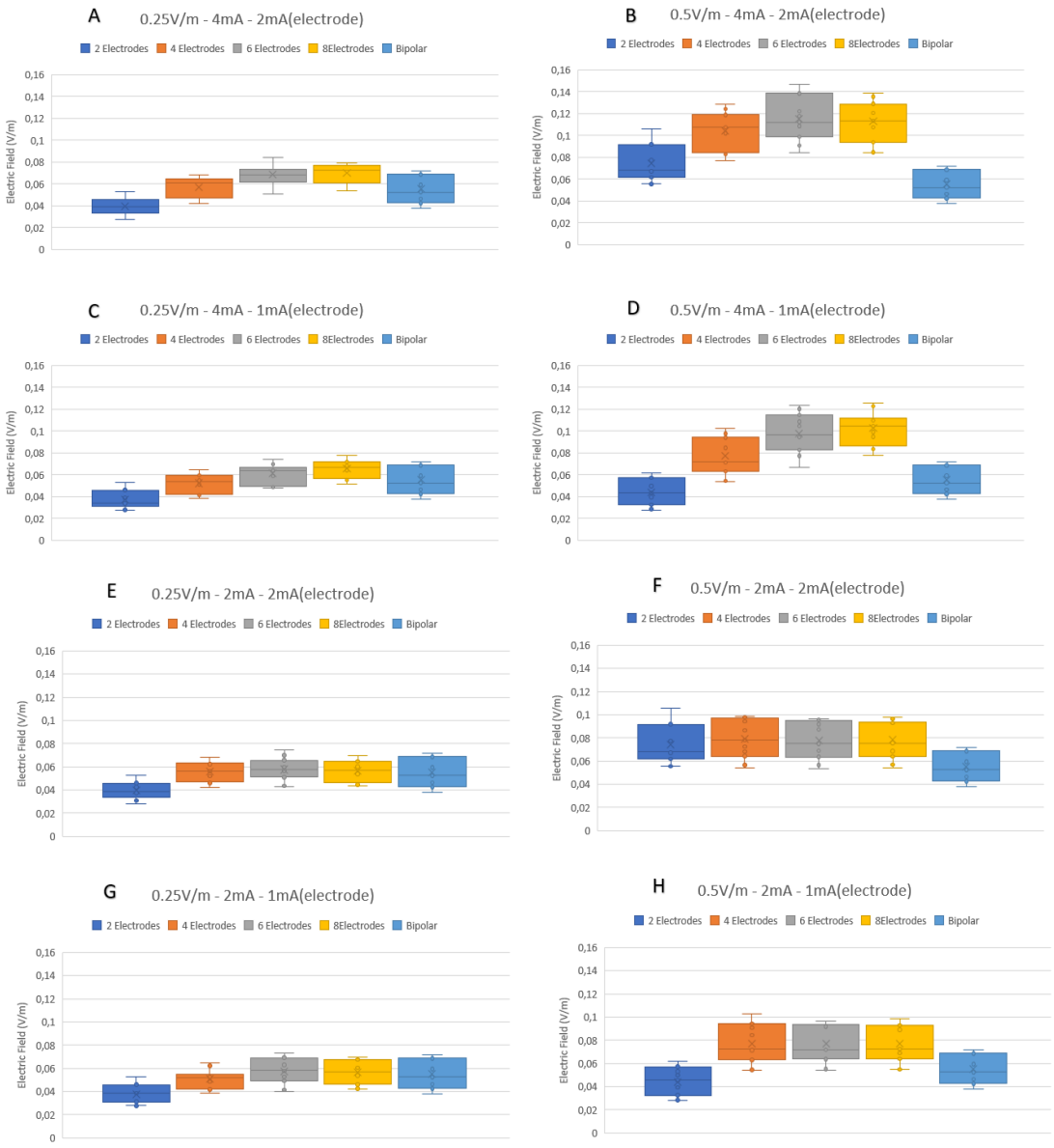

Figure 24: *Boxplots representing the electric field distribution on multichannel montages made over the IDLPFC (left dorsolateral prefrontal cortex).*

At this point we can confirm that the montage that offers a better solution is the 8-electrodes montage. Despite that in some cases, for some particular subjects, a better solution is found out for a 6-electrode montage in terms of electric field, while looking at focality, the best solution is always with 8 electrodes. To support this hypothesis, in addition to the results already shown, boxplots of the WCC and ERNI values are made for the different subjects. Figure 25 and Figure 26 shows some of the named graphs, however, given the similarities found in the structure of the results, and since we do not intend to make an exhaustive analysis of these values, not all the boxplots are shown.

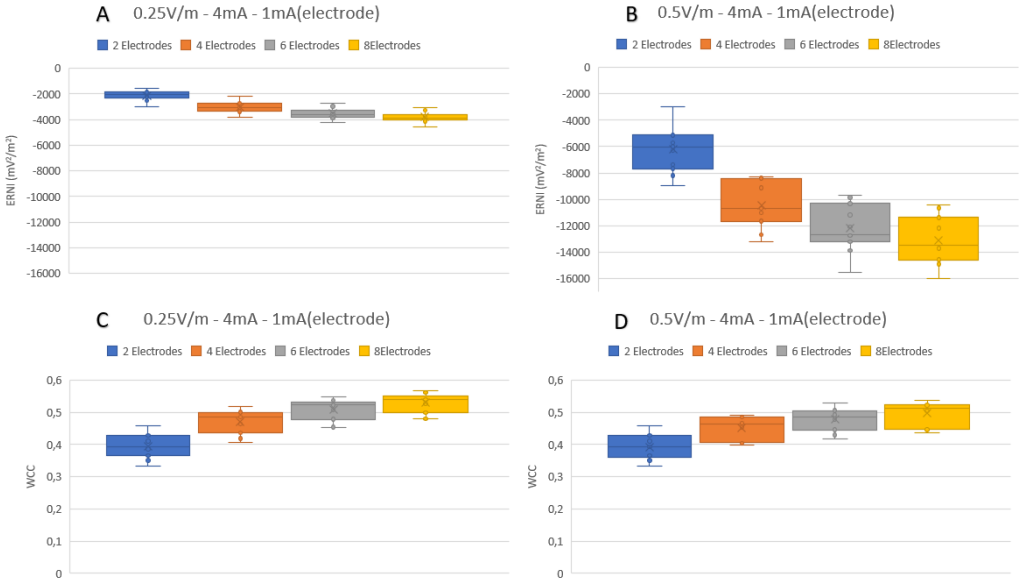

Figure 25: *Boxplots of the ERNI and WCC value for the lDLPFC*

These values can be considered as indicators of how good a solution is. It can be seen how the WCC shows a clear tendency to increase, while in the case of ERNI, it has a tendency to decrease to progressively lower (negative) values. This would indicate that the best solution, in terms of focality, is found to be in the last montage, the 8-electrode montage. Furthermore, analysing the results, these values seems to behave similarly to the electric field. In those cases where current limitation is an important factor, these values tend to stabilize, see Figure 26B, whereas in the cases that are no so restrictive in current, as in Figure 25B, this trend becomes more visible. It should also be noted that, as well as with electric field, the values obtained for the lDLPFC are higher than those of the lPMC.

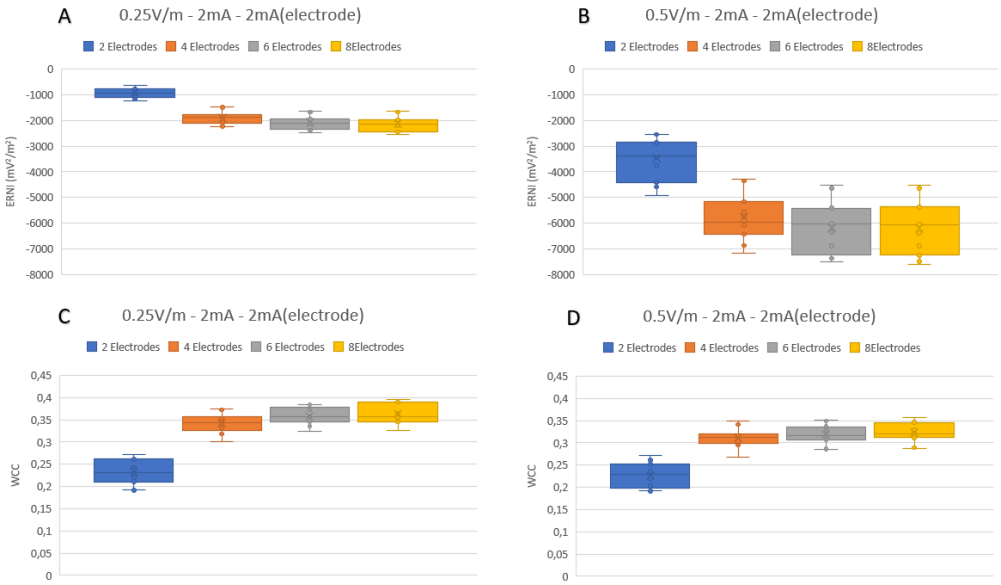

Figure 26: *Boxplots of the ERNI and WCC value for the lPMC*

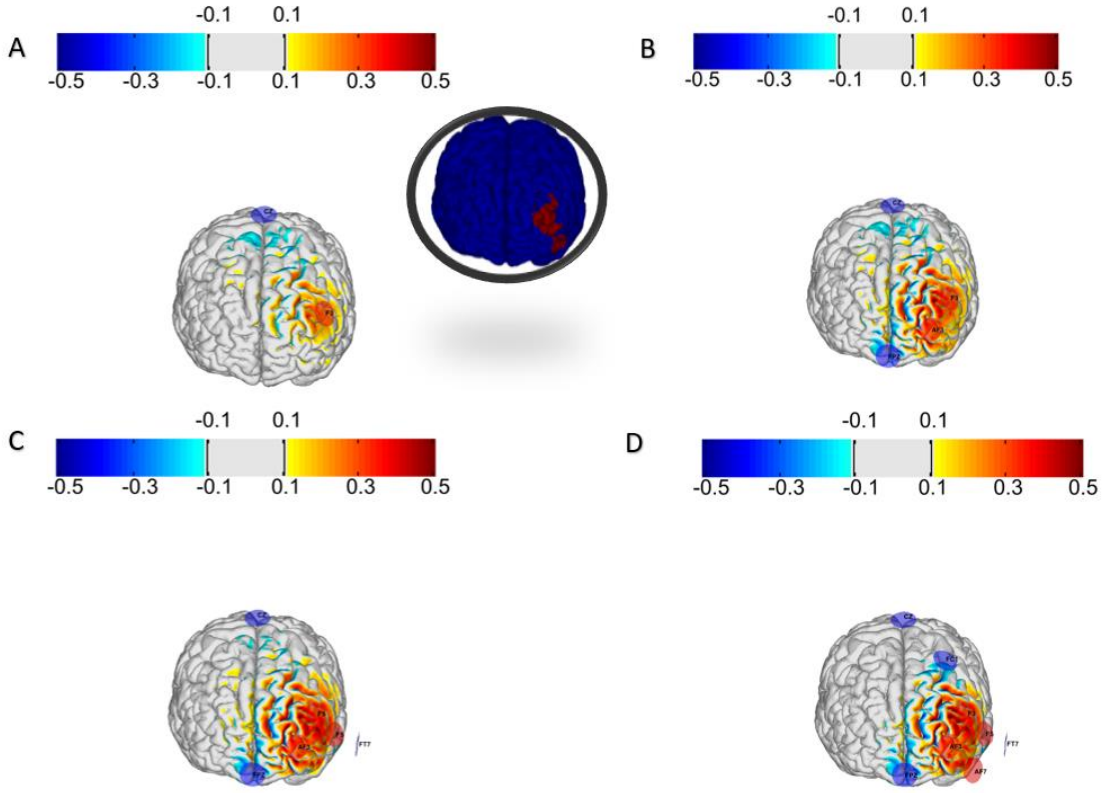

Figure 27: *Multichannel electrode montage made for IXI045 over the lDLPFC with 0.5V/m demanded electric field, 4mA maximum injected current and 1mA maximum current per electrode. (A) 2 electrode montage, (B) 4 electrode montage, (C) 6 electrode montage and (D) 8 electrode montage. (units of the scale V/m)*

Figure 27 shows how the electric field varies under the same restrictions while increasing the number of available electrodes. Due to the arguments shown above, it has been decided to select those montages with 8 electrodes for a numerical study. Table 8 and Table 9 shows the electric field mean and the standard deviation obtained for those montages over the lDLPFC and the lPMC. At this point, we can affirm that the variability (understood as the standard deviation) is related with the electric field value, and therefore with the currents used. A proportionality exists, with the standard deviation calculated being between 15-35% of the E-field magnitude.

Electrodes montages with 0.25V/m targeted E-field	E-field mean over lDLPFC (V/m)	E-field mean over lPMC (V/m)
4mA - 2mA(electrode) -8Ch	0.070 ± 0.009	0.034 ± 0.005
4mA - 1mA(electrode) -8Ch	0.065 ± 0.008	0.031 ± 0.005
2mA - 2mA(electrode) -8Ch	0.056 ± 0.009	0.025 ± 0.004
2mA - 1mA(electrode) -8Ch	0.056 ± 0.010	0.025 ± 0.005

Table 8:*Electric field mean obtained for the 8 electrode montages over the lDLPFC and the lPMC with 0.25V/m demanded E-field.*

Electrodes montages with 0.5V/m targeted E-field	E-field mean over lDLPFC (V/m)	E-field mean over lPMC (V/m)
4mA - 2mA(electrode) -8Ch	0.111 ± 0.019	0.049 ± 0.009
4mA - 1mA(electrode) -8Ch	0.101± 0.016	0.043 ± 0.007
2mA - 2mA(electrode) -8Ch	0.077 ± 0.017	0.033 ± 0.007
2mA - 1mA(electrode) -8Ch	0.075 ± 0.017	0.033 ± 0.007

Table 9 *Electric field mean obtained for the 8 electrode montages over the lDLPFC and the lPMC with 0.5V/m demanded E-field.*

In terms of electric field mean and standard deviation, no huge differences are observed while looking at the two last electrode montage configurations from Table 8 and Table 9 (2 mA TC – 2 mA MCPE / 2 mA TC – 1 mA MCPE). In Figure 28 it can be seen the different values for maximum current per electrodes for each subject for the montages limited to 2 mA-2 mA over the lPMC. Notice that, despite having the availability of 2 mA, that value is rarely completely used. For the 8 electrodes case, none of the subjects got 2 mA. This similarity on the E-field values for this concert restrictions of currents can be argued due to these values of MCPE. When limiting the MCPE to 1 mA, the currents saturates for almost all cases. Otherwise when this current is limited to 2 mA, the 8-electrode configuration tends to have values also around 1 mA as can be seen on Figure 28, generating in this way a similar E-field induced. Despite the similarity of the results, the standard deviation is reduced in two cases and the electric field is increased in one of them, when comparing 2mA maximum current per electrode with 1mA (limiting the maximum current injected to 2mA). In view of the results and given that; in no case the results obtained with 1mA of maximum injected current are better (understanding as better, a higher average electric field or a lesser standard variation), limiting this current to 2mA is advisable for these situations.

In Table 8, that represents the different values obtained with a targeted E-field of 0.25 V/m, no big variations can be observed as for standard deviation in each of the areas targeted. An increase in the mean electric field can be observed as the restrictions are less limiting, however, the standard deviation does not seem to follow a pattern and present similar values for all cases. In Table 9, where the targeted E-field is 0.5 V/m, the increment of the electric field mean as increasing the allowed total current also can be observed, with bigger differences in terms of variability. The 8-electrode configuration limited to 4 mA of maximum injected current and 2 mA maximum current per electrode with 0.5 V/m targeted E-field, is the only montage where all the subjects reached the 4 mA TC. Therefore, for this case the biggest values are obtained in terms of electric field mean, leading in turn to greater variability when compared to the other cases targeted at 0.5 V/m. These standard deviation differences that appear when modifying the currents but not the E-field, are not big enough to be considered. It can therefore be stated that with the use of 8 electrodes, the best situation is found to be with the least current restrictions, since the average electric field is increased substantially, keeping the variability between subjects minimum.

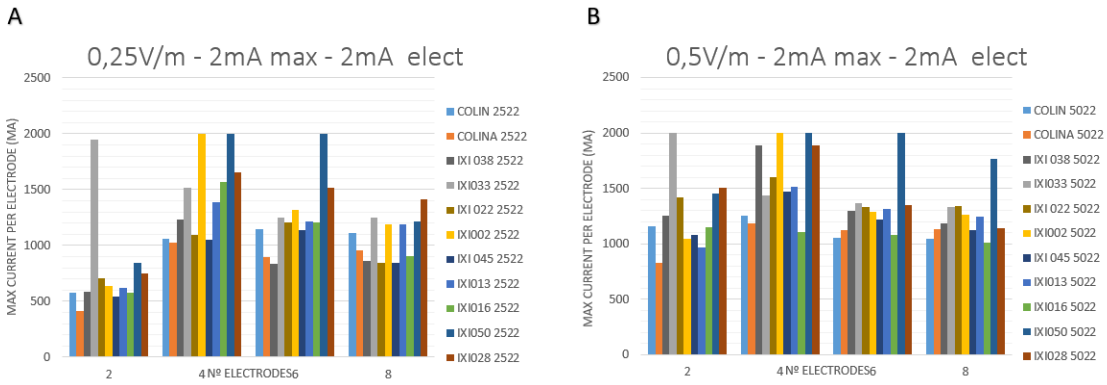

Figure 28: *Barr plots of maximum current per electrode obtained over the lPMC. In both graphs the restrictions for currents were 2mA of maximum injected current and 2mA of maximum current per electrode. On (A) the targeted E-field is 0.25V/m while on (B) is 0.5V/m.*

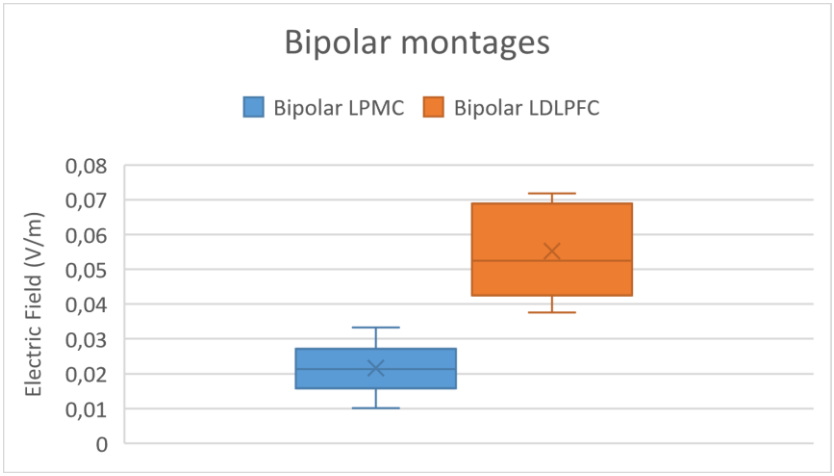

Figure 29: *Electric field induced with bipolar montages over the LDLPF and the lPMC*

As for the bipolar montages made, in Figure 29 and Table 10 a comparison of both the electric field targeted over the left dorsolateral prefrontal cortex and over the left primary motor cortex can be seen. As we have previously observed, the average value of electric field over lDLPFC is higher than over lPMC, specifically this value for the bipolar montages designed is 250% higher, while the standard deviation is increased a 280%. For the lDLPFC the standard deviation value is 24% of the E-field magnitude, while for the lPMC is 33% (both values in the range 15-35%).

E-field mean over lDLPFC with the bipolar montage (V/m)	E-field mean over lPMC with the bipolar montage (V/m)
0.054 ± 0.013	0.021 ± 0.007

Table 10*: Electric field mean and standard deviation obtained for the bipolar montage over the lDLPFC and the lPMC*

In order to study how bipolar montages electric field varies over the different areas of the brain, the following study has been designed. Firstly, by using the *tailarach.auto.xfm* file and a new generated Matlab script (Annex D), the brains of the different subjects have been mapped into the MNI standard space, two examples of this transformation can be seen on Figure 30. In this space, each brain surface was mapped to a template brain surface (Colin's surface in MNI space). To perform this transformation, the distance between the different subject brain nodes and the nodes of the Colins brains was calculated. The minimum distance between all the calculated values was taken to map the electric field to the common space. Since now, the electric field values for each of the subjects are in a common brain surface, the mean E-field and standard deviation for each node can be calculated. Figure 31 shows the results for the median and standard deviation over the lDLPFC and Figure 32 over the lPMC. In the case of the median those nodes with positive electric field values are in yellow, while the blue areas are the ones close to the cathode. As for the standard deviation is concerned, the blue areas represent low variability between the different subjects studied. Meanwhile, the green and yellow regions are the ones with big standard deviation values.

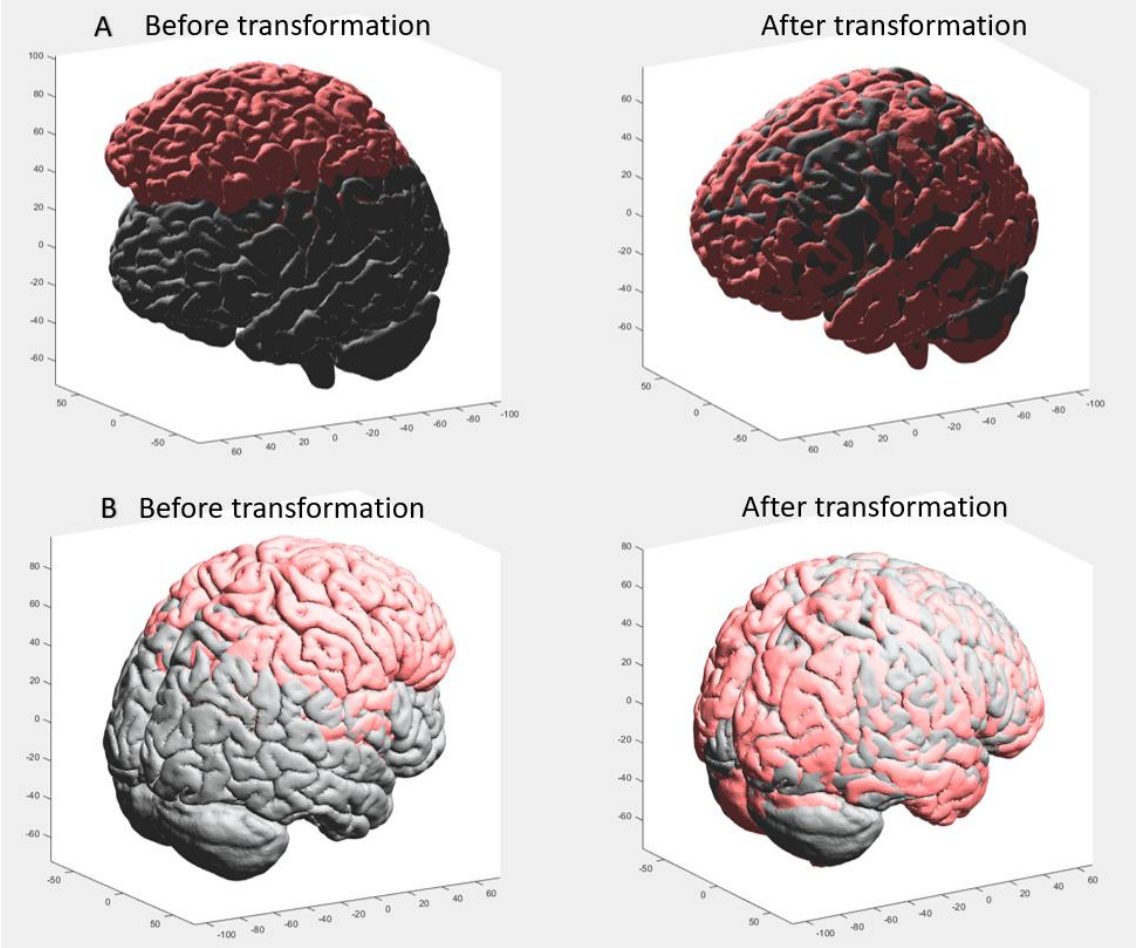

Figure 30: *Transformation into Colin space for (A) IXI 016 and (B) IXI 002*

As was expected, In Figure 31 the area around the electrode F3 presents positive electric field values while under Fp2 those values are negative. As we move away from these two located at the frontal part of the brain, the electric field values tend to drop to zero. For this reason in Figure 31B that focuses the back part of the brain, shows low values for both electric field and standard deviation. There is a clear tendency of the electric field to go from the anode to the cathode without scattering around. Given the low dispersion of the electric field, most of the variation between subjects is in the prefrontal region, most concretly at those points where positive and negative electric fields collide. For this montage, that tries to focus the electric field over lDLPFC, the main sources of variability are found to be on the zones where the two hemispheres meet over the prefrontal area. In conclusion, the electric field generated when the anode is placed over F3 and the cathode over Fp2 tends to present similar values under the stimulation area and under the cathode. The biggest differences between patients are found halfway between both electrodes.

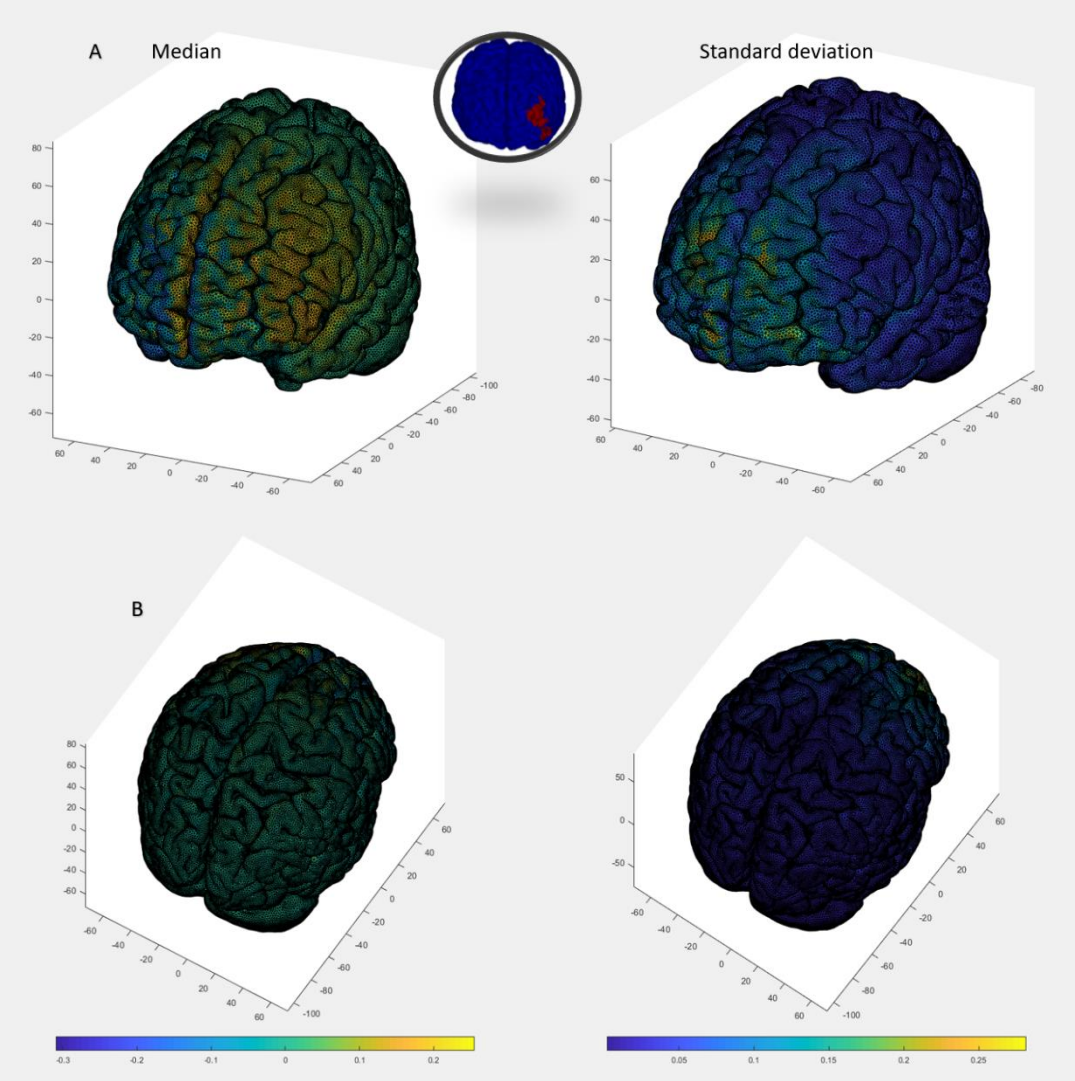

Figure 31 *Median values and standard deviation obtained for the different subjects into Colins space over the Left dorsolateral prefrontal cortex. (A) frontal view, (B) top view. (units of the scale: V/m)*

In the case of Figure 32, the results obtained are very different. For this study the anode has been located over C3 while the cathode was over FP2. Notice that, the cathode position is the same as in the previous montage, however, in this case the anode is placed at a longer distance. This distance increment between both electrodes generates a greater dispersion of the electric field, therefore the areas with positive and negative electric current are higher than in the previous scenario. Analysing the standard deviation, a larger area presents variability between subjects but the value of this variability is lower than in the previous case. As when targeting lDLPFC, the maximum values of variability are found in the prefrontal part of the brain, between both hemispheres. As we move away from this frontal area, the standard deviation values decrease, in the case of the left hemisphere, the standard deviation reaches almost the visual cortex area. In the case of the right hemisphere, from the central groove, the variability values are practically null. Notice that, those points that correspond to the lPMC present very low variability values.

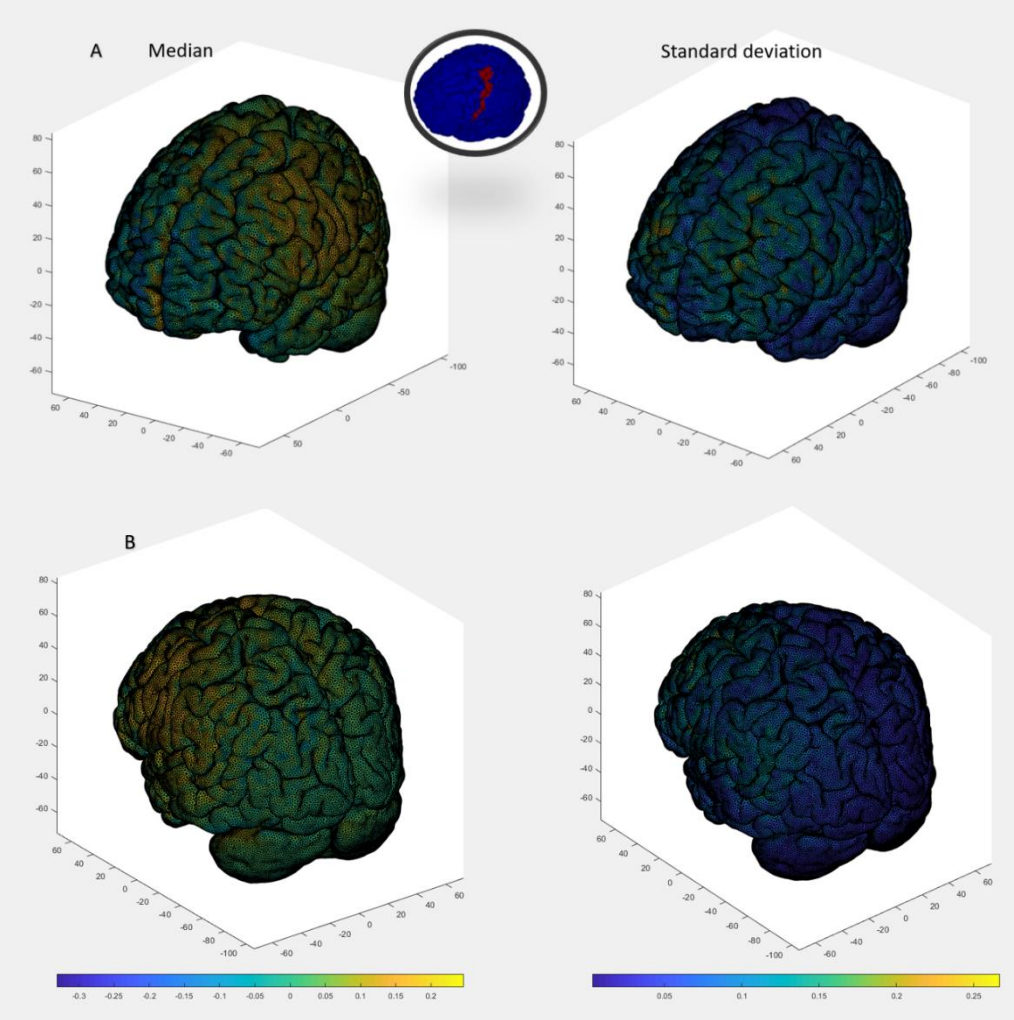

Figure 32: *Median values and standard deviation obtained for the different subjects into Colins space over the Left primary motor context. (A) frontal view (B) back view. (units of the scale: V/m)*

8. Analysis of environmental impact

Given that this project has been a study in a telematic way, based mainly on the collection and study of data, the environmental impact caused has been very low. The only considerable source of CO2 during this project is the desktop PC used. However, we cannot quantify the process of obtaining and creating the computer as CO2 emitted during the course of the project, since it was acquired for personal reasons previously to the start of this work. Furthermore, given the typology of the project, no waste of any kind was generated. Therefore, there is no need to take measures to recycle.

After consulting different pages that refer to CO2 emissions from computer products, and seeing the similarity between the data provided by all of them, an application from the Spanish government has been used. This website allows us to calculate the ecological footprint from different sources. To carry out the relevant emission calculations, the intensive and practically uninterrupted use of the computer must be taken into account. This computer has an external source of 700W, working with practically 100% CPU load. Finally, according to (Ministerio para la Transición Ecológica y el Reto Demográfico 2015), the equivalent Co2 production is estimated to be around 250Kg during the project.

9. Conclusions

A surface-based registration method has been applied for intrasubject analysis of computational electric field data. The followed procedure allows us to study the effects of tES at a group level, rather than investigating the effects on a single subject.

We must remember that the main objectives of this projects are: firstly, range of E-field values required for an effect and quantify the inter-subject variability, and secondly, implement a series of multichannel montages to see how they contribute on the E-field generation. With this purpose, we have studied two stimulation areas (lPMC and lDLPFC).

The mean electric field values have been calculated for each subject on a common brain space (Colin's space), thus allowing a visual comparison. Each subject showed variations in magnitudes and position of the E-field. However, the group analysis demonstrates that the E-field is concentrated nearby the studied areas, being the surrounding areas the ones with the highest variability. While for lPMC montages induced low variability, scattered throughout the left hemisphere, the lDLPFC variability concentrates in the prefrontal region. For this reason, we suggest for futur studies to analyse the prefrontal region with lDLPFC montages, in order not to have E-field hotspots located in this area that could induce a negative response. Given that, the studied areas have already shown their clinical efficacy with similar montages as the ones we used, we consider the average electric field values obtained with the bipolar montages as the minimum value needed on a patient for attain the desired effect (0.054 V/m as for lDLPFC and 0.021 V/m as for lPMC).

We consider multichannel montages a better alternative to bipolar distributions, since they have shown to achieve better results both in terms of focality and E-field magnitude. As it was expected, the more number of available electrodes used leads to a better solution. However, we must bear in mind the current limiting factor. Although we increase the number of electrodes, if this factor is very restrictive we are only going to get is a better focality. Neither the electric field values will increase, nor the variability between subjects will be reduced.

The variations in the electric field are mainly caused by the individuals differences of the brain. The distribution of sulci and gyri areas is different for every subject, causing the studied variability. For this reason, we consider as necessary calculating with a computational analysis the different parameters (electrodes location and currents) previous to a tES session, in order to precisly induced the desired E-field on a patient.

10. Economic analysis

In this section, the different expenses associated to the project will be evaluated. For a more detailed evaluation, this section has been divided in different parts. Starting with an analysis of the expenses associated with materials, followed by the licence needed and finishing with an analysis detailing human expenses.

Concept	Quantity	Hours used	Total price (€)
Computer	1	1100	1350€

Concept	Quantity	Price/unit	Total prince (€)
Scientific articles	26	50€	1300€
Matlab	1	800€ (1 year)	800€
SimNibs	1	-	-
ITK Snap	1	-	-
Python	1	-	-

Concept	Hours	Price/hour (€/h)	Total price (€)
Research	100	25	2500
Defining parameters of the study	20	25	500
Calculations and results	300	25	7500
Document generation	100	25	2500

Concept	*Price (€)*
Materials	1350
Licences	2100
Human resources	13000
TOTAL Price	**16450**

Table 11: *Economic analysis*

It is necessary to clarify, that the real costs associated with the project are null. Since the computer, the only material expense, has not been purchased exclusively for this job, but was previously owned. The licenses for the articles have been provided by Neuroelectrics, as well as the Matlab license that has been provided by the UPC. Finally, the human expenses in this project are null, since the student does not expect any type of economic remuneration, as has been established in the contract.

11. Bibliography

Aberra, Aman S., Boshuo Wang, Warren M. Grill, and Angel V. Peterchev. 2020. "Simulation of Transcranial Magnetic Stimulation in Head Model with Morphologically-Realistic Cortical Neurons." *Brain Stimulation* 13 (1): 175–89. https://doi.org/10.1016/j.brs.2019.10.002.

Antal, A., I. Alekseichuk, M. Bikson, J. Brockmöller, A. R. Brunoni, R. Chen, L. G. Cohen, et al. 2017. "Low Intensity Transcranial Electric Stimulation: Safety, Ethical, Legal Regulatory and Application Guidelines." *Clinical Neurophysiology*. Elsevier Ireland Ltd. https://doi.org/10.1016/j.clinph.2017.06.001.

Baumann, Stephen B., David R. Wozny, Shawn K. Kelly, and Frank M. Meno. 1997. "The Electrical Conductivity of Human Cerebrospinal Fluid at Body Temperature." *IEEE Transactions on Biomedical Engineering* 44 (3): 220–23. https://doi.org/10.1109/10.554770.

Chau, Wilkin, and Anthony R. McIntosh. 2005. "The Talairach Coordinate of a Point in the MNI Space: How to Interpret It." *NeuroImage* 25 (2): 408–16. https://doi.org/10.1016/j.neuroimage.2004.12.007.

Datta, Abhishek, Varun Bansal, Julian Diaz, Jinal Patel, Davide Reato, and Marom Bikson. 2009. "Gyri-Precise Head Model of Transcranial Direct Current Stimulation: Improved Spatial Focality Using a Ring Electrode versus Conventional Rectangular Pad." *Brain Stimulation* 2 (4): 201-207.e1. https://doi.org/10.1016/j.brs.2009.03.005.

Jurcak, Valer, Daisuke Tsuzuki, and Ippeita Dan. 2007. "10/20, 10/10, and 10/5 Systems Revisited: Their Validity as Relative Head-Surface-Based Positioning Systems." *NeuroImage* 34 (4): 1600–1611. https://doi.org/10.1016/j.neuroimage.2006.09.024.

Knotkova, Helena, Michael Nitsche, Marom Bikson, and Adam J Woods. 2019. *Practical Guide to Transcranial Direct Current Stimulation : Principles, Procedures and Applications*.

Laakso, Ilkka, Satoshi Tanaka, Soichiro Koyama, Valerio De Santis, and Akimasa Hirata. 2015. "Inter-Subject Variability in Electric Fields of Motor Cortical TDCS." *Brain Stimulation* 8 (5): 906–13. https://doi.org/10.1016/j.brs.2015.05.002.

Laakso, Ilkka, Satoshi Tanaka, Marko Mikkonen, Soichiro Koyama, Norihiro Sadato, and Akimasa Hirata. 2016. "Electric Fields of Motor and Frontal TDCS in a Standard Brain Space: A Computer Simulation Study." *NeuroImage* 137: 140–51. https://doi.org/10.1016/j.neuroimage.2016.05.032.

Lefaucheur, Jean Pascal, Andrea Antal, Samar S. Ayache, David H. Benninger, Jérôme Brunelin, Filippo Cogiamanian, Maria Cotelli, et al. 2017. "Evidence-Based Guidelines on the Therapeutic Use of Transcranial Direct Current Stimulation (TDCS)." *Clinical Neurophysiology* 128 (1): 56–92. https://doi.org/10.1016/j.clinph.2016.10.087.

Lefaucheur, Jean Pascal, and Fabrice Wendling. 2019. "Mechanisms of Action of TDCS: A Brief and Practical Overview." *Neurophysiologie Clinique*. https://doi.org/10.1016/j.neucli.2019.07.013.

Ministerio para la Transición Ecológica y el Reto Demográfico. 2015. “Guía Para El Cálculo de La Huella de Carbono y Para La Elaboración de Un Plan de Mejora de Una Organización.” *Gobierno de España*, 65. https://www.miteco.gob.es/es/cambio-climatico/temas/mitigacion-politicas-y-medidas/guia_huella_carbono_tcm30-479093.pdf.

Miranda, Pedro C., María A. Callejón-Leblic, Ricardo Salvador, and Giulio Ruffini. 2018. “Realistic Modeling of Transcranial Current Stimulation: The Electric Field in the Brain.” *Current Opinion in Biomedical Engineering* 8: 20–27. https://doi.org/10.1016/j.cobme.2018.09.002.

Miranda, Pedro Cavaleiro, Abeye Mekonnen, Ricardo Salvador, and Giulio Ruffini. 2013. “The Electric Field in the Cortex during Transcranial Current Stimulation.” *NeuroImage* 70: 48–58. https://doi.org/10.1016/j.neuroimage.2012.12.034.

Nitsche, M. A., and W. Paulus. 2000. “Excitability Changes Induced in the Human Motor Cortex by Weak Transcranial Direct Current Stimulation.” *Journal of Physiology* 527 (3): 633–39. https://doi.org/10.1111/j.1469-7793.2000.t01-1-00633.x.

Opitz, Alexander, Walter Paulus, Susanne Will, Andre Antunes, and Axel Thielscher. 2015. “Determinants of the Electric Field during Transcranial Direct Current Stimulation.” *NeuroImage* 109: 140–50. https://doi.org/10.1016/j.neuroimage.2015.01.033.

Plonsey, Robert, and Dennis B. Heppner. 1967. “Considerations of Quasi-Stationarity in Electrophysiological Systems.” *The Bulletin of Mathematical Biophysics*. https://doi.org/10.1007/BF02476917.

Radman, Thomas, Raddy L. Ramos, Joshua C. Brumberg, and Marom Bikson. 2009. “Role of Cortical Cell Type and Morphology in Subthreshold and Suprathreshold Uniform Electric Field Stimulation in Vitro.” *Brain Stimulation* 2 (4): 215-228.e3. https://doi.org/10.1016/j.brs.2009.03.007.

Reato, Davide, Ricardo Salvador, Marom Bikson, Alexander Opitz, Jacek Dmochowski, and Pedro C Miranda. 2019. “Principles of Transcranial Direct Current Stimulation (TDCS): Introduction to the Biophysics of TDCS.” In *Practical Guide to Transcranial Direct Current Stimulation: Principles, Procedures and Applications*, edited by Helena Knotkova, Michael A Nitsche, Marom Bikson, and Adam J Woods, 45–80. Cham: Springer International Publishing. https://doi.org/10.1007/978-3-319-95948-1_2.

Ruffini, Giulio, Michael D. Fox, Oscar Ripolles, Pedro Cavaleiro Miranda, and Alvaro Pascual-Leone. 2014. “Optimization of Multifocal Transcranial Current Stimulation for Weighted Cortical Pattern Targeting from Realistic Modeling of Electric Fields.” *NeuroImage* 89: 216–25. https://doi.org/10.1016/j.neuroimage.2013.12.002.

Ruffini, Giulio, Ricardo Salvador, Ehsan Tadayon, Roser Sanchez-Todo, Alvaro Pascual-Leone, and Emiliano Santarnecchi. 2020. “Realistic Modeling of Mesoscopic Ephaptic Coupling in the Human Brain.” *PLOS Computational Biology* 16 (6): e1007923. https://doi.org/10.1371/journal.pcbi.1007923.

Ruffini, Giulio, Fabrice Wendling, Isabelle Merlet, Behnam Molaee-Ardekani, Abeye Mekonnen, Ricardo Salvador, Aureli Soria-Frisch, Carles Grau, Stephen Dunne, and Pedro C. Miranda. 2013.

"Transcranial Current Brain Stimulation (TCS): Models and Technologies." *IEEE Transactions on Neural Systems and Rehabilitation Engineering* 21 (3): 333–45. https://doi.org/10.1109/TNSRE.2012.2200046.

Ruffini, Giulio, Fabrice Wendling, Roser Sanchez-Todo, and Emiliano Santarnecchi. 2018. "Targeting Brain Networks with Multichannel Transcranial Current Stimulation (TCS)." *Current Opinion in Biomedical Engineering* 8 (November). https://doi.org/10.1016/j.cobme.2018.11.001.

Ruohonen, Jarmo, and Jari Karhu. 2012. "TDCS Possibly Stimulates Glial Cells." *Clinical Neurophysiology*. https://doi.org/10.1016/j.clinph.2012.02.082.

Rush, Stanley, and Daniel A. Driscoll. 1969. "Eeg Electrode Sensitivity—An Application of Reciprocity." *IEEE Transactions on Biomedical Engineering* BME-16 (1): 15–22. https://doi.org/10.1109/TBME.1969.4502598.

Saturnino, Guilherme B., André Antunes, and Axel Thielscher. 2015. "On the Importance of Electrode Parameters for Shaping Electric Field Patterns Generated by TDCS." *NeuroImage* 120: 25–35. https://doi.org/10.1016/j.neuroimage.2015.06.067.

IXI Dataset. 2020 "Brain Development". *Brain-Development.Org*. Accessed June 5. https://brain-development.org/ixi-dataset/.

Nifti. 2020 "NIfTI ". *Neuroimaging Informatics Technology Initiative*. Accessed June 17. https://nifti.nimh.nih.gov/.

Stimtargeter. 2020. *Neuroelectrics: Reinventing Brain Health*. Accessed June 21. https://www.neuroelectrics.com/solutions/target-editor/.

Simnibs. 2020 "Simnibs User Home". *Simnibs.Drcmr.Dk*. Accessed June 23. https://simnibs.drcmr.dk/.

Annex A Numerical results for the manual corrections.

Subject	Target En-field (V/m)	Total current (mA) - Limit	Max current per electrode - Limit (mA)	Num channels	ERNI (mV^2/m^2)	WCC	Max current per electrode - Mnt (mA	Total current (mA) - Mnt	Average En on target (V/m)
Colin	0.25	4	2	2	-2170.8	0.40	1726	1726	0.040
				4	-3467.2	0.51	1999	2457	0.061
				6	-4024.7	0.54	1806	3998	0.072
				8	-4217.5	0.56	1999	3997	0.073
		2	1	2	-2287.1	0.41	1000	1000	0.042
				4	-3176.8	0.49	1000	1625	0.052
				6	-3605.5	0.52	999	1998	0.058
				8	-3756.7	0.53	999	1998	0.057
	0.5	4	2	2	-8203.5	0.39	2000	2000	0.068
				4	-12707.0	0.49	2000	3251	0.105
				6	-14929.0	0.54	2000	3999	0.112
				8	-15022.9	0.54	1998	3997	0.113
		2	1	2	-6490.0	0.36	1000	1000	0.045
				4	-10522.8	0.47	1000	2000	0.072
				6	-10955.6	0.49	1000	1997	0.072
				8	-11001.1	0.49	999	1998	0.073
	0.15	4	2	2	-781.5	0.40	1035	1035	0.024
				4	-1262.9	0.51	1613	1928	0.039
				6	-1443.4	0.54	848	1726	0.045
				8	-1620.3	0.58	1660	3950	0.051
Colin-Corr	0.25	4	2	2	-7945.3	0.39	2000	1878	0.070
				4	-12370.8	0.49	2000	3250	0.103
				6	-15675.5	0.51	1998	3550	0.099
				8	-15022.9	0.54	1998	3997	0.113
		2	1	2	-2287.1	0.41	1000	1000	0.042
				4	-3189.8	0.49	1000	1625	0.049
				6	-3785.8	0.48	1000	1998	0.055
				8	-3756.7	0.53	999	1998	0.057
	0.5	4	2	2	-2287.1	0.41	1000	1000	0.042
				4	-3189.8	0.49	1000	1625	0.049
				6	-3785.8	0.48	1000	1998	0.055
				8	-4217.5	0.56	1999	3997	0.073
		2	1	2	-6490.0	0.35	1000	1000	0.045
				4	-10405.7	0.47	1000	2000	0.072
				6	-10736.5	0.50	1000	2000	0.073
				8	-11001.1	0.49	1000	2000	0.073
	0.15	4	2	2	-781.5	0.40	1035	1035	0.024
				4	-1279.0	0.51	2000	2781	0.036
				6	-1438.3	0.54	862	1664	0.044
				8	-1620.3	0.58	1660	3950	0.051

Subject	Target En-field (V/m)	Total current (mA) - Limit	Max current per electrode - Limit (mA)	Num channels	ERNI (mV^2/m^2)	WCC	Max current per electrode - Mnt (mA	Total current (mA) - Mnt	Average En on target (V/m)
Colina	0.25	4	2	2	-2070.0	0.40	686	686	0.039
				4	-2975.2	0.48	1119	1378	0.056
				6	-3573.6	0.52	1768	2376	0.068
				8	-3942.2	0.55	2000	3654	0.071
		2	1	2	-2070.0	0.40	686	686	0.039
				4	-2965.8	0.48	999	1311	0.055
				6	-3357.4	0.51	1000	1672	0.063
				8	-3564.7	0.53	1000	1996	0.057
	0.5	4	2	2	-8280.1	0.40	1372	1372	0.079
				4	-11863.9	0.48	2000	2624	0.110
				6	-13802.6	0.51	1999	3743	0.122
				8	-14511.5	0.53	2000	3995	0.124
		2	1	2	-7670.0	0.40	1000	1000	0.057
				4	-10689.4	0.45	1000	1891	0.097
				6	-11558.4	0.48	1000	1998	0.092
				8	-11909.4	0.49	999	1996	0.091
	0.15	4	2	2	-745.2	0.40	411	411	0.024
				4	-1207.5	0.51	1265	1465	0.039
				6	-1338.0	0.53	1394	1992	0.043
				8	-1437.7	0.55	1954	2996	0.046
Colina-Corr	0.25	4	2	2	-8280.1	0.40	1372	1372	0.079
				4	-11863.9	0.48	2000	2624	0.110
				6	-13531.7	0.52	2000	4000	0.116
				8	-14376.4	0.53	2000	4000	0.125
		2	1	2	-7670.0	0.40	1000	1000	0.057
				4	-10829.9	0.45	1000	1782	0.099
				6	-11851.6	0.47	1000	1997	0.089
				8	-14115.6	0.42	998	1993	0.089
	0.15	4	2	2	-674.4	0.42	525	525	0.026
				4	-1207.5	0.51	1265	1465	0.039
				6	-1380.4	0.52	1098	1335	0.040
				8	-1489.3	0.54	984	2077	0.040

Annex B Results for the target area 'lDLPFC'

B1. Numerical results

Subject	Target E-n field (V/m)	Total current (mA) - Limit	Max current per electrode - Limit (mA)	Num channels	ERN (mV^2/m^2)	WCC	Max current per electrode - Mnt (mA)	Total current (mA) - Mnt	Average Eron target (V/m)
Colin	0.25	4	2	2	-217.08	0.40	1726	1726	0.040
				4	-346.72	0.51	1999	2457	0.061
				6	-402.47	0.54	1806	3998	0.072
				8	-421.75	0.56	1999	3997	0.073
		4	1	2	-205.19	0.39	999	999	0.034
				4	-317.48	0.49	1000	1625	0.052
				6	-390.64	0.54	1000	2446	0.066
				8	-404.21	0.55	1000	2932	0.068
		2	2	2	-207.16	0.39	1114	1114	0.038
				4	-345.83	0.50	1993	1993	0.063
				6	-371.90	0.53	1093	1999	0.058
				8	-375.70	0.54	1026	1997	0.057
	0.5	4	2	2	-820.35	0.39	2000	2000	0.088
				4	-1270.70	0.49	2000	3251	0.105
				6	-1492.90	0.54	2000	3999	0.112
				8	-1502.29	0.54	1998	3997	0.113
		4	1	2	-630.71	0.36	1000	1000	0.044
				4	-1052.28	0.47	1000	2000	0.072
				6	-1208.56	0.48	1000	2966	0.084
				8	-1371.44	0.51	999	3832	0.103
		2	2	2	-820.35	0.39	2000	2000	0.088
				4	-1095.43	0.47	1999	1999	0.078
				6	-1117.97	0.49	1545	1999	0.075
				8	-1119.74	0.48	1542	1997	0.076
		2	1	2	-649.00	0.36	1000	1000	0.045
				4	-1052.28	0.47	1000	2000	0.072
				6	-1095.56	0.49	1000	1997	0.072
				8	-1100.11	0.49	999	1998	0.073
Subject	Target E-n field (V/m)	Total current (mA) - Limit	Max current per electrode - Limit (mA)	Num channels	ERN (mV^2/m^2)	WCC	Max current per electrode - Mnt (mA)	Total current (mA) - Mnt	Average Eron target (V/m)
Colina	0.25	4	2	2	-207.0.0	0.40	686	686	0.039
				4	-297.5.2	0.48	1119	1378	0.056
				6	-357.3.6	0.52	1768	2376	0.068
				8	-384.2.2	0.55	2000	3654	0.071
		4	1	2	-207.0.0	0.40	686	686	0.039
				4	-296.6.0	0.47	999	1311	0.055
				6	-342.2.0	0.51	999	1820	0.061
				8	-369.1.0	0.53	1000	2568	0.067
		2	2	2	-207.0.0	0.40	686	686	0.039
				4	-297.5.2	0.47	1119	1378	0.056
				6	-355.0.3	0.50	1321	1999	0.060
				8	-363.1.9	0.53	1121	1998	0.061
		2	1	2	-207.0.0	0.40	686	686	0.039
				4	-296.5.8	0.48	999	1311	0.055
				6	-335.7.4	0.51	1001	1672	0.063
				8	-356.4.7	0.53	1000	1996	0.057
	0.5	4	2	2	-828.0.1	0.40	1372	1372	0.079
				4	-1186.3.9	0.48	2000	2624	0.110
				6	-1380.2.6	0.51	1999	3743	0.122
				8	-1451.1.5	0.53	2000	3995	0.124
		4	1	2	-767.0.0	0.40	1000	1000	0.057
				4	-1082.9.9	0.45	1000	1999	0.094
				6	-1268.6.6	0.49	1000	2550	0.109
				8	-1346.2.1	0.51	1000	2999	0.110
		2	2	2	-828.0.1	0.40	1372	1372	0.079
				4	-1186.3.9	0.48	2000	2624	0.110
				6	-1380.2.6	0.51	1999	3743	0.122
				8	-1451.1.5	0.53	2000	3995	0.124
		2	1	2	-767.0.0	0.40	1000	1000	0.057
				4	-1082.9.9	0.45	1000	1999	0.094
				6	-1268.6.6	0.49	1000	2550	0.109
				8	-1346.2.1	0.51	1000	2999	0.110
	0.5	4	2	2	-828.0.1	0.40	1372	1372	0.079
				4	-1114.3.3	0.47	1383	1999	0.087
				6	-1177.6.7	0.49	926	1998	0.087
				8	-1194.0.2	0.49	1131	1997	0.089
		2	2	2	-767.0.0	0.40	1000	1000	0.057
				4	-1068.9.4	0.45	1000	1891	0.097
				6	-1155.8.4	0.48	1000	1998	0.092
				8	-1190.9.4	0.49	999	1996	0.091

Subject	Target En-field (V/m)	Total current (mA) - Limit	Max current per electrode - Limit (mA)	Num channels	ERNI (mV^2/m^2)	WCC	Max current per electrode - Mnt (mA)	Total current (mA) - Mnt	Average En-on target (V/m)
IXI 038	0.25	4	2	2	-2986.1	0.46	996	996	0.053
				4	-3853.3	0.52	1334	1786	0.068
				6	-4509.0	0.56	2000	3017	0.078
				8	-4504.5	0.56	1999	3327	0.079
		4	1	2	-2986.1	0.46	996	996	0.053
				4	-3798.8	0.52	1000	1588	0.064
				6	-4260.9	0.55	1000	2027	0.074
				8	-4555.0	0.57	1000	2701	0.078
		2	2	2	-2986.1	0.46	996	996	0.053
				4	-3853.3	0.52	1334	1786	0.068
				6	-4310.5	0.55	1261	1999	0.074
				8	-4368.3	0.56	1027	1998	0.070
		2	1	2	-2986.1	0.46	996	996	0.053
				4	-3798.8	0.52	999	1587	0.064
				6	-4259.8	0.55	999	1998	0.073
				8	-4364.6	0.56	990	1997	0.069
	0.5	4	2	2	-11944.5	0.46	1993	1993	0.106
				4	-15195.4	0.52	2000	3176	0.129
				6	-17039.2	0.55	2000	3999	0.147
				8	-17471.4	0.56	2000	3998	0.139
		4	1	2	-2986.1	0.46	996	996	0.053
				4	-13184.7	0.49	1000	1999	0.098
				6	-15566.0	0.53	1000	3000	0.123
				8	-15978.9	0.54	999	3167	0.123
		2	2	2	-11944.5	0.46	1993	1993	0.106
				4	-13772.8	0.51	1999	1999	0.099
				6	-14071.8	0.52	1664	1999	0.096
				8	-14103.6	0.52	1683	1998	0.097
		2	1	2	-8977.4	0.46	1000	1000	0.053
				4	-13265.7	0.51	999	1998	0.091
				6	-13803.6	0.52	1000	1998	0.094
				8	-13883.3	0.52	999	1997	0.094
IXI 033	0.25	4	2	2	-2359.7	0.41	999	999	0.034
				4	-3334.9	0.49	1000	1874	0.055
				6	-3802.2	0.52	1000	2381	0.064
				8	-4056.4	0.54	1000	3104	0.068
		2	1	2	-2359.7	0.41	999	999	0.034
				4	-3334.9	0.49	1000	1874	0.055
				6	-3802.2	0.52	1000	2381	0.064
				8	-4056.4	0.54	1000	3104	0.068
		2	2	2	-2360.4	0.41	1260	1260	0.042
				4	-3723.7	0.52	2000	2304	0.064
				6	-3959.3	0.53	1999	2815	0.067
				8	-4340.0	0.56	2000	3999	0.073
		4	2	2	-2360.4	0.41	1260	1260	0.042
				4	-3634.0	0.52	1779	1999	0.056
				6	-3739.2	0.51	1315	1999	0.057
				8	-3769.1	0.53	1295	1998	0.057
	0.5	2	1	2	-2259.7	0.41	999	999	0.034
				4	-3334.9	0.49	1000	1874	0.055
				6	-3683.2	0.52	999	1998	0.058
				8	-3753.3	0.53	998	1997	0.056
		4	2	2	-9038.7	0.41	2000	2000	0.067
				4	-13339.5	0.49	1999	3748	0.109
				6	-14796.8	0.53	1999	3998	0.109
				8	-15005.9	0.53	1999	3998	0.110
		4	2	2	-6005.2	0.41	999	999	0.034
				4	-10698.7	0.47	999	1998	0.071
				6	-12753.1	0.49	1000	3000	0.096
				8	-13678.8	0.51	999	3670	0.099
	0.5	2	1	2	-9038.7	0.41	2000	2000	0.067
				4	-10926.2	0.48	1587	1999	0.068
				6	-11005.7	0.49	1218	1998	0.069
				8	-11044.2	0.49	1199	1997	0.069
		2	2	2	-6005.2	0.41	1000	1000	0.034
		4	4	4	-10698.7	0.47	1000	2000	0.071
		6	6	6	-10945.5	0.48	974	1999	0.072
		8	8	8	-11030.5	0.49	999	1998	0.069

Subject	Target En-field (V/m)	Total current (mA) - Limit	Max current per electrode - Limit (mA)	Num channels	ERNI (mV^2/m^2)	WCC	Max current per electrode - Mnt (mA)	Total current (mA) - Mnt	Average En on target (V/m)
IXI 002	0.25	4	2	2	-2325.6	0.43	921	921	0.046
				4	-3231.7	0.50	1323	1664	0.064
				6	-3692.1	0.54	1909	2827	0.073
				8	-3891.3	0.55	1882	3849	0.077
		4	1	2	-2325.6	0.43	921	921	0.046
				4	-3178.4	0.50	1000	1481	0.059
				6	-3546.5	0.53	1000	1981	0.070
				8	-3742.8	0.54	1000	2614	0.072
		2	2	2	-2325.6	0.43	921	921	0.046
				4	-3231.7	0.50	1323	1664	0.064
				6	-3549.6	0.53	1149	1969	0.070
				8	-3639.8	0.54	892	1998	0.065
		2	1	2	-2325.6	0.43	921	921	0.046
				4	-2893.5	0.48	999	999	0.048
				6	-3546.5	0.53	1000	1981	0.070
				8	-3584.0	0.53	1000	1999	0.070
	0.5	4	2	2	-9302.5	0.43	1842	1842	0.092
				4	-12713.6	0.50	2000	2962	0.119
				6	-14186.1	0.53	2000	3964	0.139
				8	-14560.7	0.54	1793	3998	0.129
		4	1	2	-7358.3	0.43	1000	1000	0.050
				4	-11012.5	0.49	1000	2000	0.084
				6	-12995.1	0.51	1000	2869	0.115
				8	-13431.1	0.52	1000	2998	0.112
		2	2	2	-9302.5	0.43	1842	1842	0.092
				4	-11573.9	0.48	1999	1999	0.097
				6	-11754.1	0.49	1744	1997	0.095
				8	-11783.5	0.50	1668	1998	0.094
		2	1	2	-7358.3	0.43	999	999	0.050
				4	-11012.5	0.49	1000	1999	0.084
				6	-11570.1	0.49	1000	1999	0.093
				8	-11644.9	0.50	1000	1997	0.089

Subject	Target En-field (V/m)	Total current (mA) - Limit	Max current per electrode - Limit (mA)	Num channels	ERNI (mV^2/m^2)	WCC	Max current per electrode - Mnt (mA)	Total current (mA) - Mnt	Average En on target (V/m)
IXI 022	0.25	4	2	2	-1641.1	0.35	785	785	0.031
				4	-2450.7	0.43	1420	1658	0.046
				6	-2708.8	0.45	1333	2162	0.051
				8	-3229.5	0.49	2000	3416	0.056
		4	1	2	-1641.1	0.35	785	785	0.031
				4	-2200.0	0.41	873	1310	0.041
				6	-2747.4	0.45	999	1953	0.049
				8	-3058.9	0.48	1000	2984	0.055
		2	2	2	-1641.1	0.35	785	785	0.031
				4	-2450.7	0.43	1420	1658	0.046
				6	-2794.3	0.46	1327	1999	0.051
				8	-2870.2	0.47	791	1998	0.047
		2	1	2	-1641.1	0.35	785	785	0.031
				4	-2379.7	0.42	1000	1401	0.042
				6	-2742.8	0.45	999	1839	0.049
				8	-2870.2	0.47	774	1996	0.046
	0.5	4	2	2	-6564.5	0.35	1571	1571	0.062
				4	-8799.8	0.41	1747	2622	0.083
				6	-10989.8	0.45	2000	3909	0.099
				8	-11480.9	0.47	1561	3998	0.094
		4	1	2	-5696.7	0.35	999	999	0.039
				4	-8298.4	0.40	1000	1999	0.064
				6	-9717.3	0.43	1000	2699	0.083
				8	-10389.3	0.45	1000	2998	0.087
		2	2	2	-6564.5	0.35	1571	1571	0.062
				4	-8781.0	0.41	1999	1999	0.072
				6	-9153.7	0.43	1446	1998	0.069
				8	-9194.7	0.43	1353	1997	0.069
		2	1	2	-5696.7	0.35	999	999	0.039
				4	-8298.4	0.40	1000	1999	0.064
				6	-9046.3	0.43	999	1998	0.065
				8	-9105.4	0.43	999	1998	0.066

Subject	Target En-field (V/m)	Total current (mA) - Limit	Max current per electrode - Limit (mA)	Num channels	ERNI (mV^2/m^2)	WCC	Max current per electrode - Mrt (mA)	Total current (mA) - Mrt	Average En on target (V/m)
IXI 013	0.25	4	2	2	-1596.3	0.33	976	976	0.028
				4	-2830.0	0.45	1998	1998	0.042
				6	-3203.9	0.47	2000	3759	0.056
				8	-3408.1	0.49	2000	3999	0.053
		4	1	2	-1596.3	0.33	976	976	0.028
				4	-2493.2	0.42	1648	1999	0.039
				6	-2954.5	0.45	1000	2378	0.048
				8	-3262.7	0.48	1000	3185	0.051
		2	2	2	-1596.3	0.33	976	976	0.028
				4	-2830.0	0.45	1998	1998	0.042
				6	-2884.9	0.46	1555	1998	0.043
				8	-2924.7	0.45	852	1999	0.043
		2	1	2	-1596.3	0.33	976	976	0.028
				4	-2493.2	0.42	999	1648	0.039
				6	-2877.1	0.46	1000	1999	0.041
				8	-2924.3	0.46	859	1998	0.042
	0.5	4	2	2	-4863.9	0.33	999	999	0.028
				4	-8410.2	0.41	999	1998	0.055
				6	-9867.2	0.42	1000	2984	0.077
				8	-10643.5	0.44	1000	3521	0.078
		4	1	2	-4863.9	0.33	999	999	0.028
				4	-8410.2	0.41	999	1998	0.055
				6	-9867.2	0.42	1000	2984	0.077
				8	-10643.5	0.44	1000	3521	0.078
		2	2	2	-6385.3	0.33	1953	1953	0.056
				4	-8554.5	0.42	1427	1999	0.054
				6	-8708.9	0.43	1230	1998	0.053
				8	-8738.1	0.43	1206	1997	0.054
		2	1	2	-4863.9	0.33	999	999	0.028
				4	-8410.2	0.41	999	1998	0.055
				6	-8705.9	0.42	1000	1998	0.055
				8	-8727.0	0.42	999	1997	0.055
IXI 045	0.25	4	2	2	-10101.7	0.43	1510	1510	0.093
				4	-13523.0	0.50	1987	2660	0.124
				6	-15109.8	0.53	2000	3375	0.139
				8	-16258.9	0.55	1834	3998	0.136
		4	2	2	-8948.9	0.43	1000	1000	0.061
				4	-12665.0	0.49	999	1998	0.103
				6	-13879.9	0.50	1000	2680	0.120
				8	-14902.7	0.52	1000	2998	0.126
	0.5	4	1	2	-10101.7	0.43	1510	1510	0.093
				4	-12810.1	0.49	1261	1999	0.098
				6	-13319.8	0.51	984	1998	0.096
				8	-13512.2	0.52	949	1998	0.098
		2	2	2	-8948.9	0.43	1000	1000	0.061
				4	-12665.0	0.49	1000	2000	0.103
				6	-13319.8	0.51	984	1998	0.096
				8	-13523.8	0.52	970	1998	0.098
		2	1	2	-8948.9	0.43	1000	1000	0.061
				4	-12665.0	0.49	1000	2000	0.103
				6	-13319.8	0.51	984	1998	0.096
				8	-13523.8	0.52	970	1998	0.098

Subject	Target En-field (V/m)	Total current (mA) - Limit	Max current per electrode - Limit (mA)	Num channels	ERNI (mV^2/m^2)	WCC	Max current per electrode - Mnt (mA)	Total current (mA) - Mnt	Average En on target (V/m)
IXI 050	0.25	4	2	2	-1955.1	0.37	1211	1211	0.034
				4	-3075.5	0.46	1998	1998	0.047
				6	-3785.3	0.51	1999	3944	0.062
				8	-3833.4	0.51	1978	3998	0.061
		4	1	2	-1895.3	0.37	999	999	0.028
				4	-2730.1	0.44	999	1756	0.042
				6	-3250.0	0.48	1000	2416	0.048
				8	-3599.2	0.50	1000	3554	0.057
		2	2	2	-1955.1	0.37	1211	1211	0.034
				4	-3075.5	0.46	1998	1998	0.047
				6	-3166.9	0.48	1678	1999	0.043
				8	-3176.3	0.48	1703	1997	0.044
		2	1	2	-1895.3	0.37	999	999	0.028
				4	-2730.1	0.44	999	1756	0.042
				6	-3073.2	0.48	999	2416	0.040
				8	-3092.1	0.48	999	3998	0.042
		4	2	2	-1895.3	0.37	999	999	0.028
				4	-2730.1	0.44	999	1756	0.042
				6	-3073.2	0.48	999	2416	0.040
				8	-3092.1	0.48	999	3998	0.042
	0.5	2	1	2	-7581.1	0.37	1999	1999	0.056
				4	-10920.5	0.44	3515	3515	0.084
				6	-12096.0	0.46	2000	3999	0.091
				8	-12372.6	0.48	1999	3998	0.084
		4	2	2	-5121.6	0.37	999	999	0.038
				4	-8297.2	0.40	999	1998	0.054
				6	-10309.8	0.45	1000	2998	0.067
				8	-11380.9	0.45	999	3832	0.084
		2	1	2	-5121.6	0.37	999	999	0.028
				4	-8297.2	0.40	999	1998	0.054
				6	-8825.4	0.42	999	1998	0.054
				8	-8900.5	0.43	999	1998	0.054
		4	2	2	-7581.1	0.37	1999	1999	0.056
				4	-9212.5	0.43	2000	2000	0.057
				6	-9325.4	0.44	1999	1999	0.057
				8	-9347.6	0.44	1999	1999	0.057
IXI 016	0.25	4	2	2	-8801.8	0.39	1354	1354	0.077
				4	-12234.5	0.46	1738	2314	0.108
				6	-14577.5	0.51	1999	3584	0.118
				8	-15560.2	0.53	1999	3998	0.121
		4	1	2	-8200.0	0.39	999	999	0.057
				4	-11655.0	0.45	1000	1911	0.094
				6	-13200.8	0.48	1000	2703	0.104
				8	-14577.7	0.51	1000	3379	0.110
		2	1	2	-8200.0	0.39	999	999	0.057
				4	-11655.0	0.45	1000	1911	0.094
				6	-12376.8	0.47	1171	1991	0.092
				8	-12524.9	0.48	1019	1997	0.093
		2	2	2	-8200.0	0.39	999	999	0.057
				4	-11655.0	0.45	1000	1911	0.094
				6	-12332.1	0.47	999	1998	0.093
				8	-12519.4	0.48	1000	1998	0.093
	0.5	2	1	2	-8801.8	0.39	1354	1354	0.077
				4	-12234.5	0.46	2314	2314	0.108
				6	-14577.5	0.51	1999	3584	0.118
				8	-15560.2	0.53	1999	3998	0.121
		4	2	2	-8801.8	0.39	1354	1354	0.077
				4	-12234.5	0.46	2314	2314	0.108
				6	-14577.5	0.51	1999	3584	0.118
				8	-15560.2	0.53	1999	3998	0.121

Subject	Target En-field (V/m)	Total current (mA) - Limit	Max current per electrode - Limit (mA)	Num channels	ERNI (mV^2/m^2)	WCC	Max current per electrode - Mnt (mA)	Total current (mA) - Mnt	Average En on target (V/m)
IXI 028	0.25	4	2	2	-1910.0	0.39	1202	1202	0.037
				4	-3563.9	0.53	1999	2439	0.064
				6	-4303.8	0.58	1975	3884	0.084
				8	-4412.3	0.59	1999	3998	0.079
		4	1	2	-1855.6	0.39	999	999	0.031
				4	-3016.3	0.49	999	1826	0.051
				6	-3602.8	0.53	1000	2507	0.065
				8	-3897.3	0.56	999	3121	0.064
		2	2	2	-1910.0	0.39	1202	1202	0.037
				4	-3417.3	0.54	1998	1998	0.052
				6	-3530.4	0.55	1268	1999	0.052
				8	-3556.9	0.55	1144	1997	0.054
	0.5	4	2	2	-7422.5	0.39	2000	2000	0.062
				4	-12065.1	0.49	1999	3654	0.102
				6	-14128.5	0.55	2000	3999	0.109
				8	-14223.3	0.55	1999	3996	0.108
		4	1	2	-5128.5	0.38	1000	1000	0.033
				4	-9128.2	0.46	999	1998	0.063
				6	-11184.2	0.49	1000	2598	0.083
				8	-12273.1	0.50	1000	3994	0.095
		2	2	2	-7422.5	0.39	2000	2000	0.062
				4	-9458.8	0.48	1999	1999	0.064
				6	-9688.5	0.50	1145	1998	0.064
				8	-9713.9	0.50	1150	1997	0.064
		2	1	2	-5128.5	0.38	999	999	0.033
				4	-9128.2	0.46	1000	2000	0.063
				6	-9880.0	0.50	1000	1999	0.064
				8	-9703.5	0.50	1000	1997	0.064

B2. Graphical results for the average E-field

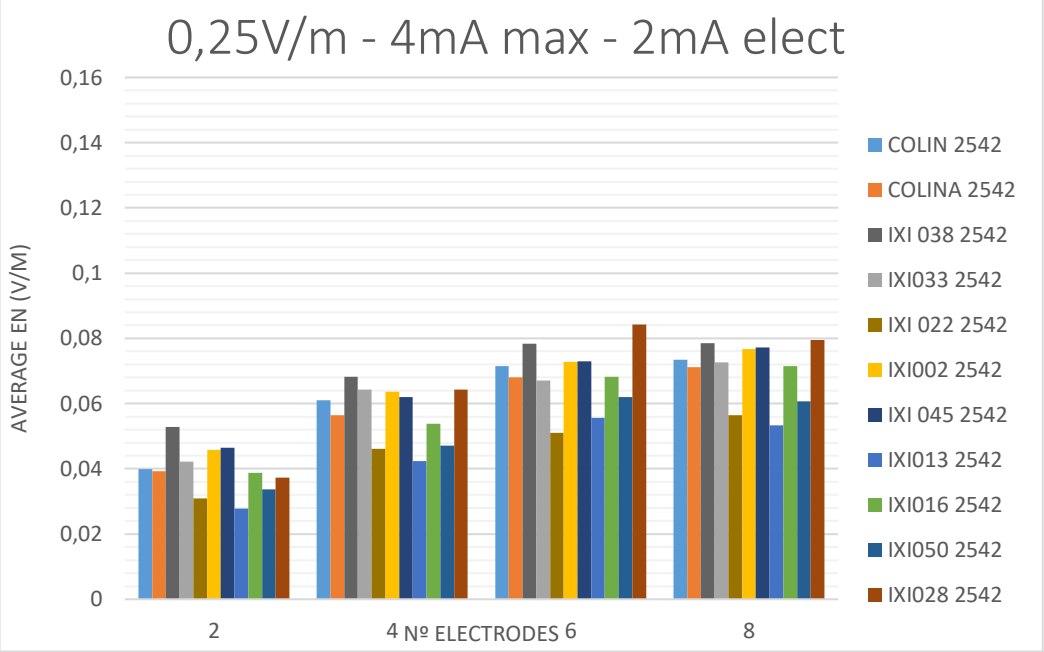

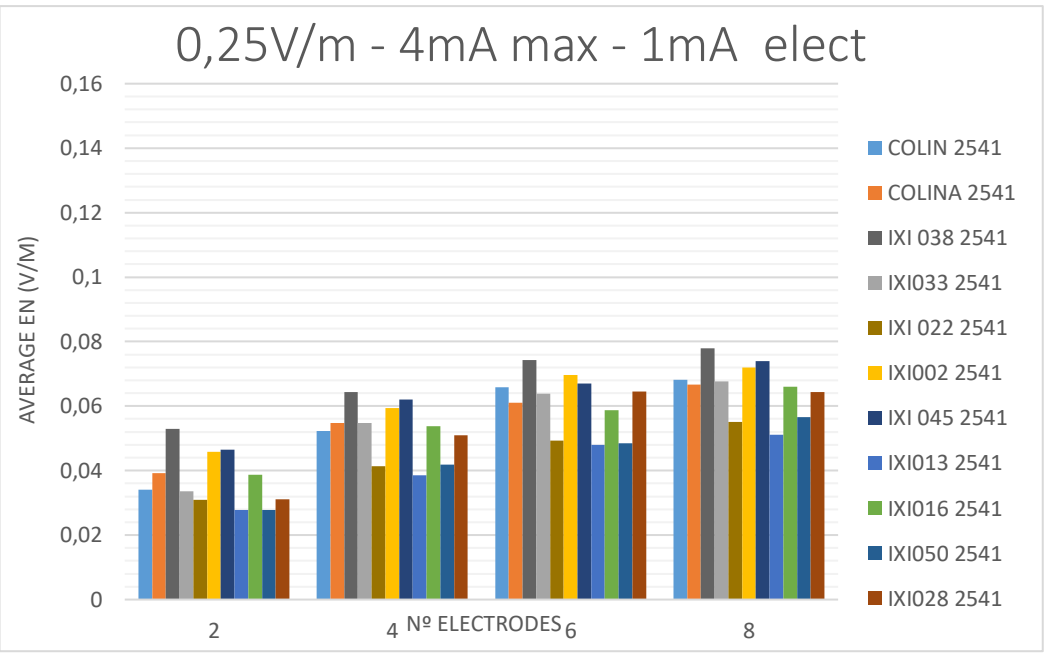

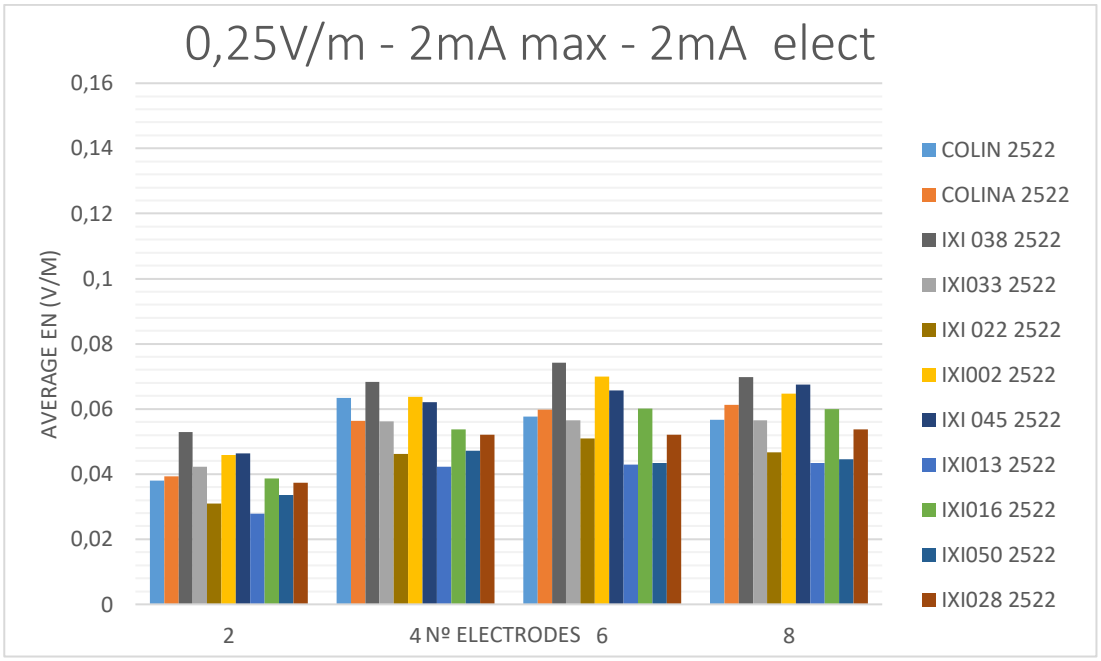
0,25V/m - 2mA max - 2mA elect
AVERAGE EN (V/M)
0,16
0,14
0,12
0,1
0,08
0,06
0,04
0,02
0
2
4
6
8
Nº ELECTRODES
COLIN 2522
COLINA 2522
IXI 038 2522
IXI033 2522
IXI 022 2522
IXI002 2522
IXI 045 2522
IXI013 2522
IXI016 2522
IXI050 2522
IXI028 2522

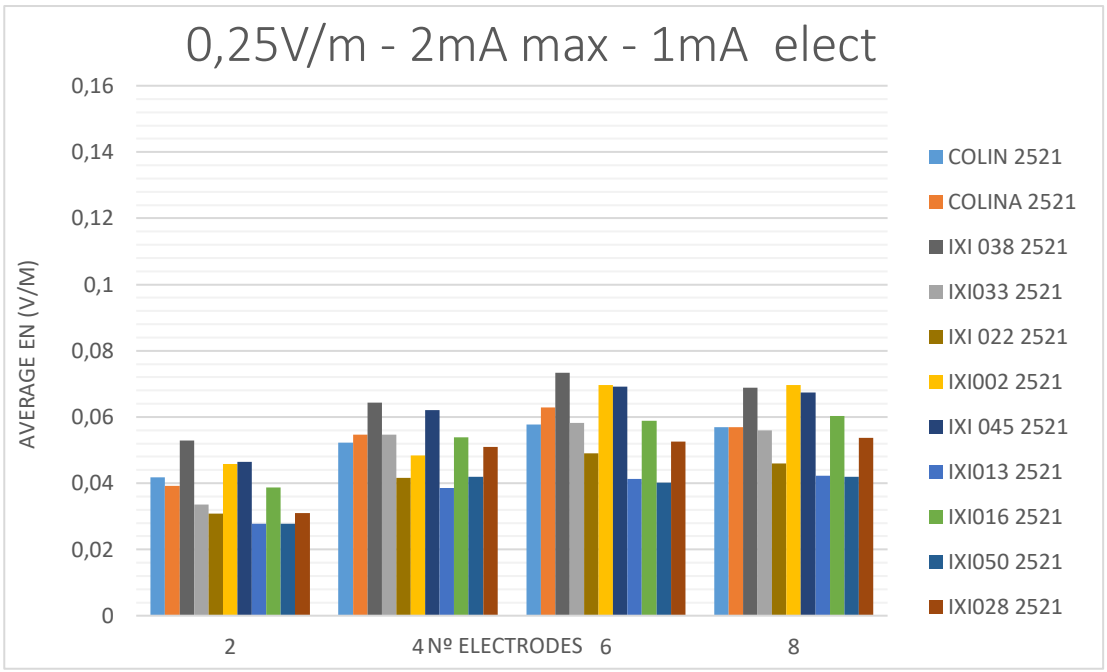
0,25V/m - 2mA max - 1mA elect
AVERAGE EN (V/M)
0,16
0,14
0,12
0,1
0,08
0,06
0,04
0,02
0
2
4
6
8
Nº ELECTRODES
COLIN 2521
COLINA 2521
IXI 038 2521
IXI033 2521
IXI 022 2521
IXI002 2521
IXI 045 2521
IXI013 2521
IXI016 2521
IXI050 2521
IXI028 2521

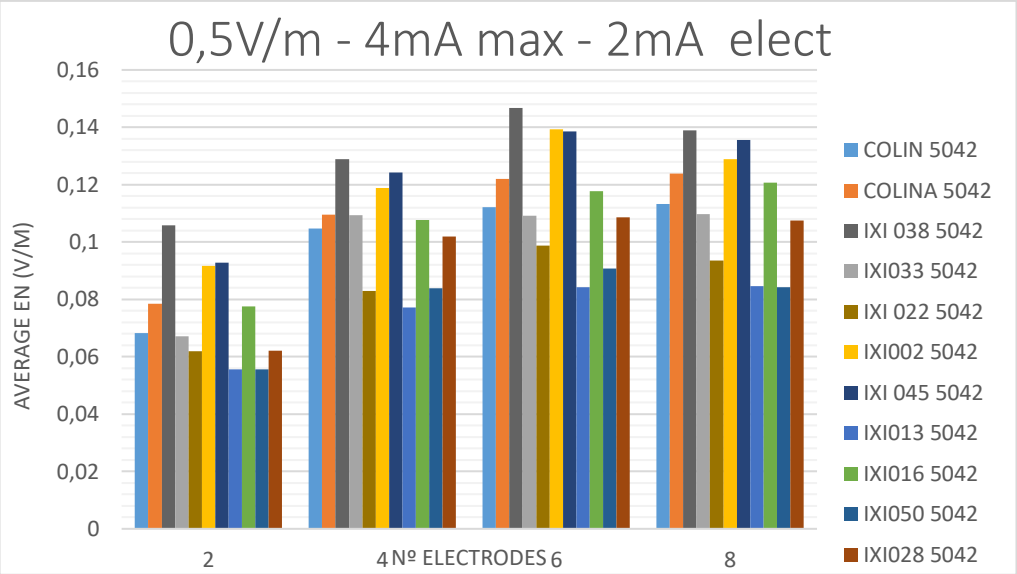
0,5V/m - 4mA max - 2mA elect
AVERAGE EN (V/M)
0,16
0,14
0,12
0,1
0,08
0,06
0,04
0,02
0
2
4
6
8
Nº ELECTRODES
COLIN 5042
COLINA 5042
IXI 038 5042
IXI033 5042
IXI 022 5042
IXI002 5042
IXI 045 5042
IXI013 5042
IXI016 5042
IXI050 5042
IXI028 5042

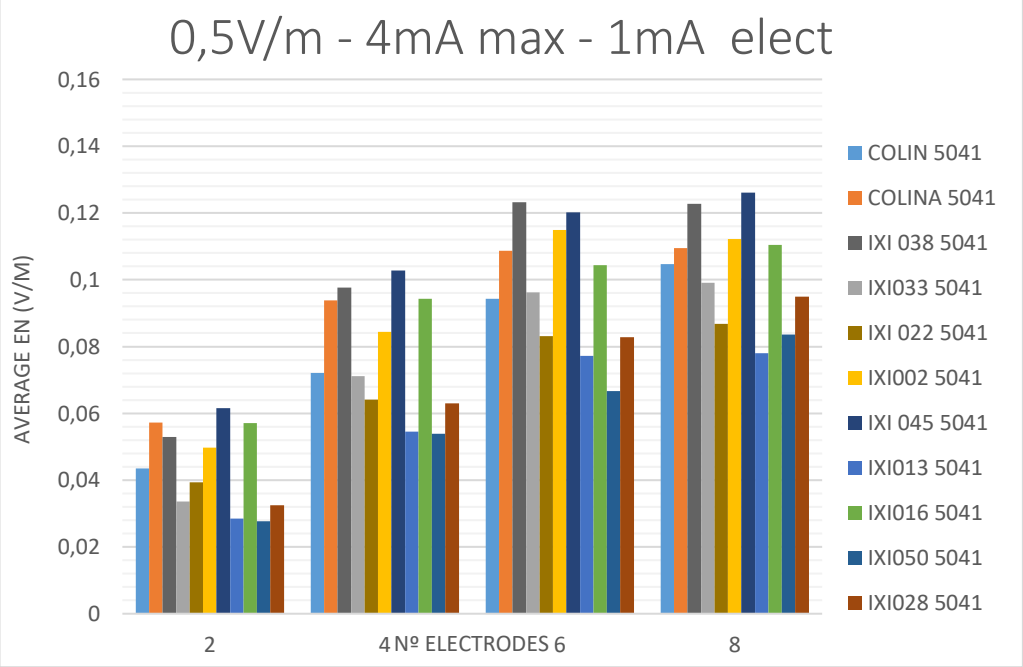
0,5V/m - 4mA max - 1mA elect
AVERAGE EN (V/M)
0,16
0,14
0,12
0,1
0,08
0,06
0,04
0,02
0
2
4
6
8
Nº ELECTRODES
COLIN 5041
COLINA 5041
IXI 038 5041
IXI033 5041
IXI 022 5041
IXI002 5041
IXI 045 5041
IXI013 5041
IXI016 5041
IXI050 5041
IXI028 5041

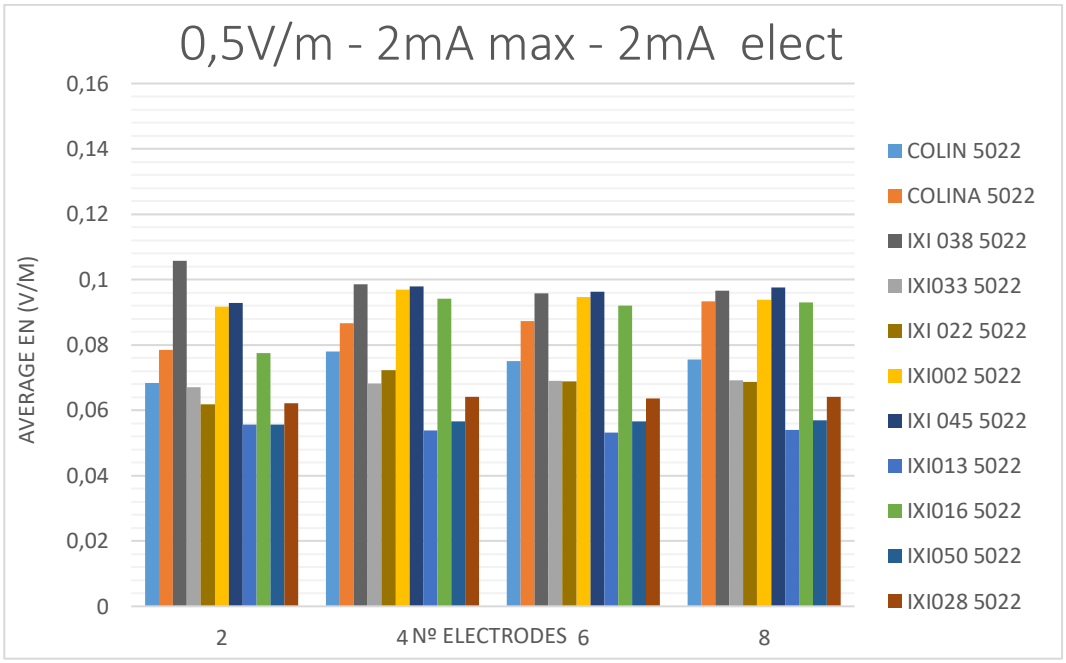

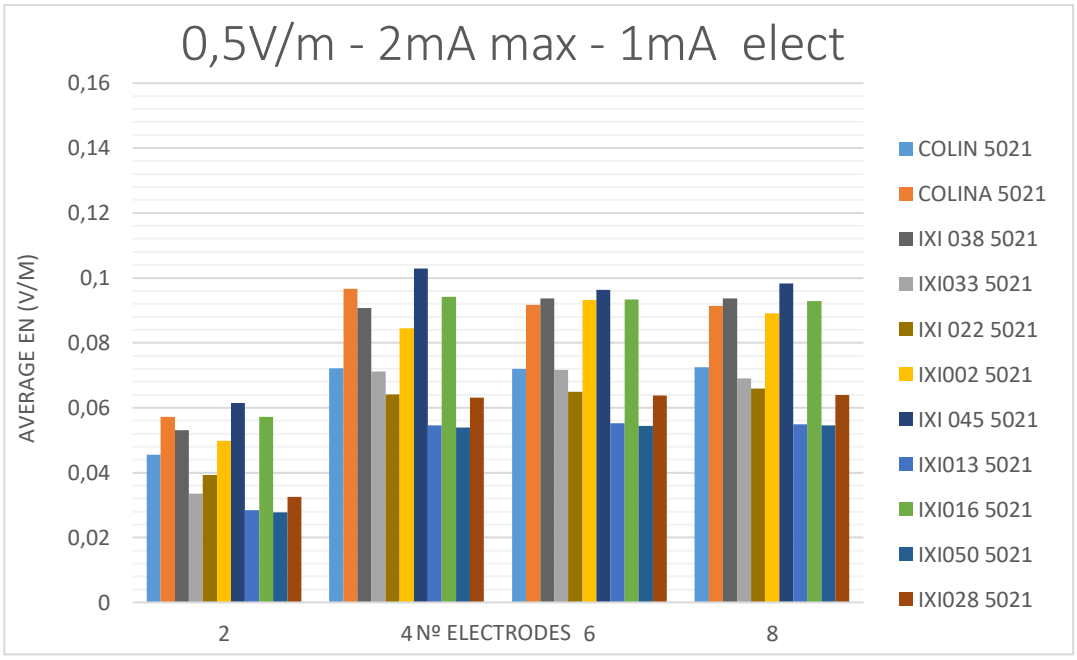

B3. Bipolar configuration results (V/m)

Colin	Colina	IXI038	IXI033	IXI022	IXI002	IXI045	IXI013	IXI016	IXI050	IXI028
0.046	0.069	0.059	0.049	0.052	0.069	0.072	0.038	0.069	0.043	0.043

MEAN	MEADIAN	SD
0.054	0.052	0.013

Annex C Results for the target area 'IPMC'

C1. Numerical results

Subject	Target En-field (V/m)	Total current (mA) - Limit	Max current per electrode - Limit (mA)	Num channels	ERNI (mV^2/m^2)	WCC	Max current per electrode - Mmt (mA)	Total current (mA) - Mmt	Average En on target (V/m)
Colin	0.25	4	2	2	-634.8	0.19	577	577	0.009
				4	-1818.3	0.33	1999	3692	0.022
				6	-2076.6	0.35	1999	3998	0.029
				8	-2260.7	0.37	1718	3999	0.027
		4	1	2	-634.8	0.19	577	577	0.009
				4	-1455.7	0.30	1000	2000	0.017
				6	-1820.1	0.33	1000	2673	0.022
				8	-1997.8	0.34	1000	3562	0.026
		2	2	2	-634.8	0.19	577	577	0.009
				4	-1458.3	0.30	1057	1999	0.017
				6	-1670.0	0.32	1144	1999	0.019
				8	-1675.1	0.33	1107	1998	0.019
		2	1	2	-634.8	0.19	577	577	0.009
				4	-1455.7	0.30	1000	2000	0.017
				6	-1652.2	0.32	1000	1999	0.019
				8	-1672.9	0.33	1000	1997	0.019
	0.5	4	2	2	-2539.2	0.19	1155	1155	0.018
				4	-5712.6	0.30	2000	3800	0.033
				6	-6652.8	0.32	2000	3999	0.038
				8	-6700.0	0.32	1999	3997	0.038
		4	1	2	-2496.5	0.19	999	999	0.017
				4	-4214.3	0.26	999	1998	0.022
				6	-5540.7	0.30	1000	3000	0.030
				8	-6125.5	0.31	1000	3969	0.034
		2	1	2	-2496.5	0.19	1000	1000	0.017
				4	-4215.0	0.28	999	1998	0.021
				6	-4641.6	0.28	999	1998	0.024
				8	-4602.5	0.28	865	1998	0.024
Subject	Target En-field (V/m)	Total current (mA) - Limit	Max current per electrode - Limit (mA)	Num channels	ERNI (mV^2/m^2)	WCC	Max current per electrode - Mmt (mA)	Total current (mA) - Mmt	Average En on target (V/m)
Colina	0.25	4	2	2	-579.7	0.18	414	414	0.0094
				4	-1582.7	0.30	1005	1750	0.0230
				6	-2090.3	0.35	1648	3062	0.0304
				8	-2177.9	0.35	1595	3965	0.0316
		4	1	2	-635.8	0.19	414	414	0.0092
				4	-1757.6	0.32	1000	1855	0.0251
				6	-1990.0	0.34	1000	2592	0.0286
				8	-2088.4	0.35	1000	2694	0.0273
		2	2	2	-635.8	0.19	414	414	0.0092
				4	-1758.4	0.32	1027	1886	0.0255
				6	-1940.1	0.34	894	1997	0.0260
				8	-1981.5	0.34	957	1997	0.0240
		2	1	2	-579.7	0.18	414	414	0.0084
				4	-1757.6	0.32	1000	1855	0.0251
				6	-1940.1	0.34	894	1999	0.0260
				8	-1986.4	0.35	1000	1999	0.0239
	0.5	4	2	2	-2318.8	0.18	828	828	0.0168
				4	-7030.5	0.32	2000	3711	0.0502
				6	-7686.2	0.34	1999	3998	0.0460
				8	-7945.6	0.35	1999	3998	0.0478
		4	1	2	-2318.8	0.18	828	828	0.0168
				4	-5456.8	0.32	1000	2000	0.0271
				6	-6426.5	0.31	999	2844	0.0391
				8	-6952.3	0.32	1000	3410	0.0422
		2	2	2	-2543.3	0.19	828	828	0.0185
				4	-5577.4	0.31	1186	1999	0.0286
				6	-5974.5	0.31	1119	1998	0.0337
				8	-5986.4	0.31	1131	1997	0.0326
		2	1	2	-2543.3	0.19	828	828	0.0185
				4	-5456.8	0.32	1000	2000	0.0271
				6	-5786.8	0.30	999	1998	0.0340
				8	-5986.9	0.31	998	1997	0.0329

Subject	Target En-field (V/m)	Total current (mA) - Limit	Max current per electrode - Limit (mA)	Num channels	ERNI (mV^2/m^2)	WCC	Max current per electrode - Mrt (mA)	Total current (mA) - Mrt	Average En on target (V/m)
IXI 038	0.25	4	2	2	851.2	0.22	589	589	0.012
				4	2158.0	0.35	1511	2624	0.030
				6	2386.4	0.36	1175	3077	0.033
				8	2734.5	0.39	1402	3998	0.034
		4	1	2	1148.1	0.25	628	628	0.016
				4	1991.5	0.34	1000	1924	0.023
				6	2379.0	0.37	1000	2997	0.027
				8	2539.7	0.38	999	2916	0.032
		2	2	2	851.2	0.22	589	589	0.012
				4	2069.8	0.34	1232	1999	0.025
				6	2138.7	0.35	837	1999	0.025
				8	2216.4	0.36	865	1998	0.026
		2	1	2	1148.1	0.25	628	628	0.016
				4	1834.0	0.32	1000	1762	0.024
				6	2203.7	0.35	882	1999	0.026
				8	2262.6	0.36	757	1998	0.026
	0.5	4	2	2	3404.9	0.22	1178	1178	0.024
				4	7336.0	0.32	1999	3523	0.047
				6	8681.6	0.36	1825	3999	0.049
				8	9046.9	0.36	1519	3998	0.052
		4	1	2	4400.0	0.25	1000	1000	0.025
				4	5953.3	0.30	1000	2000	0.032
				6	7613.0	0.33	999	2860	0.048
				8	8332.1	0.36	999	3798	0.049
		2	2	2	4392.2	0.25	1257	1257	0.032
				4	6430.3	0.30	1809	1999	0.039
				6	6885.3	0.32	1295	1998	0.038
				8	6888.0	0.32	1187	1997	0.038
		2	1	2	4400.0	0.25	1000	1000	0.025
				4	5930.7	0.29	1000	2000	0.034
				6	6848.9	0.32	999	1998	0.037
				8	6853.9	0.32	999	1998	0.037
IXI 033	0.25	4	2	2	714.2	0.24	999	999	0.008
				4	1398.3	0.35	1000	1656	0.014
				6	1647.9	0.33	1000	2400	0.021
				8	1792.7	0.34	1000	3240	0.025
		2	1	2	936.9	0.24	1951	1951	0.015
				4	1484.3	0.32	1515	1999	0.017
				6	1647.2	0.35	1253	1998	0.019
				8	1647.8	0.34	1246	1997	0.019
		2	2	2	936.9	0.24	1951	1951	0.015
				4	1983.6	0.36	1999	3269	0.029
				6	2080.5	0.36	2000	3999	0.029
				8	2163.5	0.38	1999	3998	0.028
	0.5	4	2	2	2856.6	0.24	1999	1999	0.015
				4	5593.1	0.35	1999	3311	0.029
				6	6306.9	0.34	1999	3998	0.036
				8	6467.4	0.34	1999	3997	0.037
		4	1	2	2553.9	0.21	1000	1000	0.016
				4	3885.6	0.25	999	1998	0.025
				6	5003.0	0.29	1000	3000	0.031
				8	5600.4	0.32	1000	4000	0.032
		2	2	2	2856.6	0.24	2000	2000	0.015
				4	4285.1	0.29	1433	1999	0.023
				6	4506.8	0.29	1365	1998	0.026
				8	4510.0	0.29	1335	1998	0.026
		2	1	2	2553.9	0.21	999	999	0.016
				4	3933.0	0.26	999	1998	0.025
				6	4389.8	0.28	1000	1999	0.025
				8	4446.9	0.29	999	1999	0.025

Subject	Target En-field (V/m)	Total current (mA) - Limit	Max current per electrode - Limit (mA)	Num channels	ERNI (mV²/m²)1	WCC	Max current per electrode - Mnt (mA)	Total current (mA) - Mnt	Average En on target (V/m)
IXI 022	0.25	4	2	2	-1227.7	0.27	709	709	0.018
				4	-2359.9	0.38	1402	2705	0.036
				6	-2855.5	0.40	2000	3266	0.040
				8	-2812.4	0.41	1689	3998	0.040
		4	1	2	-1227.7	0.27	709	709	0.018
				4	-2214.4	0.37	999	1998	0.027
				6	-2434.8	0.38	999	2653	0.033
				8	-2694.9	0.40	1000	3248	0.036
		2	2	2	-1227.7	0.27	709	709	0.018
				4	-2234.6	0.37	1092	1999	0.028
				6	-2382.3	0.38	1203	1999	0.031
				8	-2435.7	0.39	844	1997	0.030
		2	1	2	-1227.7	0.27	709	709	0.018
				4	-2214.4	0.37	999	1998	0.027
				6	-2376.9	0.39	1000	1999	0.030
				8	-2430.1	0.39	937	1998	0.029
		4	2	2	-4910.7	0.27	1419	1419	0.037
				4	-8857.6	0.37	1999	3998	0.054
				6	-9325.4	0.38	1999	3998	0.060
				8	-9762.5	0.39	1803	3998	0.061
		4	1	2	-4481.2	0.27	999	999	0.026
				4	-8136.1	0.34	1000	2000	0.032
				6	-7534.4	0.34	1000	2823	0.049
				8	-8844.7	0.37	1000	3464	0.055
	0.5	2	1	2	-4481.2	0.27	999	999	0.026
				4	-5891.2	0.32	1000	2000	0.033
				6	-7099.3	0.34	1000	1999	0.042
				8	-7236.8	0.35	999	1997	0.040
		2	2	2	-4910.7	0.27	1419	1419	0.037
				4	-6864.0	0.34	1602	1999	0.038
				6	-7239.1	0.35	1335	1998	0.041
				8	-7256.5	0.35	1343	1998	0.040
		4	2	2	-4910.7	0.27	1419	1419	0.037
				4	-8857.6	0.37	1999	3998	0.054
				6	-9325.4	0.38	1999	3998	0.060
				8	-9762.5	0.39	1803	3998	0.061
		4	1	2	-4481.2	0.27	999	999	0.026
				4	-8136.1	0.34	1000	2000	0.032
				6	-7534.4	0.34	1000	2823	0.049
				8	-8844.7	0.37	1000	3464	0.055
IXI 002	0.25	2	1	2	-769.5	0.21	639	639	0.011
				4	-1733.9	0.32	1000	1699	0.022
				6	-2065.1	0.36	999	1998	0.023
				8	-2125.4	0.37	999	1998	0.023
		2	2	2	-3077.9	0.21	1279	1279	0.022
				4	-6935.5	0.32	2000	3398	0.044
				6	-8260.3	0.36	1999	3998	0.047
				8	-8506.2	0.37	1998	3997	0.047
		4	2	2	-2848.8	0.20	1000	1000	0.020
				4	-5431.4	0.31	1000	2000	0.028
				6	-6867.0	0.33	1000	2997	0.037
				8	-7603.2	0.34	999	3980	0.044
		4	1	2	-2853.4	0.20	1041	1041	0.021
				4	-5760.2	0.30	1000	1999	0.033
				6	-6004.7	0.31	1299	1998	0.032
				8	-6011.1	0.32	1287	1998	0.032
	0.5	2	1	2	-2848.8	0.20	1000	1000	0.020
				4	-5431.4	0.31	1000	2000	0.028
				6	-5970.1	0.31	999	1998	0.032
				8	-5985.6	0.32	998	1997	0.032

Subject	Target En-field (V/m)	Total current (mA) - Limit	Max current per electrode - Limit (mA)	Num channels	ERNI (mV*s/m^2)	WCC	Max current per electrode - Mnt (mA)	Total current (mA) - Mnt	Average En on target (V/m)
IXI 045	0.25	4	2	2	-1103.9	0.26	540	540	0.017
				4	-2267.9	0.37	1266	2286	0.035
				6	-2551.8	0.40	1373	2871	0.040
				8	-2833.8	0.42	1475	3998	0.043
		4	1	2	-1103.9	0.26	540	540	0.017
				4	-2233.4	0.37	1000	1986	0.032
				6	-2438.2	0.40	841	1998	0.032
				8	-2483.6	0.39	1000	2560	0.038
				8	-2662.8	0.41	1000	3161	0.039
		2	2	2	-1103.9	0.26	540	540	0.017
				4	-2240.5	0.37	1051	1999	0.032
				6	-2354.5	0.38	1134	1998	0.033
				8	-2438.2	0.40	841	1998	0.032
		2	1	2	-1103.9	0.26	540	540	0.017
				4	-2233.4	0.37	1000	1986	0.032
				6	-2399.8	0.39	820	1999	0.032
				8	-2420.3	0.39	843	1997	0.033
	0.5	4	2	2	-4391.3	0.26	1000	1000	0.032
				4	-6612.5	0.34	1000	1998	0.039
				6	-8334.7	0.39	999	2997	0.047
				8	-8804.2	0.38	999	3373	0.056
		4	1	2	-4415.6	0.26	1080	1080	0.034
				4	-7159.1	0.35	1469	1999	0.043
				6	-7523.9	0.35	1220	1999	0.048
				8	-7614.9	0.36	1125	1999	0.047
		2	2	2	-4415.6	0.26	1080	1080	0.034
				4	-8933.4	0.37	2000	3972	0.065
				6	-9599.2	0.39	1660	3999	0.064
				8	-9724.4	0.39	1610	3999	0.064
		4	2	2	-4391.3	0.26	1000	1000	0.032
				4	-8334.7	0.39	999	2997	0.047
				6	-9599.2	0.39	1660	3999	0.064
				8	-9724.4	0.39	1610	3999	0.064
	0.25	4	2	2	-962.5	0.23	617	617	0.013
				4	-2386.8	0.36	1000	2000	0.032
				6	-2646.0	0.39	2000	3999	0.030
				8	-2748.2	0.40	1998	3997	0.032
		2	1	2	-962.5	0.23	617	617	0.013
				4	-2011.4	0.34	1000	2000	0.023
				6	-2233.7	0.35	1000	2667	0.028
				8	-2375.9	0.36	1000	3050	0.030
		4	2	2	-962.5	0.23	617	617	0.013
				4	-2106.6	0.36	1390	1999	0.022
				6	-2119.6	0.36	1211	1998	0.023
				8	-2138.0	0.36	1188	1998	0.023
		2	1	2	-707.5	0.20	484	484	0.010
				4	-2011.4	0.34	999	1998	0.023
				6	-2103.9	0.35	1000	1998	0.023
				8	-2131.9	0.36	999	1998	0.023
		4	2	2	-3849.9	0.23	1235	1235	0.027
				4	-8045.6	0.34	1999	3998	0.047
				6	-8415.7	0.35	2000	3998	0.046
				8	-8527.5	0.36	1999	3998	0.046
	0.5	4	2	2	-2829.9	0.20	969	969	0.020
				4	-5642.5	0.31	999	1998	0.027
				6	-6754.1	0.32	1000	2998	0.037
				8	-7856.4	0.34	1000	3952	0.044
		2	1	2	-2829.9	0.20	969	969	0.020
				4	-5996.8	0.32	1516	1999	0.029
				6	-6204.3	0.32	1310	1999	0.030
				8	-6056.5	0.32	1242	1999	0.030
		2	2	2	-3710.3	0.23	999	999	0.022
				4	-5642.5	0.31	1000	2000	0.027
				6	-5995.2	0.31	999	1998	0.030
				8	-6043.3	0.31	999	1998	0.030

Subject	Target En field (V/m)	Total current (mA) - Limit	Max current per electrode - Limit (mA)	Num channels	ERN (mV*s)/(m^2)	WCC	Max current per electrode - Mxt (mA)	Total current (mA) - Mxt	Average En on target (V/m)
IXI 016	0.25	4	2	2	-801.7	0.21	427	427	0.011
				4	-1947.2	0.33	1999	2299	0.024
				6	-2682.3	0.39	3000	3154	0.036
				8	-2966.0	0.41	1790	3998	0.041
		4	1	2	-862.3	0.22	575	575	0.012
				4	-1689.3	0.31	1000	1533	0.021
				6	-2420.4	0.37	999	2019	0.032
				8	-2782.3	0.40	999	2827	0.036
		2	2	2	-862.3	0.22	575	575	0.012
				4	-1876.2	0.33	1567	1999	0.022
				6	-2489.7	0.38	1208	1998	0.031
				8	-2541.0	0.39	907	1998	0.029
		2	1	2	-862.3	0.22	575	575	0.0127
				4	-1689.3	0.31	1000	1533	0.0211
				6	-2443.2	0.37	999	1999	0.0322
				8	-2542.4	0.39	805	1998	0.0301
		4	2	2	-3206.7	0.21	854	854	0.0233
				4	-6757.3	0.31	1999	3065	0.0411
				6	-9432.9	0.36	1999	3880	0.0631
				8	-10070.9	0.39	1562	3999	0.0571
		4	1	2	-3389.3	0.22	999	999	0.0211
				4	-6137.9	0.30	1000	1999	0.0341
				6	-7750.4	0.34	999	2843	0.0401
				8	-9071.4	0.35	1000	3424	0.0391
		2	2	2	-3389.3	0.22	1000	1000	0.0211
				4	-6117.9	0.30	2000	2000	0.0371
				6	-7372.0	0.34	1079	1999	0.0401
				8	-7482.9	0.35	1006	1997	0.0391
		2	1	2	-3389.3	0.22	1000	1000	0.0211
				4	-6117.9	0.30	1000	1999	0.0371
				6	-7329.6	0.34	1000	1999	0.0391
				8	-7491.7	0.35	1000	1997	0.0391
IXI 050	0.25	4	2	2	-3485.3	0.23	1352	1352	0.027
				4	-6707.5	0.32	1999	3586	0.047
				6	-8183.3	0.36	1999	3998	0.055
				8	-8354.6	0.37	1999	3997	0.055
		4	1	2	-3918.8	0.27	1000	1000	0.022
				4	-5367.8	0.30	1000	1999	0.034
				6	-6610.9	0.33	1000	2997	0.044
				8	-7707.0	0.36	1000	4000	0.047
		2	2	2	-1172.0	0.27	840	840	0.018
				4	-1864.0	0.34	1999	1753	0.024
				6	-2009.2	0.36	1998	2290	0.028
				8	-2079.7	0.36	1211	1999	0.028
		4	1	2	-1172.0	0.27	840	840	0.018
				4	-1676.9	0.32	1000	1753	0.024
				6	-2035.6	0.37	999	2290	0.028
				8	-2300.2	0.38	1000	3127	0.031
		2	1	2	-1172.0	0.27	840	840	0.018
				4	-1864.0	0.34	1999	1999	0.026
				6	-2009.2	0.36	1998	1998	0.027
				8	-2079.7	0.36	1211	1999	0.028
		4	2	2	-1172.0	0.27	840	840	0.018
				4	-1732.8	0.34	999	1998	0.021
				6	-2042.9	0.36	1000	1999	0.028
				8	-2086.6	0.37	999	1997	0.027
	0.5	4	2	2	-3485.3	0.23	1352	1352	0.027
				4	-6707.5	0.32	1999	3586	0.047
				6	-8183.3	0.36	1999	3998	0.055
				8	-8354.6	0.37	1999	3997	0.055
		4	1	2	-3918.8	0.27	1000	1000	0.022
				4	-5367.8	0.30	1000	1999	0.034
				6	-6610.9	0.33	1000	2997	0.044
				8	-7707.0	0.36	1000	4000	0.047
		2	2	2	-3918.8	0.27	1000	1000	0.022
				4	-5367.8	0.30	1000	1999	0.034
				6	-6341.4	0.33	1998	1998	0.038
				8	-6381.0	0.33	1765	1999	0.036
		4	2	2	-3918.8	0.27	1000	1000	0.022
				4	-5367.8	0.30	1000	1999	0.034
				6	-6149.9	0.33	1000	1999	0.035
				8	-6223.7	0.34	1000	1999	0.035

Subject	Target E-n-field (V/m)	Total current (mA) - Limit	Max current per electrode - Limit (mA)	Num.channels	ERNI (mV²/m^2)	WCC	Max current per electrode - Mnt (mA)	Total current (mA) - Mnt	Average E-n on Target (V/m)
IXI 028	0.25	4	2	2	-942.9	0.24	751	751	0.014
				4	-2315.2	0.37	1999	3946	0.033
				6	-2453.3	0.38	2000	3999	0.035
				8	-2611.8	0.40	1904	3998	0.031
		4	1	2	-942.9	0.24	751	751	0.014
				4	-1724.5	0.37	1000	2000	0.017
				6	-2039.4	0.35	999	2438	0.025
				8	-2295.9	0.38	1000	3549	0.027
		2	2	2	-942.9	0.24	751	751	0.014
				4	-1881.8	0.34	1650	1999	0.022
				6	-1963.5	0.35	1514	1999	0.024
				8	-1969.1	0.35	1415	1999	0.023
		2	1	2	-942.9	0.24	751	751	0.014
				4	-1724.5	0.37	1000	2000	0.017
				6	-1876.8	0.35	1000	1999	0.022
				8	-1941.8	0.36	999	1996	0.022
	0.5	4	2	2	-3771.7	0.24	1503	1503	0.028
				4	-6898.2	0.37	2000	4000	0.034
				6	-7639.1	0.35	1999	3998	0.044
				8	-7764.7	0.36	1999	3998	0.044
		4	1	2	-3348.9	0.24	999	999	0.019
				4	-4568.9	0.30	999	1998	0.021
				6	-5913.8	0.31	999	2796	0.024
				8	-6671.0	0.33	1000	3996	0.038
		2	2	2	-3771.7	0.24	1503	1503	0.028
				4	-5157.1	0.32	1889	1999	0.026
				6	-5413.6	0.31	1348	1999	0.028
				8	-5376.1	0.31	1138	1997	0.028
		2	1	2	-3348.9	0.24	1000	1000	0.019
				4	-4383.9	0.28	1000	1999	0.022
				6	-5348.3	0.31	999	1998	0.028
				8	-5375.0	0.31	999	1998	0.028

C2. Graphical results for the average E-field

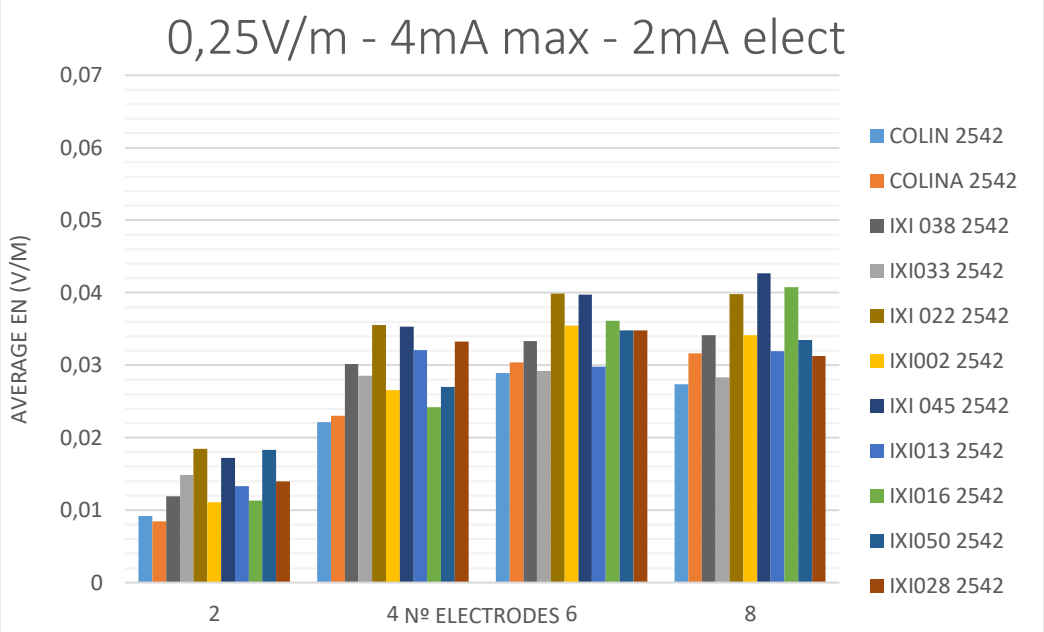

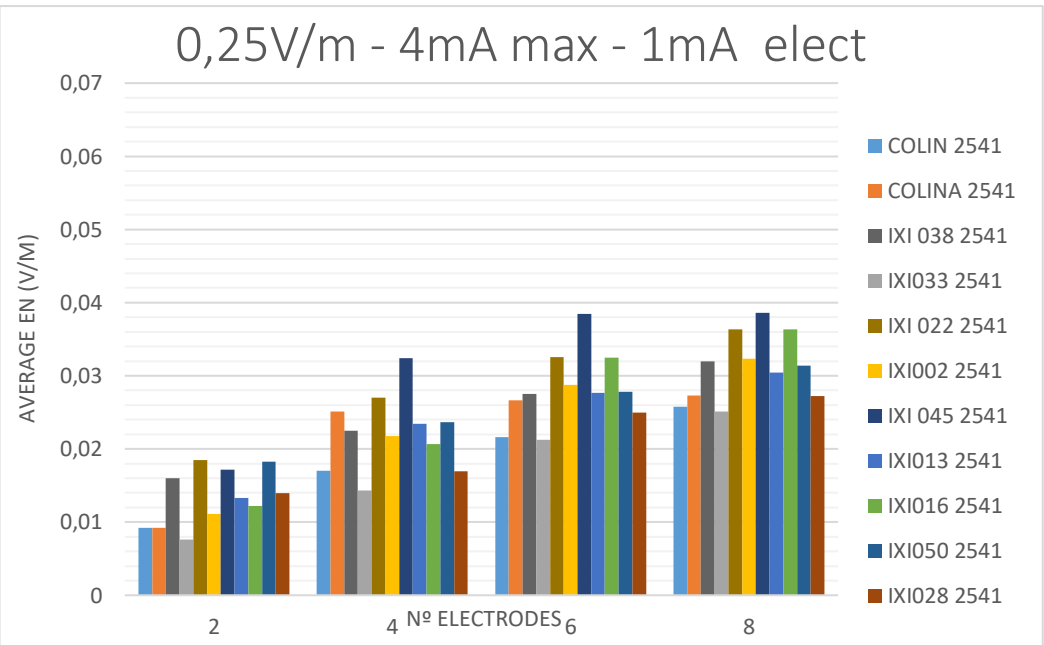

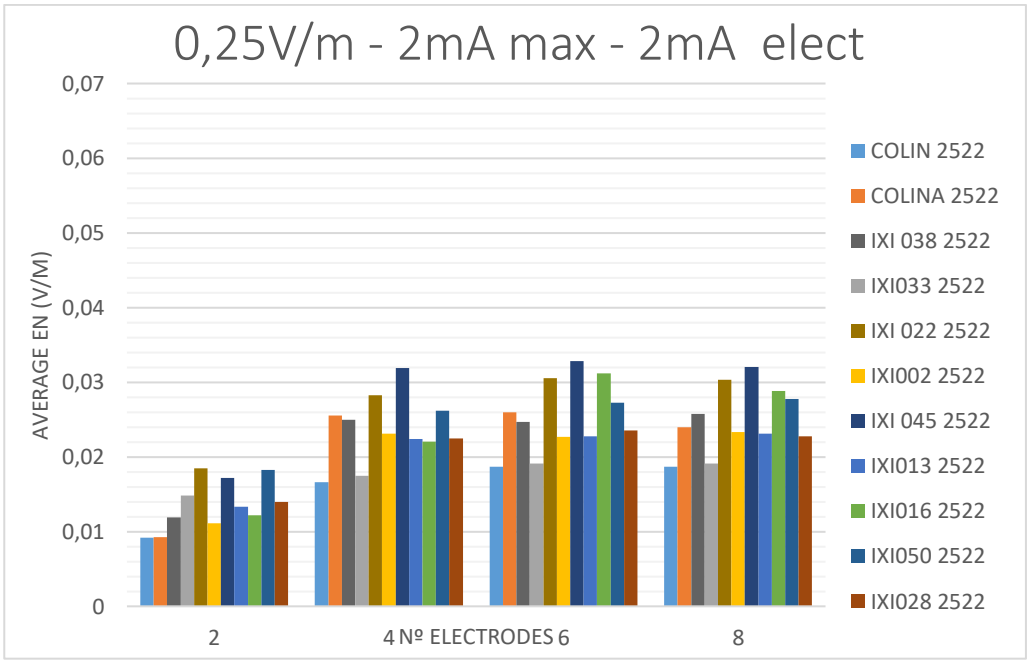
0,25V/m - 2mA max - 2mA elect
AVERAGE EN (V/M)
0,07
0,06
0,05
0,04
0,03
0,02
0,01
0
2
4
Nº ELECTRODES
6
8
COLIN 2522
COLINA 2522
IXI 038 2522
IXI033 2522
IXI 022 2522
IXI002 2522
IXI 045 2522
IXI013 2522
IXI016 2522
IXI050 2522
IXI028 2522

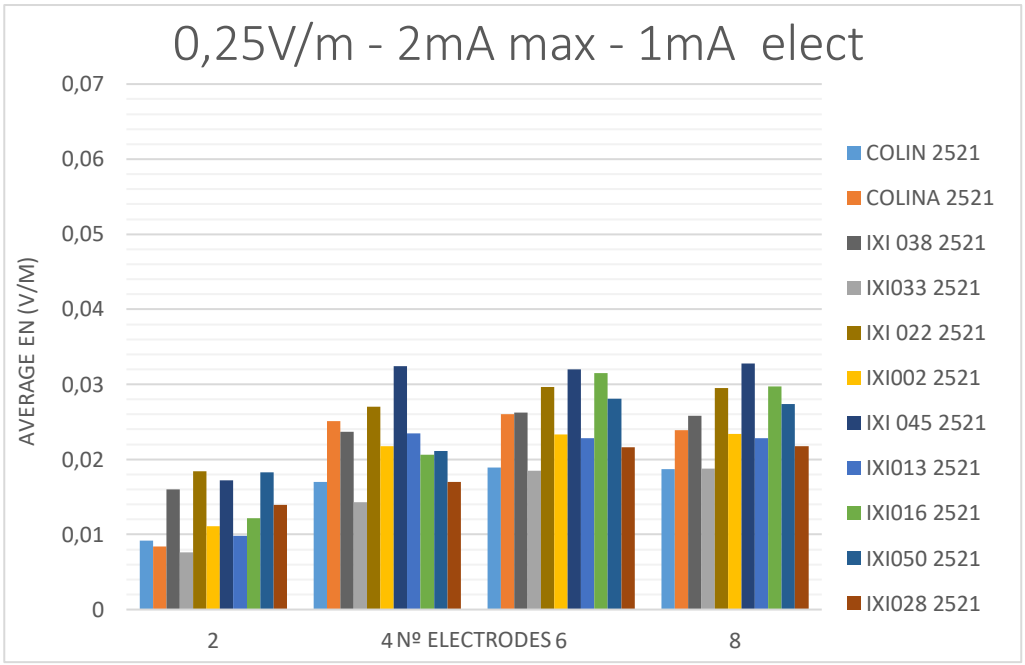
0,25V/m - 2mA max - 1mA elect
AVERAGE EN (V/M)
0,07
0,06
0,05
0,04
0,03
0,02
0,01
0
2
4
Nº ELECTRODES
6
8
COLIN 2521
COLINA 2521
IXI 038 2521
IXI033 2521
IXI 022 2521
IXI002 2521
IXI 045 2521
IXI013 2521
IXI016 2521
IXI050 2521
IXI028 2521

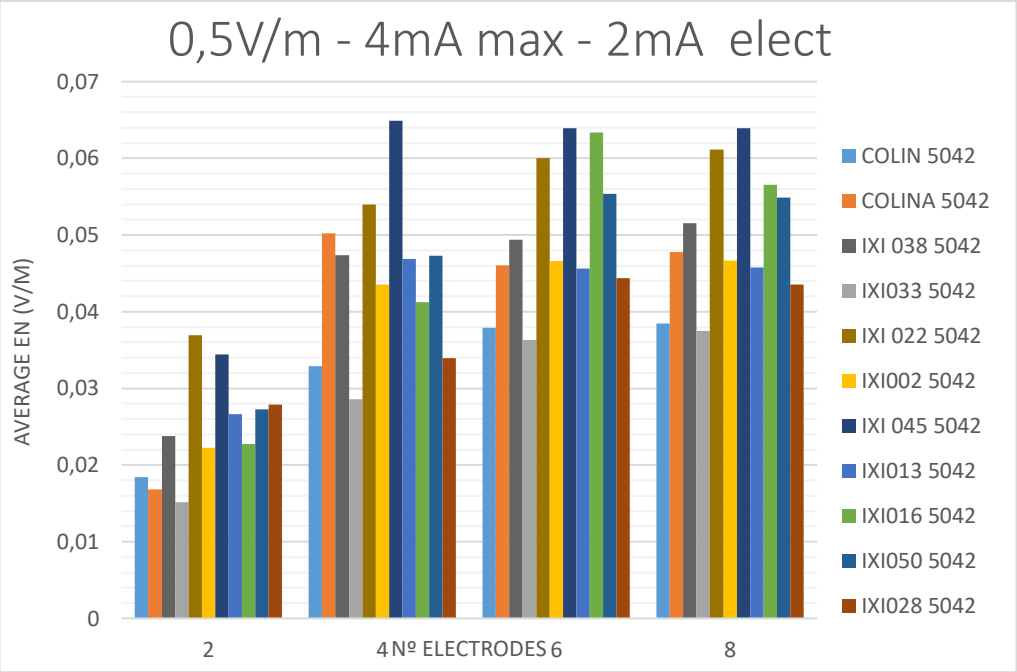
0,5V/m - 4mA max - 2mA elect
AVERAGE EN (V/M)
0,07
0,06
0,05
0,04
0,03
0,02
0,01
0
2
4
Nº ELECTRODES
6
8
COLIN 5042
COLINA 5042
IXI 038 5042
IXI033 5042
IXI 022 5042
IXI002 5042
IXI 045 5042
IXI013 5042
IXI016 5042
IXI050 5042
IXI028 5042

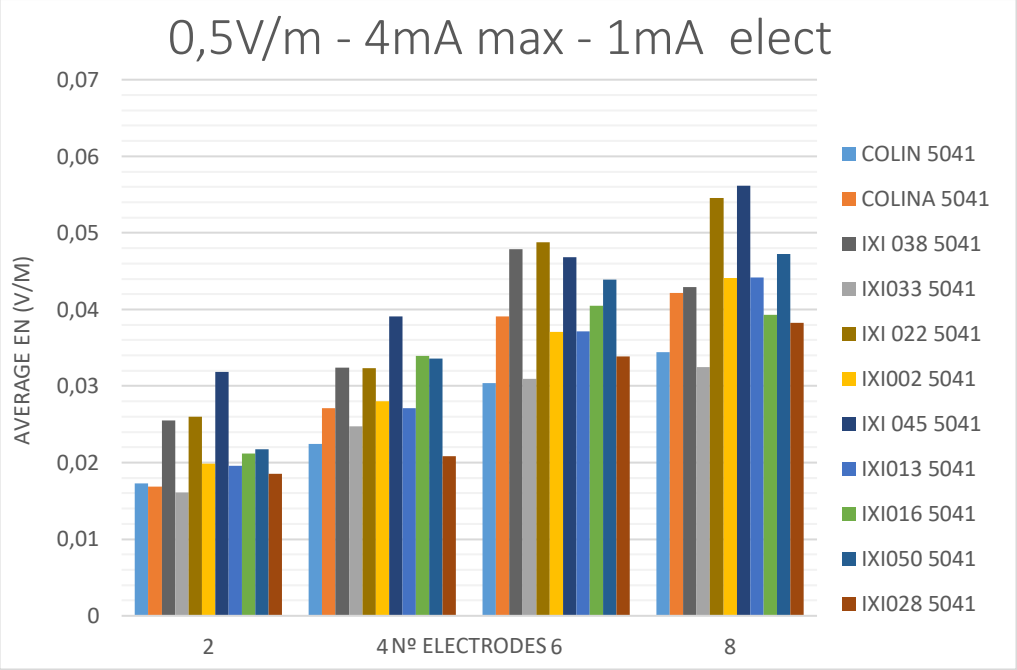
0,5V/m - 4mA max - 1mA elect
AVERAGE EN (V/M)
0,07
0,06
0,05
0,04
0,03
0,02
0,01
0
2
4
Nº ELECTRODES
6
8
COLIN 5041
COLINA 5041
IXI 038 5041
IXI033 5041
IXI 022 5041
IXI002 5041
IXI 045 5041
IXI013 5041
IXI016 5041
IXI050 5041
IXI028 5041

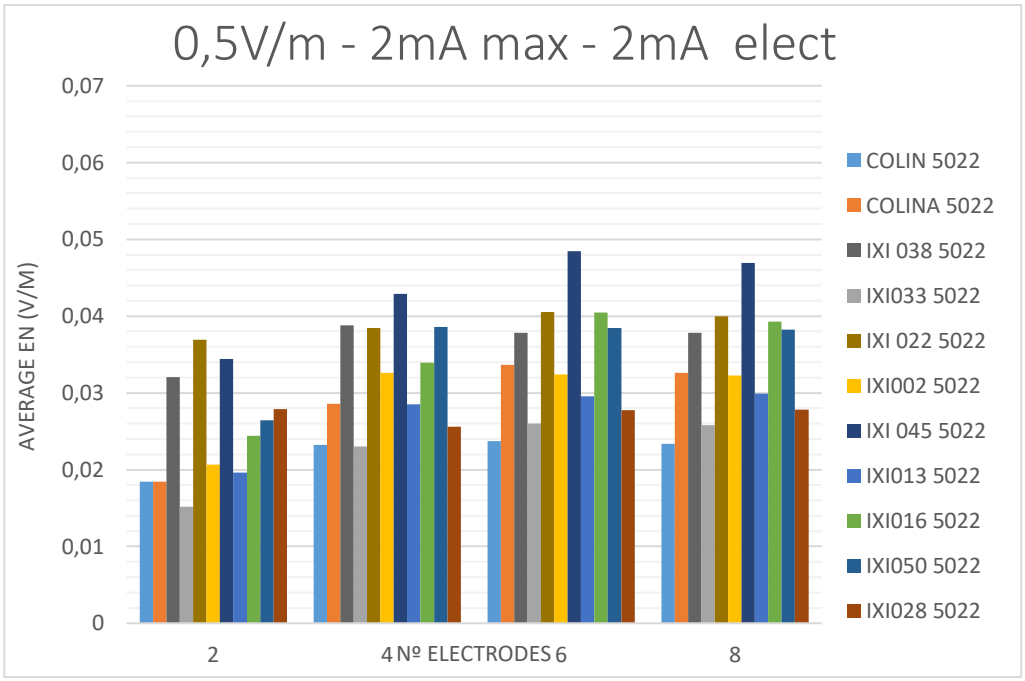

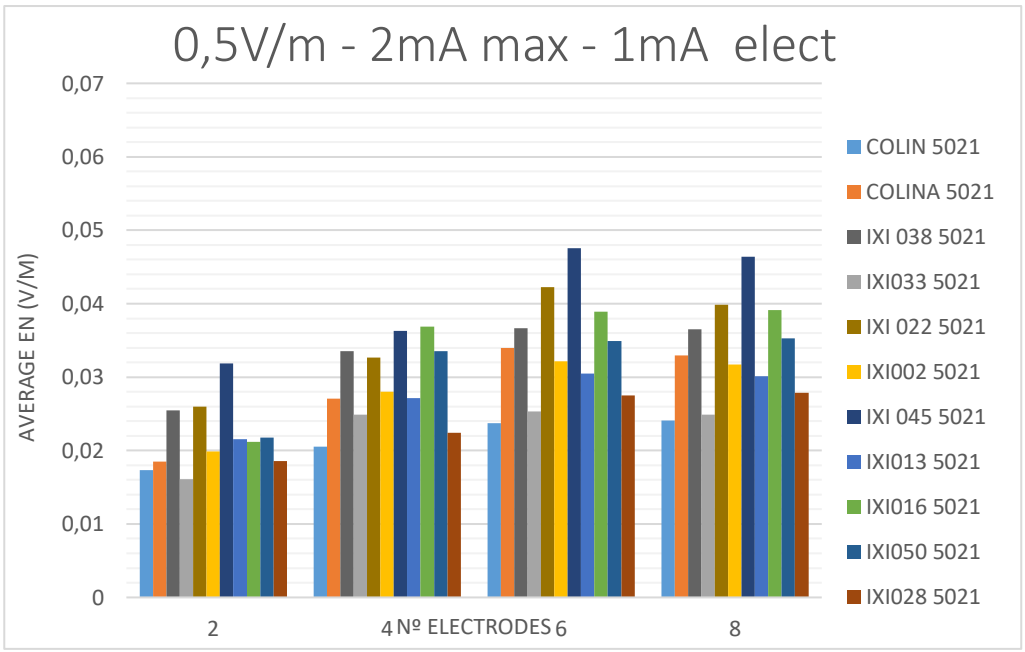

C3. Bipolar configuration results (V/m)

Colin	Colina	IXI038	IXI033	IXI022	IXI002	IXI045	IXI013	IXI016	IXI050	IXI028
0.013	0.021	0.020	0.027	0.023	0.025	0.030	0.019	0.033	0.010	0.016

MEAN	MEADIAN	SD
0.021	0.021	0.007

Annex D Code created for meshing into Colin's space

```
%First, we copy the values for the tailarach.auto.xfm file

transformation_colin = [0.968872 -0.003120 -0.013832 -0.165924
0.006807 0.969138 0.049886 -2.106155
0.014437 0.028974 0.954776 0.091980];

transformation_subject = [1.039743 -0.018241 0.005892 1.207916
-0.018279 0.991003 0.170336 -19.046707
-0.009698 -0.112450 1.119335 -29.364792];

%Map from subject's space to Colin's space

nodes_Colin_mni = (transformation_colin(1:3,1:3)*NodesColin.nodes_g' +
repmat(transformation_colin(1:3,4),1,length(NodesColin.nodes_g)))';
nodes_Subject_mni =
(transformation_subject(1:3,1:3)*NodesSubject.nodes_g' +
repmat(transformation_subject(1:3,4),1,length(NodesSubject.nodes_g)))';

%Plots
subplot(1,2,1);
title('Before transform')
plotmesh(NodesColin.nodes_g,NodesColin.faces_g,'EdgeColor','none','FaceCo
lor',uint8([126,128,128]));material dull;light;
hold on;
plotmesh(NodesSubject.nodes_g,NodesSubject.faces_g,'EdgeColor','none','Fa
ceColor',uint8([256,128,128]));material dull;light;
subplot(1,2,2);
title('After transform')
plotmesh(nodes_Colin_mni,NodesColin.faces_g,'EdgeColor','none','FaceColor
',uint8([126,128,128]));material dull;light;
hold on;
plotmesh(nodes_Subject_mni,NodesSubject.faces_g,'EdgeColor','none','FaceC
olor',uint8([256,128,128]));material dull;light;

%Map the E-field from the subject to Colin

mapping_matrix = zeros(length(nodes_Colin_mni),1);

h = waitbar(0,'Please wait...')
for i=1:length(nodes_Colin_mni)
    distance = (nodes_Colin_mni(i,1)-
nodes_Subject_mni(:,1)).^2+(nodes_Colin_mni(i,2)-
nodes_Subject_mni(:,2)).^2+(nodes_Colin_mni(i,3)-
nodes_Subject_mni(:,3)).^2;
    [~,mapping_matrix(i,1)] = min(distance);
    waitbar(i / length(nodes_Colin_mni))
end
close(h);

%Plot E.field in Colin's mesh

figure;
```

```
plotmesh([nodes_Colin_mni
nEgmsurfdataexportedLDLPFC(mapping_matrix)],NodesColin.faces_g,'EdgeColor
','none');material dull; light; colormap jet; colorbar;
title('E-field (normal component to the cortical surface) in Colin''s
space LDLPFC');

figure;
plotmesh([nodes_Colin_mni
nEgmsurfdataexportedLPMC(mapping_matrix)],NodesColin.faces_g,'EdgeColor',
'none');material dull; light; colormap jet; colorbar;
title('E-field (normal component to the cortical surface) in Colin''s
space LPMC');

%For each subject, the E-field distrubtion is mapped into Colin and saved

IXI02_LDLPFC=nEgmsurfdataexported(mapping_matrix)

%Calculations for median and STD with plots

SS_LPMC=[IXI50_LDLPFC IXI45_LDLPFC IXI38_LDLPFC IXI33_LDLPFC IXI28_LDLPFC
IXI22_LDLPFC IXI16_LDLPFC IXI13_LDLPFC IXI02_LDLPFC Colin Colina];
Median_SS=median(SS,2);
st_SS=std(SS,0,2);
subplot(1,2,1);title('Median');plotmesh([Nodes.nodes_g
Median_SS],Nodes.faces_g);colorbar('southoutside');
subplot(1,2,2);title('STD');plotmesh([Nodes.nodes_g
st_SS],Nodes.faces_g);colorbar('southoutside');
```